Silvie Müller

Reaction Engineering Studies of Cold Plasma Partial Oxidation of Methane

Scientific Report Series Volume 47

2024

Scientific Report Series
Laboratory of Engineering Thermodynamics (LTD)
RPTU Kaiserslautern
P.O. Box 3049
67663 Kaiserslautern
Germany

ISSN 2195-7606
ISBN 978-3-944433-46-2

© LTD all rights reserved

Reaction Engineering Studies of Cold Plasma Partial Oxidation of Methane

Vom Fachbereich Maschinenbau und Verfahrenstechnik
der Rheinland-Pfälzischen Technischen Universität
Kaiserslautern-Landau
zur Verleihung des akademischen Grades

Doktor-Ingenieur (Dr.-Ing.)
genehmigte
Dissertation

von
M.Sc. Silvie Müller
aus Ludwigshafen am Rhein

Dekan:	Prof. Dr. rer. nat. Roland Ulber
Berichterstattende:	Prof. Dr.-Ing. Hans Hasse
	Prof. Dr.-Ing. Erik von Harbou
	Jun.-Prof. Dr.-Ing. Maximilian Kohns

Tag der mündlichen Prüfung: 19.04.2024

D 386

Danksagung

Diese Arbeit entstand während meiner Tätigkeit als wissenschaftliche Mitarbeiterin am Lehrstuhl für Thermodynamik (LTD) an der Rheinland-Pfälzischen Technischen Universität Kaiserslautern-Landau.

Hans Hasse danke ich als Doktorvater dieser Arbeit für die hervorragende Betreuung und die fachliche sowie persönliche Unterstützung insbesondere durch die sehr motivierenden Besprechungen. Maximilian Kohns danke ich für die Begleitung meiner Zeit am LTD als Kollege, Junior-Professor und Betreuer. Erik von Harbou danke ich für viele vortreffliche Impulse, unter Anderem mir eine Promotion vorzuschlagen. Eckhard Ströfer als Flammen- und Innovations-Spezialist danke ich für prägende Gespräche und für die Idee Kaltes Plasma zum LTD zu bringen. Kerstin Münnemann und dem NMR-Team danke ich für den Support bezüglich meiner NMR-Messungen und -Auswertungen.

Jürgen Brauch, Berthold Mrawek, Julian Peter und Dirk Feddeck stellen für mich den Inbegriff eines Ingenieurs dar und ich danke ihnen allen sehr für den maßgeblichen Beitrag in Konzeption und Konstruktion der Plasma-Anlage. Insbesondere Jürgen Brauch danke ich für die außerordentliche Beratung im Labor hinsichtlich Gefährdung und Inbetriebnahme. Jörg Brutscher von GBS Elektronik GmbH danke ich für den eigens für meine Anwendung gebauten Plasmagenerator und die kompetente Begleitung der ersten Versuche. Kirsten Brunn und Nicole Hevert danke ich für stets gut gelaunte fachliche Unterstützung im Labor. Im Team mit Tanja Breug-Nissen und Luciana Ninni Schäfer ließ sich jeder Frust im Laboralltag überwinden.
Marlies Mangold, Ilona Stein und Jennifer Bergmann sind für mich als Expertinnen für alle Bürobelange das Herzstück des LTD und ich danke ihnen für die wunderbare Unterstützung bei jeglichen Anfragen. Daniel Fröscher danke ich für jeden glänzenden Einsatz bei allen IT-Fragestellungen. Fabian Jirasek und Nicolas Hayer danke ich für das „zu Hause Gefühl“, viel Spaß und tiefgründigen Gesprächen im Penthouse. Allen

weiteren Freunden und Kollegen am LTD danke ich für viele großartige und prägende Erfahrungen und die Gewissheit immer miteinander verbunden zu sein.

Besonderer Dank geht an die Studierenden, die im Rahmen von Experimenten, Messungen, Auswertungen oder Optimierungen einen wertvollen Beitrag zu dieser Dissertation geleistet haben. Dazu gehören die studentischen und wissenschaftlichen Hilfskräfte Ferdinand Breit, Annemarie Rätz, Maximilian Koch und Florian Jager sowie die Studierenden Tess Seip, Craig McQuillan, André Bender, Lena Magel, Daniel Stolte, Jana Heiß und Tobias Laufer, die ihre studentischen Projekt- und Abschlussarbeiten bei mir durchgeführt haben.

Elmar Kessler und Ellen Steimers danke ich für die unschätzbar wertvolle Freundschaft und für die gemeinsame Zeit in der RWTH51, in der ich für die Promotion von Anfang bis Ende perfekt unterstützt wurde. Ein herzliches Dankeschön geht auch an meine Familie und Freunde, die mir viel Verständnis entgegengebracht und immer Zuspruch vermittelt haben.

Kaiserslautern, Mai 2024
Silvie Müller

Abstract

Cold plasma is a partially ionized state of matter that unites high reactivity and mild conditions. Therefore, cold plasma reactors are intriguing for reaction engineering. In this work, a laboratory scale dielectric barrier discharge (DBD) cold plasma reactor was designed, set up, and used for studying the application of the technology for the partial oxidation of methane. Experiments were carried out near ambient conditions and in addition to the reactants the feed also contained the inert carrier gas argon. The product stream was split into a condensable fraction and the remaining gaseous fraction. The latter was analyzed at-line in a gas chromatograph equipped with a dual column and two carrier gases. The condensable fraction was analyzed by NMR spectroscopy, Karl Fischer titration, and sodium sulfite titration. In the product stream, 16 product components were identified and quantified: acetic acid, acetone, carbon dioxide, carbon monoxide, ethanol, ethane, ethene, ethylene glycol, formaldehyde, formic acid, hydrogen, methanol, methyl acetate, methyl hydroperoxide, methyl formate, and water. The conversion of the reactants and the selectivities to the products were measured varying the molar reactant ratio in the feed, the mole fraction of argon in the feed, the residence time in the reactor, and the electrical power input. The influence of the variation of the electrical power input, the residence time, and the argon mole fraction can be described well by lumping the three factors into a newly introduced specific energy input *SEI**, such that the dependencies of conversions and selectivities can be described by using only the *SEI** and the molar reactant ratio in the feed. The results from 43 experiments carried out in the present work and the sundry trends found in the comprehensive data set extend the available knowledge on DBD cold plasma partial oxidation of methane considerably and are useful for testing mechanistic models

.

Kurzfassung

Kaltes Plasma ist ein teilweise ionisierter Zustand, der eine hohe Reaktivität und milde Bedingungen miteinander verbindet. Daher sind Reaktoren mit kaltem Plasma für die Reaktionstechnik sehr interessant. In dieser Arbeit wurde ein solcher Reaktor mit dielektrischer Barriereentladung (DBD) im Labormaßstab entworfen, in Betrieb genommen und verwendet, um die Anwendung der Technologie für die partielle Oxidation von Methan zu untersuchen. Die Experimente wurden bei Umgebungsbedingungen durchgeführt, und neben den Reaktanden enthielt der Feed auch das inerte Trägergas Argon. Der Produktstrom wurde in eine kondensierbare Fraktion und die verbleibende gasförmige Fraktion aufgeteilt. Letztere wurde at-line mit einem Gaschromatographen mittels Doppelsäule und zwei Trägergasen analysiert. Die kondensierbare Fraktion wurde mittels NMR-Spektroskopie, Karl-Fischer-Titration und Natriumsulfit-Titration analysiert. Im Produktstrom wurden 16 Produkte identifiziert und quantifiziert: Aceton, Ameisensäure, Ethanol, Ethan, Ethen, Ethylenglykol, Essigsäure, Formaldehyd, Kohlendioxid, Kohlenmonoxid, Methanol, Methylacetat, Methylformiat, Methylhydroperoxid, Wasser und Wasserstoff. Der Umsatz der Reaktanten und die Selektivität zu den Produkten wurden unter Variation des Reaktanten-Einsatzstoffverhältnisses, des Argon-Molanteils im Feed, der Verweilzeit im Reaktor und des elektrischen Leistungseintrags gemessen. Der Einfluss der Variation des elektrischen Leistungseintrags, der Verweilzeit und des Argon-Molanteils lässt sich gut beschreiben, indem die drei Faktoren zu einem neu eingeführten spezifischen Energieeintrag *SEI** zusammengefasst werden, so dass die Abhängigkeiten von Umsatz und Selektivität nur durch den *SEI** und das molare Reaktanten-Einsatzstoffverhältnis im Feed beschrieben werden können. Die Ergebnisse von 43 in der vorliegenden Arbeit durchgeführten Experimenten und die unterschiedlichen Trends aus dem umfassenden Datensatz erweitern das verfügbare Wissen über die partielle Oxidation von Methan in DBD-Reaktoren erheblich und sind anwendbar für die Prüfung mechanistischer Modelle.

Contents

Abstract **XI**

Kurzfassung **XIII**

Contents **XV**

1 Introduction **19**

1.1 Cold Plasma Technology 19

1.2 Cold Plasma Partial Oxidation of Methane 19

1.3 Goals of this Work 3

2 Materials and Methods **5**

2.1 Chemicals 5

2.2 Experimental Set-up 6

2.2.1 Cold Plasma Reactor 6

2.2.2 Laboratory Scale Plant 8

2.3 Experimental Procedure 12

2.4 Analysis of the Product Stream 14

2.4.1 Overview 14

2.4.2 Wet-chemistry 17

2.4.3 NMR Spectroscopy 18

2.4.3.1 Sample Preparation 18

2.4.3.2 Qualitative NMR Spectroscopy 18
2.4.3.3 Quantitative NMR Spectroscopy 24
2.4.4 Gas Chromatography 25
2.5 Conversions and Selectivities 27
2.6 Specific Energy Input 28

3 Results and Discussion 29

3.1 Overview of Experiments 29
3.2 Influence of the Mole Fraction of Argon 30
3.3 Lumping of the Data 32
3.4 Conversions 32
3.5 Selectivities 34
3.6.1 H-Selectivity to Products without Carbon 35
3.6.2 C-Selectivity to Products without Hydrogen 36
3.6.3 C-Selectivity to Products without Oxygen 37
3.6.4 C-Selectivity to Products that Contain One Carbon Atom and Hydrogen and Oxygen 38
3.6.5 C-Selectivity to Products that Contain More than One Carbon Atom and Hydrogen and Oxygen 40
3.6 Temperature Increase 41
3.7 Comparison with the Literature 42

4 Conclusions 47

References 51

Appendix 63

A Supporting Information on Experiments 63

A.1 Setting of the Two-Position Valves of the Analytical System 63
A.2 Feed Composition 67

B Supporting Information on Measurements 69

B.1 Measurement Uncertainties 69
B.2 Wet-chemistry 72
B.3 NMR Spectroscopy 73
B.3.1 Acquisition and Processing Parameters 73
B.3.2 Structure Elucidation 74
B.4 Gas Chromatography 85
B.4.1 Acquisition Parameters and Specification of the Methods 85
B.4.2 Retention Times and Quantitative Evaluation 86
B.5 Stability of the Condensable Fraction 89

C Influence of Argon **91**
C.1 Conversions 91
C.2 Selectivities 92
C.2.1 H-Selectivity to Products without Carbon 92
C.2.2 C-Selectivity to Products without Hydrogen 93
C.2.3 C-Selectivity to Products without Oxygen 94
C.2.4 C-Selectivity to Products that Contain One Carbon and Hydrogen and Oxygen 95
C.2.5 C-Selectivity to Products that Contain More than One Carbon Atom and Hydrogen and Oxygen 95

D Individual Results **97**
D.1 Conversions 97
D.2 Selectivities 98
D.2.1 H-Selectivity to Products without Carbon 99
D.2.2 C-Selectivity to Products without Hydrogen 100
D.2.3 C-Selectivity to Products without Oxygen 101
D.2.4 C-Selectivity to Products that Contain One Carbon Atom and Hydrogen and Oxygen 102

D.2.5 C-Selectivity to Products that Contain More than One Carbon Atom and Hydrogen and Oxygen 103

E Results without a High Temperature Difference 105

E.1 General Remarks 105

E.2 Conversions 107

E.3 Selectivities 108

E.3.1 H-Selectivity to Products without Carbon 108

E.3.2 C-Selectivity to Products without Hydrogen 109

E.3.3 C-Selectivity to Products without Oxygen 110

E.3.4 C-Selectivity to Products that Contain One Carbon and Hydrogen and Oxygen 111

E.3.5 C-Selectivity to Products that Contain More than One Carbon Atom and Hydrogen and Oxygen 112

F Elemental Balance 113

G Numerical Experimental Data 115

G.1 Lumped Experimental Data 115

G.2 Individual Experimental Data 119

G.3 Numerical Data for the Elemental Balance 124

1 Introduction

1.1 Cold Plasma Technology

Cold plasma technology is interesting as the presence of excited species, radicals, ions, and free electrons in the plasma opens up new reaction pathways at mild conditions [1]. Dielectric barrier discharge (DBD) cold plasma technology is particularly suited for applications in reaction engineering: it is comparatively easy to operate, works at ambient conditions [2, 3], and it has a large volume excitation in an energy range capable for the excitation of atomic and molecular species and the breaking of chemical bonds to initiate chemical reactions [4, 5].

The most important application of DBD cold plasma is the generation of ozone, first described in 1857 by Siemens [6]. Due to the high oxidizing effect of ozone and its effective and low-cost production with DBD cold plasma, ozone generators are currently widely used in both commercial and industrial sectors and the underlying physical mechanisms are well understood [2, 7–11]. Today, there is also a growing number of additional possible applications of DBD cold plasma besides ozone generation, such as the decomposition of volatile organic compounds [12] and the synthesis of value-added products in organic chemistry [5, 13–19].

1.2 Cold Plasma Partial Oxidation of Methane

The partial oxidation of methane in DBD cold plasma has been studied experimentally by many authors [10, 13–15, 20–51] and several reviews [52–55] provide an overview of the results. Many of those investigations also combine the DBD cold plasma with a catalyst [36–40] and in some investigations, also other educts were added, which

undergo reactions, such as water [14, 33, 35, 42], hydrogen [34], and starch [46]. Further, inert components are added to the feed, such as the noble gases helium or argon or the inert gas nitrogen [56–58], to avoid explosion limits, improve the discharge uniformity, or decrease the breakdown voltage.

In general, investigations of cold plasma reaction technology are challenging not only because it requires applying high voltage, but in particular because a plethora of different components are formed which need to be analyzed, both qualitatively and quantitatively. Moreover, as the very broad product spectrum strongly depends on the experimental conditions it is even more difficult to quantify or even only elucidate the products spectrum completely when varying electrical or process parameters. As a result, many studies have covered only few products and a narrow range of conditions. Thus, little is still known about the influence of electrical and process parameters on the methane and oxygen conversion and the selectivities to the product components of partial oxidation of methane in DBD cold plasma.

In the literature, the analysis of the product stream from cold plasma partial oxidation of methane (CH_4) with pure oxygen (O_2) usually focuses on synthesis gas products, i.e., hydrogen and carbon monoxide, as well as on a few oxygen-containing compounds, such as methanol or formaldehyde. The most comprehensive studies of cold plasma partial oxidation of CH_4 in terms of product analysis have been carried out by Larkin et al. [31], Chawdhury et al. [40], and Goujard et al. [49]. But even in these, quantitative data on products such as acetic acid, ethanol, and methyl formate are often only available for a single experiment. Astonishingly, one important product does not seem to have been analyzed quantitatively in the literature investigations so far: water.

Against this background, the fragmented data strongly hamper the development of mechanistic models of the process, so that, despite considerable efforts [10, 37, 40, 42–49, 51, 59–61], no commonly accepted model has emerged and a holistic understanding of the processes is still lacking. This is also a major drawback for assessing the technological potential of partial oxidation of methane in DBD cold plasma.

1.3 Goals of this Work

Most of the mentioned above studies were carried out with a focus on chemistry in the plasma and not with a focus on reaction engineering aspects. For this reason, the present work contributes to closing this gap and, thus, focus on the basic reaction system of the partial oxidation of CH_4 with pure O_2 in the presence of the inert gas argon (Ar). Moreover, the present work refers only to uncatalyzed partial oxidation of methane with pure oxygen in DBD cold plasma.

In the present work, a DBD cold plasma reactor is designed, set-up and used for studies on partial oxidation of CH_4 with O_2 with Ar as carrier gas. To overcome the challenge of a plethora of product components, the product stream from the reactor was split into a fraction that was condensed in a cold trap and the remaining gaseous fraction. The gaseous fraction of the product stream was analyzed at-line in a gas chromatograph (GC) with a thermal conductivity detector. The use of a double column and two different carrier gases allowed for the analysis of a variety of components, including: CH_4, O_2, Ar, carbon monoxide, carbon dioxide, ethane, ethene, and hydrogen. The fraction from the cold trap containing components such as alcohols, acids, water, and formaldehyde was analyzed offline. The main tool applied for the offline analysis was qualitative and quantitative nuclear magnetic resonance (NMR) spectroscopy, which was complemented by titration techniques (Karl Fischer titration for water and sodium sulfite titration for formaldehyde). The analytical procedures for the fraction from the cold trap were based on previous experience of our group with similar systems [62–67].

With this experimental and analytical set-up, a series of 43 experiments was conducted, in which the reactor was always operated at ambient pressure and near-ambient temperature in steady-state, while varying the electrical and process parameters. The process parameters were the reactant ratio CH_4:O_2 in the feed, the mole fraction of the inert carrier gas argon in the feed x_{Ar}^{in}, and the residence time τ in the reactive zone of the reactor. The electrical parameter was the electrical power P fed to the reactor. The latter two parameters, i.e., residence time τ and electrical power P, are typically combined and expressed with the parameter SEI in the literature. In this this work, a new parameter SEI^* is introduced which combines and

expresses the three parameters: the mole fraction of the inert carrier gas argon in the feed $x_{\mathrm{Ar}}^{\mathrm{in}}$, the residence time τ in the reactive zone of the reactor, and the electrical power P fed to the reactor.

By the means of the sophisticated product analysis and the wide range of parameters covered in the series of experiments, this work aims to complete the fragmented data available in literature. Finally, from this comprehensive data and following reaction kinetic modeling a holistic understanding of the processes can be derived to assess the technological potential of partial oxidation of methane in DBD cold plasma. The developments of such reaction kinetic models were, however, out of the scope of the present study and are left open for future work.

2 Materials and Methods

2.1 Chemicals

Table **1** provides information on the chemicals that were used in the experiments and analytical measurements. All chemicals were used without further purification. The feed of the DBD cold plasma reactor consisted of a mixture of CH_4, O_2, and Ar.

Table 1: Overview of the chemicals that were used in the experiments and analytical measurements.

Chemical	Supplier	Purity / g g^{-1}
Argon	Air Liquide	0.99999
Methane		0.99500
Oxygen		0.99998
Carbon dioxide		0.99995
Helium		0.99999
Hydrogen		0.99999
Nitrogen		0.99990
1,4-dioxane	Sigma-Aldrich	0.99900
Hydranal composite 5	Honeywell	-
Hydranal methanol dry		0.99990
Hydranal water standard 10.0		0.99000
Sodium sulfite		0.98000
Reference gas mixture [a]	Linde	0.99900

[a] 0.76 mol mol^{-1} carbon monoxide, 0.19 mol mol^{-1} ethane, 0.05 mol mol^{-1} ethene.

2.2 Experimental Set-up

2.2.1 Cold Plasma Reactor

The cold plasma reactor consists of an outer tube (outer diameter: 14 mm, width of the wall: 1 mm), in which an inner tube is mounted concentrically (outer diameter 6 mm, width of the wall: 1 mm). The entire reactor has a length of 350 mm. It is made from borosilicate glass and surrounded by a thermostatization jacket, through which water was circulated.

Figure 1 shows a technical drawing of the outer tube and the thermostatization jacket of the cold plasma reactor.

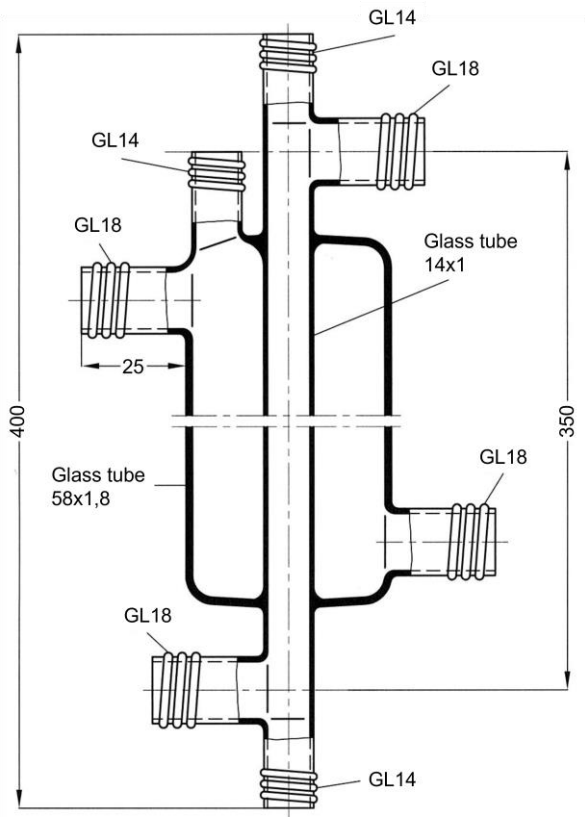

Figure 1: Technical drawing of the outer tube and the thermostatization jacket of the cold plasma reactor with dimensions in mm and size of the threads (indicated with the prefix GL).

The thermostatization jacket contained the ground electrode and the inner tube contained the high voltage high frequency electrode. The cold plasma is generated in the annular gap between the inner and outer glass tubes. The active volume of the reactor in the zone, where plasma can be generated, is about 26.3 cm^3.

2.2.2 Laboratory Scale Plant

Figure 2 shows the set-up of the cold plasma reactor and its feed gases, the connection of the electrodes to the electrical equipment, as well as the position of the pressure and the temperature measurement in the periphery.

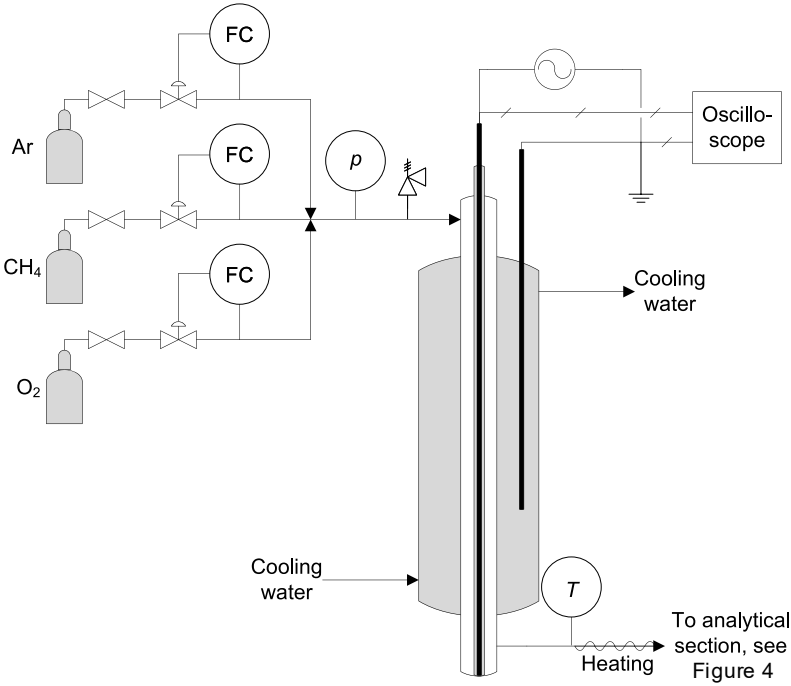

Figure 2: The DBD cold plasma reactor with mass flow controllers (FC) for argon (Ar), methane (CH_4), and oxygen (O_2), the connection of the electrodes to the electrical equipment, as well as the position of the pressure p and temperature T measurement in the periphery.

Both electrodes were made from 1.4571 stainless steel (X6CrNiMoTi17-12-2). They were connected to a high voltage generator from GBS Elektronik (MINIPULS Universal). The primary voltage supply of the MINIPULS Universal was adjustable

in a range from 0 to 60 V with a frequency from 0.5 to 50 kHz. The output signal of the generator is a sinusoidal, high frequency high voltage and the maximal effective output power is 700 W (averaged over the cycle). The effective electrical power P fed to the reactor is calculated from Equation (1)

$$P = \frac{1}{\bar{t}} \int_{t=0}^{\bar{t}} u(t)\, i(t)\, \mathrm{d}t \tag{1}$$

where i is the instantaneous current, u the instantaneous voltage, t the time, and $\bar{t}$ the time of one period. Figure 3 shows an oscillogram of the instantaneous current i, the instantaneous voltage u, and the calculated instantaneous electrical power p_{el} with a) no plasma and b) plasma generated.

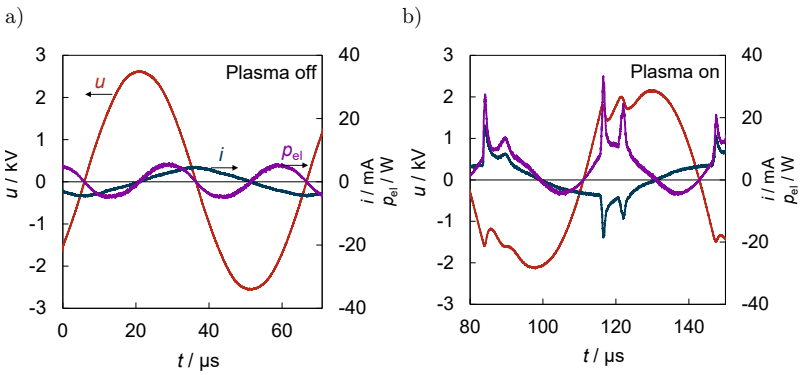

Figure 3: Oscillograms of the measured variables instantaneous current i and the instantaneous voltage u plotted with the calculated instantaneous electrical power p_{el} with a) no plasma and b) plasma generated in the cold plasma reactor.

The calculation of the electrical power P fed to the reactor by Equation (1) yields results which are equivalent to those from the Lissajous method and was recommended for plasma applications by Holub [68]. The instantaneous current i between the electrodes was measured with a current probe from Pearson Electronics

(Model 6585). Both signals, u and i, were recorded as a function of time with a digital storage oscilloscope from Tektronix (TBS2104) with a sample interval of $8 \cdot 10^{-9}$ s.

The three feed gases, i.e., CH_4, O_2, and Ar, were supplied from high-pressure cylinders equipped with pressure-reducing valves, which were set to pressures slightly above 1 bar. For monitoring and safety purposes, a pressure gauge (WIKA P-30) and a pressure relief valve were installed in the feed line of the plasma reactor. An electrical heating tape was installed around the line at the outlet of the reactor, as condensation was detected there. The product stream exiting the cold plasma reactor is connected to the analytical system of the laboratory scale plant. Figure 4 shows the set-up of the analytical system.

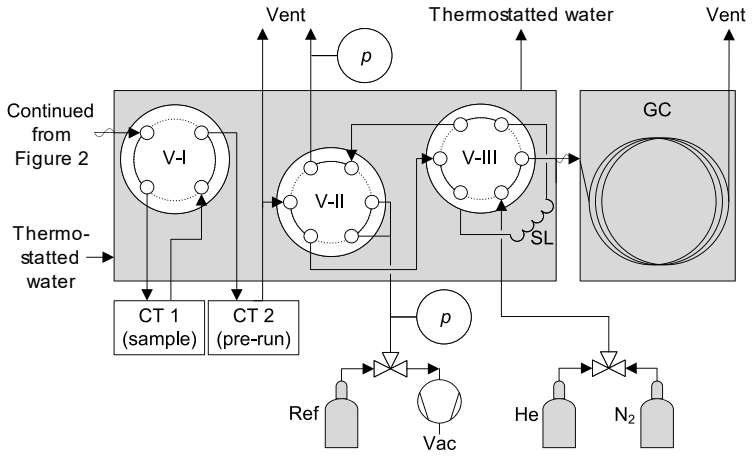

Figure 4: Analytical system consisting of a temperature-controlled sampling unit with three multi-way valves, V-I to V-III. The valves provide connections to two cold traps (CT) and to a sample loop (SL) for the gas chromatographic analysis (GC). The sample loop can also be evacuated (Vac) or filled with an external reference gas (Ref). The GC can be operated with two carrier gases, helium (He) and nitrogen (N_2).

For analytical purposes, two pressure gauges (WIKA P-30 and MKS 690A13TRA) were installed in the analytical system. The uncertainty of the pressure measurement

is 0.5 mbar for all gauges. The readings of the WIKA instrument were recorded with the WIKA Easy-Com 2011 software and noted manually for the MKS instrument. The flow rates of the three gases were controlled individually by three mass flow controllers from Bronkhorst (EL-FLOW Prestige). Additionally, the mass flow controllers measured and recorded the inlet temperature of the feed gases. The relative uncertainty of the mass flow measurement including the uncertainty of the temperature was 0.4% according to the manufacturer. The outlet temperature of the product stream was measured with a resistance thermometer from Temperatur Messelemente Hettstedt GmbH (Pt100). The readings of the thermometer and the Bronkhorst instruments were recorded using LabVIEW 2013. The inlet and outlet temperatures were averaged over the duration of each experiment. The measurement uncertainty of these average values is specified including the standard deviation of the temperature fluctuations over the course of the experimental duration. The uncertainty of the average temperature at the reactor inlet is 1 K. Since the outlet temperature was additionally influenced by the following heating, the uncertainty of its mean value is 2 K. The cooling water for the thermostatization jacket was taken from a central supply line with an inlet temperature of about 291 K. The part of the analytical system containing the three multi-port valves and the sample loop (cf. Figure 4), was thermostatted to 313 K using a thermostat from Julabo (model F25) with water as medium.

The residence time τ was calculated from Equation (2)

$$\tau = \frac{V}{\dot{V}^{\mathrm{in}}} \tag{2}$$

where V is the active reactor volume and $\dot{V}^{\mathrm{in}}$ is the volumetric feed flow rate. The volumetric feed flow rate $\dot{V}^{\mathrm{in}}$ was calculated from the mass flow rates of the three feed gases and the results for the feed temperature and pressure using the ideal gas law.

In the analytical system, the product stream was split by means of a cold trap into a condensable fraction for offline analysis and into the remaining gaseous fraction that was analyzed at-line. Furthermore, the analytical system was equipped such that it can be evacuated, purged, and connected to a calibration gas supply. To achieve this, several valves were installed as shown in Figure 4. V-I was a 4-way, 2-position valve

from Swagelok (SS-45YF4); V-II and V-III were 6-way, 2-position valves from VICI (DC6WE). There are two cold traps (CT). The first cold trap CT 1 was used for the sampling of the condensable fraction and the second cold trap CT 2 was used during the preparations of the experiments (pre-run mode). The cold traps were made of glass and were operated at 195 K with a mixture of solid carbon dioxide and isopropanol. The valve position depicted in Figure 4 is the one in which the condensable fraction is collected in cold trap CT 1 and the gaseous fraction is led to the gas chromatograph (GC) for analysis. The position of the multi-port valves in the modes pre-run, sampling, and calibration is shown in the Appendix A.1.

2.3 Experimental Procedure

For the start-up of the plant, V-I was switched to the pre-run mode, so that the product stream only passed the cold trap CT 2. The primary voltage was set to a target value and subsequently, the frequency was reduced beginning from its maximum value until cold plasma was present in the reactor. During this start-up, the cold plasma was not homogeneous, but lightning-type fluctuating luminous effects were observed, accompanied occasionally by a loud sizzling noise. Once homogeneous plasma was obtained and the noise stopped, the electrical parameters were kept constant; then, a steady-state in the reactor was reached, which took only a few minutes. V-I was then switched to sampling mode and the product stream was led to cold trap CT 1. The remaining gaseous fraction from the outlet of CT 1 was first led through CT 2 and then split up. A part was released, the other part was led to the sampling valve V-III, which was equipped with a 100 µl sample loop. By switching V-III, samples from the sample loop were injected to the GC. This procedure was repeated several times during one steady-state run. V-II was installed to switch between the experiment and calibration.

The duration of the runtime in steady-state was chosen such that enough liquid sample was accumulated for analysis (about 3 ml) and so that at least six measurements in the GC were carried out, i.e., three for each carrier gas. On average, the duration of a single experiment was five hours. Figure 5 shows two photographs of the cold plasma reactor during operation in daylight and in dimmed light in the laboratory.

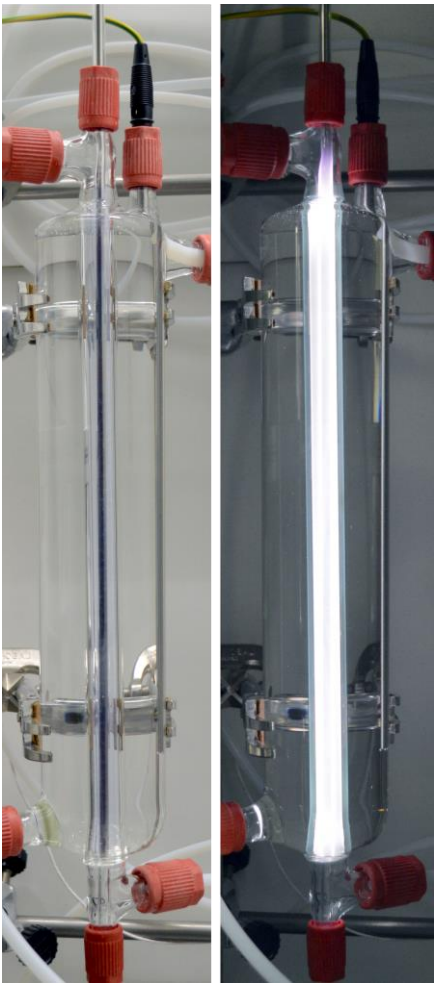

Figure 5: Photographs of the cold plasma reactor during operation (left: daylight, right: dimmed light in laboratory).

The electrical power input P is calculated from Equation (1) and is varied by adjusting the time of one period, i.e., the frequency and the primary voltage fed to the plasma generator. The volumetric feed flow rate $\dot{V}^{\text{in}}$ is directly proportional to the residence

time τ, cf. Equation (2), and is varied by adjusting the mass flow controllers of the three feed gases.

2.4 Analysis of the Product Stream

2.4.1 Overview

At the end of the experiment the cold trap CT 1 was sealed, and the trapped solid material was allowed to melt overnight. The mass of the sample of the condensable fraction in the cold trap was determined by means of differential weighing of the cold trap CT 1 before and after the experiment using a balance from Mettler Toledo (PR1203, accuracy 1 mg). The sample of the condensable fraction was analyzed with NMR spectroscopy and wet-chemistry methods, which provided the mass fractions of the different components. The obtained mass fractions in the sample of the condensable fraction, the total mass of the sample from differential weighing, and the sampling time were used to calculate the molar component flows of the analyzed components in the condensable fraction. Further, the gaseous fraction of the product stream was analyzed with GC, which provided the mole fractions of the different components. The obtained mole fractions and the known molar flow of Ar were then used to calculate the molar component flows of the components in the gaseous fraction. Table 2 lists all components analyzed in the product stream. There, each component is provided with an abbreviation, which will be used hereafter for the sake of clarity.

Table 2: Overview on quantified components in the condensable or gaseous fraction of the product stream and the corresponding analysis methods.

Component	Abbreviation	Fraction	Analysis method
Feed			
Argon	Ar	Gaseous	GC
Methane	CH_4		
Oxygen	O_2		
Products without carbon			
Hydrogen	H_2	Gaseous	GC
Water	H_2O	Condensable	Karl Fischer titration
Products without hydrogen			
Carbon monoxide	CO	Gaseous	GC
Carbon dioxide	CO_2		
	$CO_{2,condensable}$	Condensable	NMR
Products without oxygen			
Ethane	C_2H_6	Gaseous	GC
Ethene	C_2H_4		
Products that contain one carbon and hydrogen and oxygen			
Formaldehyde	FA	Condensable	Sodium sulfite titration
Formic acid	FAc		NMR
Methanol	MeOH		
Methyl hydroperoxide	MeOOH		
Products that contain more than one carbon and hydrogen and oxygen			
Acetone	Ace	Condensable	NMR
Acetic acid	HAc		
Ethanol	EtOH		
Ethylene glycol	EG		
Methyl acetate	MeAc		
Methyl formate	MeFo		

The condensable fraction contains product components that are reactive at ambient conditions also when they are not exposed to cold plasma. Here, only the classes of reactions are mentioned that have consequences for the present work: with H_2O, FA reacts to methylene glycol (MG) and with alcohols, FA reacts to hemiformals [67]. In the case of MeOH as alcohol, the reaction product is hemiformal (HF) and in case of MeOOH as alcohol, the reaction product is hemiformal hydroperoxide (HFO). The reactions of FA that are relevant for the present work are:

$$\mathrm{FA} + \mathrm{H_2O} \rightleftharpoons \mathrm{MG} \tag{I}$$

$$\mathrm{FA} + \mathrm{MeOH} \rightleftharpoons \mathrm{HF} \tag{II}$$

$$\mathrm{FA} + \mathrm{MeOOH} \rightleftharpoons \mathrm{HFO} \tag{III}$$

Hemiformals and methylene glycols can react further with FA yielding oligomers (in the case of MeOH as alcohol, these are polyoxymethylene glycols and polyoxymethylene hemiformals). The titration methods used in the present work break up the reaction products, yielding what is referred here to overall concentrations of FA and H_2O. It makes no sense to state the quantitative amount of MG, HF, and HFO individually in the condensable fraction as the species distribution in formaldehyde containing mixtures changes completely upon condensation. In particular, it is known that most of the FA is present as the monomer in the gas phase, whereas in the liquid phase, the concentration of monomeric FA is very low [62, 64, 65, 69–71] – so low that it could not be detected here. Hence, the Reactions (I) – (III) are neglected and instead the overall concentrations that are obtained from the sodium sulfite titration for FA and from the Karl Fischer titration for H_2O are directly reported. Similar to Reactions (I) – (III), reactions also occur with other aldehydes [72, 73], but reaction products of acetaldehyde with H_2O or alcohols were not found in the present work. However, it should be noted, that acetaldehyde has been detected in the condensate of cold plasma oxidation of CH_4 in the literature by Larkin et al. [31, 32] and Goujard et al. [49].

In contrast to the titration methods used in this work, the quantitative NMR analysis yields true concentrations, i.e., also information on the reaction products into reactants. From NMR spectroscopy, the reaction products HF and HFO were only quantified to account for their amount in the overall amount of MeOH and MeOOH. Formaldehyde oligomers were only detected in very small amounts in the present work and thus not quantified.

Regarding the other products, the following is to be noted: interestingly, CO_2 was only found in its molecular form and not as bicarbonate, as it might have been expected since the samples contain water. The reason is that the sample contains many acids, which leads to low pH values (about pH 2), which, in turn, favors the presence of monomeric CO_2. Furthermore, alcohols and acids can undergo esterification reactions [57–61]. The compounds involved in the esterification reactions could also have been formed in the gas phase. Therefore, esters were accounted for explicitly. The two esters that were quantified are MeAc and MeFo.

Although H_2O has been reported as a product of the partial oxidation of CH_4 with O_2, it appears that the present work is the first to have quantified its amount. In the literature, the selectivity to H_2O is calculated – if at all – only from mass balance. MeOOH has been quantified for only one experiment by Goujard et al. [49] so far, who used ^{1}H NMR spectroscopy. Further, in the present work, MeAc and EG have been detected and quantified in the sample of the condensable fraction. The occurrence of neither of the components has been reported previously, not even qualitatively. Finally, it was possible to identify and quantify additional components as products in the sample of the condensable fraction, namely MeFo, HAc, EtOH, and Ace. Even though these products of cold plasma oxidation of CH_4 with O_2 have been reported previously (MeFo [26, 31, 32, 43], HAc [40], EtOH [40, 47], Ace [40]), little quantitative data were available.

2.4.2 Wet-chemistry

The mass fraction of H_2O in the sample of the condensable fraction was measured with the Karl Fischer titration method [74]. The mass fraction of FA in the sample of the condensable fraction was measured with the sodium sulfite titration method with hydrochloric acid as titer [75]. Both wet-chemistry methods used in the present

work directly provide the overall mass fractions [62, 64, 66, 75–78]. The uncertainties of the quantitative results from wet-chemistry are 0.01 g g^{-1} for the mass fraction of H_2O and 0.02 g g^{-1} for the mass fraction of FA. They were specified from the average deviation from repeated measurements including the weighing error.

2.4.3 NMR Spectroscopy

2.4.3.1 Sample Preparation

As the total number of moles in the sample of the condensable fraction was unknown, an internal standard, 1,4-dioxane (Diox), was used for calibration. The amount of Diox added to the sample was chosen so that the mass fraction of Diox in the resulting mixture was about 0.05 g g^{-1}. An analytical balance from Mettler Toledo (AG204 Delta Range, accuracy 0.1 mg) was used for preparation. Then, the sample was transferred to a 5 mm NMR tube and analyzed in a 400 MHz NMR spectrometer from Bruker (magnet: Ascend 400, console: Avance 3 HD 400, Double Resonance Broad Band Probe).

2.4.3.2 Qualitative NMR Spectroscopy

For the qualitative evaluation, a structure elucidation was carried out by combining information, such as the chemical shift and multiplicity of peaks, from one- and two-dimensional NMR techniques. In total, six types of NMR spectra were recorded:

- ^{1}H,
- ^{13}C inverse-gated ^{1}H-decoupled (hereafter referred to as ^{13}C),
- ^{13}C Distortionless Enhancement by Polarization Transfer (DEPT-135),
- ^{13}C without ^{1}H decoupling,
- ^{1}H,^{13}C Heteronuclear Single Quantum Coherence (HSQC), and
- ^{1}H,^{13}C Heteronuclear Multiple Bond Correlation (HMBC).

Figure 6 and Figure 7 show the ^{1}H and ^{13}C NMR spectra of the sample of the condensable fraction gathered in one exemplary experiment (experiment 15, see Appendix G, Table G.3).

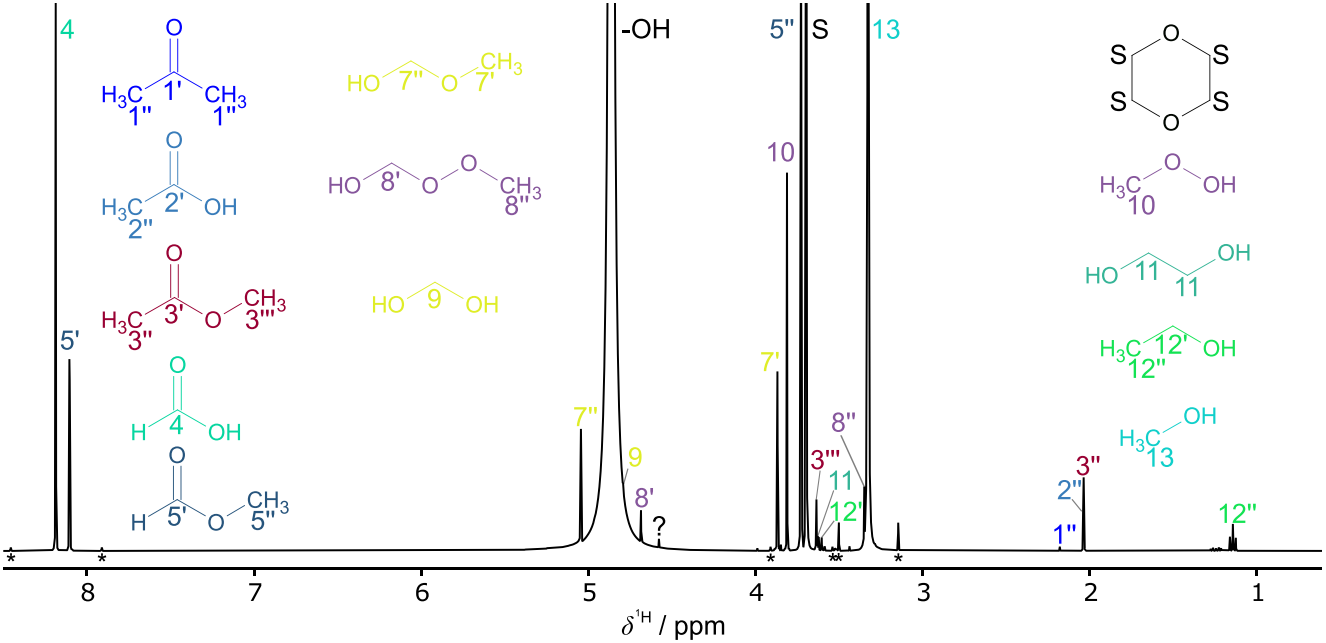

Figure 6: ^{1}H NMR spectrum of the sample of the condensable fraction of experiment 15. The full intensities of some peaks are truncated for better visibility.

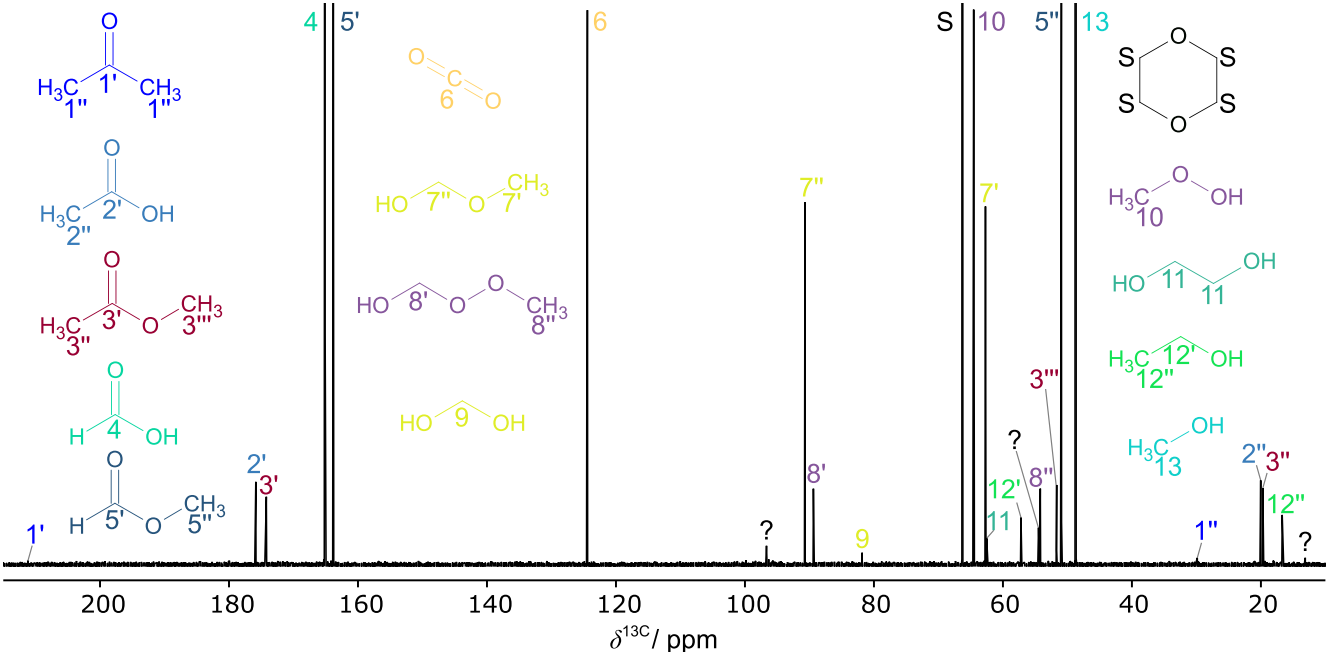

Figure 7: ^{13}C NMR spectrum of the sample of the condensable fraction of experiment 15. The full intensities of some peaks are truncated for better visibility.

For some peaks in the ^{1}H NMR spectrum, cf. Figure 6, also the ^{13}C satellites are visible, which are labeled with an asterisk (*) below the baseline. In Figure 6 and Figure 7, peaks labeled with a question mark (?) have not been assigned. Table 3 gives an overview of all assigned components and the corresponding peak labels.

Table 3: Peak assignment in the ^{1}H and ^{13}C NMR spectra obtained from the analysis of the sample of the condensable fraction and the chemical shifts in ^{1}H and ^{13}C spectrum (δ^{1H} and δ^{13C}). The bold and underlined font indicates the functional group of the chemical formula corresponding to the peak. The values of the shifts are those for the sample of the condensable fraction of experiment 15.

Label	Component	Chemical formula	δ^{1H} / ppm	δ^{13C} / ppm
1'	Ace	$(CH_3)_2\underline{\mathbf{C}}O$		211.17
2'	HAc	$CH_3\underline{\mathbf{C}}OOH$		175.85
3'	MeAc	$CH_3\underline{\mathbf{C}}OOCH_3$		174.20
4	FAc	$\underline{\mathbf{HC}}OOH$	8.19	165.10
5'	MeFo	$\underline{\mathbf{HC}}OOCH_3$	8.10	163.82
6	$CO_{2,liq}$	$\underline{\mathbf{C}}O_2$		124.43
7''	HF	$HO(\underline{\mathbf{CH_2}}O)CH_3$	5.04	90.70
8'	HFO	$HO(\underline{\mathbf{CH_2}}O)OCH_3$	4.68	89.38
9	MG	$HO(\underline{\mathbf{CH_2}}O)H$	4.79	81.85
S	Internal standard Diox	$C_4H_8O_2$	3.70	66.30
10	MeOOH	$\underline{\mathbf{CH_3}}OOH$	3.81	64.54
7'	HF	$HO(CH_2O)\underline{\mathbf{CH_3}}$	3.87	62.70
11	EG	$HO(\mathbf{CH_2})_2OH$	3.63	62.52
12'	EtOH	$CH_3\underline{\mathbf{CH_2}}OH$	3.61	57.20
8''	HFO	$HO(CH_2O)O\underline{\mathbf{CH_3}}$	3.35	54.20
3'''	MeAc	$CH_3COO\underline{\mathbf{CH_3}}$	3.64	51.67
5''	MeFo	$HCOO\underline{\mathbf{CH_3}}$	3.73	50.93
13	MeOH	CH_3OH	3.33	48.72
1''	Ace	$(\mathbf{CH_3})_2CO$	2.18	29.86
2''	HAc	$\underline{\mathbf{CH_3}}COOH$	2.04	20.05
3''	MeAc	$\underline{\mathbf{CH_3}}COOCH_3$	2.04	19.70
12''	EtOH	$\underline{\mathbf{CH_3}}CH_2OH$	1.14	16.70
-OH	H_2O, hydroxyl groups	H_2O, -OH	4.86	

The remaining four types of acquired NMR spectra, i.e., ^{13}C without ^{1}H-decoupling; ^{13}C DEPT-135; ^{1}H,^{13}C HSQC; and ^{1}H,^{13}C HMBC as well as further details on the structure elucidation are presented in Appendix B.3. Also, ^{1}H and ^{13}C NMR spectra of the sample of the condensable fraction from two additional experiments are provided there (i.e., experiments 3 and 43, see Appendix G, Table G.3). From the structure elucidation, 14 individual components were assigned. Among them, MG, HF, and HFO stem from the reactions of FA with H_2O, MeOH, and MeOOH (cf. Section 2.4). For more information on NMR spectroscopic analysis of formaldehyde-containing samples, see [62, 63, 66, 69, 79]).

2.4.3.3 Quantitative NMR Spectroscopy

For the quantitative evaluation, ^{1}H and ^{13}C NMR spectra were acquired at 303 K. The phase and baseline corrections were performed using automatic routines from MestReNova (version 14.2.2). The full set of acquisition and processing parameters is listed in Appendix B.3, Table B.2. The mass fractions of the components in the NMR sample were determined according to Equation (3)

$$x_i^{(\mathrm{m}),\mathrm{NMR}} = \zeta_i \, x_{\mathrm{Diox}}^{(\mathrm{m}),\mathrm{NMR}} \frac{M_i}{M_{\mathrm{Diox}}} \tag{3}$$

where ζ_i is the molar ratio of component i to the internal standard and M_i is the molar mass of component i. The molar ratio ζ_i was calculated from the peak areas A_i^{NMR} accounting for the corresponding number of atoms N_i as indicated in Equation (4).

$$\zeta_i = \frac{A_i^{\mathrm{NMR}}}{A_{\mathrm{Diox}}^{\mathrm{NMR}}} \frac{N_{\mathrm{Diox}}}{N_i} \tag{4}$$

The peak areas A_i^{NMR} were determined for peaks that were available for direct integration, i.e., where no overlapping with other peaks occurred. In general, peaks in

the ^{1}H NMR spectra show more overlap than peaks in the ^{13}C NMR spectra due to coupling effects and relatively high exchange rate of H atoms in contrast to C atoms. The latter is especially valid for those peaks of the hydroxyl (-OH) groups. Hence, most of the components were quantified with ^{13}C NMR spectroscopy only, which was possible as quantitative NMR measurement techniques were used.

For components for which more than one peak was available for direct integration, both peaks were used, and the obtained molar ratios were averaged. In Equations (3) – (4), i refers to either of the components Ace, $CO_{2,liq}$, EG, EtOH, FAc, HAc, MeOH (incl. HF), MeOOH (incl. HFO), MeAc, and MeFo. The uncertainties of the mass fractions of the components obtained from quantitative NMR results are derived from the deviations between the results from ^{1}H and ^{13}C NMR spectra including the weighing error and are 0.01 g g^{-1}.

2.4.4 Gas Chromatography

The gaseous fraction of the product stream was analyzed at-line in a GC equipped with a thermal conductivity detector and a dual column from Agilent (GC: Series 6890, column: CP7430 comprised of PoraBOND Q and Molsieve 5 Å). Two different carrier gases, helium (He) and nitrogen (N_2), were used in all experiments, except for the experiments 2 – 5 and 8 – 10 (see Appendix G, Table G.3), as only He was available. The two carrier gases were applied subsequently. In the GC analysis, five products: CO, CO_2, C_2H_6, C_2H_4, and H_2, as well as the educts CH_4 and O_2, and the inert gas Ar were quantified. The assignment of retention times was done using reference components. In some experiments, a slight elevation of the baseline was detected in the chromatogram, which is probably caused by traces of the highly reactive ozone. This was verified by operating the DBD cold plasma reactor with only O_2 and Ar, which led to the same baseline elevation. It can be assumed that ozone damages and reacts with the stationary phase of the column and, thus, does not elute giving a well-defined retention time but rather a broad baseline elevation.

For the quantitative evaluation, a calibration using reference gases was carried out in which the calibration factors k_i were determined by linear regression of known pairs of partial pressure p_i and area A_i^{GC} in the chromatogram. The accuracy of the GC analysis depends strongly on the uncertainty of the calibration factor. Where more

than one signal was obtained for the same component for both carrier gases, the one with the higher calibration accuracy was used.

The areas from the chromatograms and determined calibration factors k_i are used to calculate the partial pressure p_i of the components in the gaseous fraction of the product stream as in Equation (5).

$$p_i = k_i A_i^{GC} \tag{5}$$

In Equation (5), i refers to either of the components Ar, CH_4, O_2, CO_2, CO, H_2, C_2H_6, and C_2H_4. Each time V-III was switched to injection mode, the in-line pressure p (cf. analytical system in Figure 3) was recorded. Assuming a mixture of ideal gases, the mole fractions x_i in the gaseous fraction of the product stream can be calculated according to Equation (6)

$$x_i = \frac{p_i}{p} \tag{6}$$

where p_i refers to the partial pressure of either of the components Ar, CH_4, O_2, CO_2, CO, H_2, C_2H_6, and C_2H_4. For each experiment, at least three chromatograms were recorded for each carrier gas during the steady-state operation. The resulting values for the mole fractions were then averaged for each component. The only exception is the noble gas Ar, which is quantified as it is not converted in the cold plasma reactions and for which the solubility in the CT sample is neglected. Hence, Ar was used as an internal reference gas with a known molar flow, allowing for the calculation of the total molar flow of the gaseous fraction of the product stream. Two typical chromatograms – one for each carrier gas – with the retention times and information on GC acquisition parameters as well as the calibration factors and individual standard uncertainties are compiled in Appendix B.4.

2.5 Conversions and Selectivities

The conversion X_j of the reactants j is defined by Equation (7)

$$X_j = \frac{\dot{n}_j^{\text{in}} - \dot{n}_j^{\text{out}}}{\dot{n}_j^{\text{in}}} \tag{7}$$

where j is either CH_4 or O_2 and $\dot{n}_j^{\text{in}}$ is the molar flow of reactant j at the inlet and $\dot{n}_j^{\text{out}}$ is the corresponding number at the outlet of the reactor.

Two types of selectivities are reported here: one refers to hydrogen (referred to as H-selectivity $S_{i,\text{H}}$) and one refers to carbon (referred to as C-selectivity $S_{i,\text{C}}$). The H-selectivity was used for the two products without carbon, i.e., H_2O and H_2. The C-selectivity was used for all products that contain carbon and can be understood as a measure of the route that the carbon from the methane takes. The selectivities are defined in Equations (8) and (9)

$$S_{i,\text{H}} = \frac{\dot{n}_i^{\text{out}}}{\dot{n}_{\text{CH}_4}^{\text{in}} - \dot{n}_{\text{CH}_4}^{\text{out}}} \frac{4}{\nu_{i,\text{H}}} \tag{8}$$

$$S_{i,\text{C}} = \frac{\dot{n}_i^{\text{out}}}{\dot{n}_{\text{CH}_4}^{\text{in}} - \dot{n}_{\text{CH}_4}^{\text{out}}} \frac{1}{\nu_{i,\text{C}}} \tag{9}$$

where $\dot{n}_i^{\text{out}}$ refers to the molar flow of the product component i at the outlet of the reactor, $\nu_{i,\text{H}}$ is the number of H atoms in component i, and $\nu_{i,\text{C}}$ is the number of C atoms in component i.

2.6 Specific Energy Input

The specific energy input *SEI* supplied to the DBD cold plasma reactor is broadly used in the literature for describing the combined influence of the electrical power input P and the volumetric feed flow rate $\dot{V}^{in}$, as given by Equation (10).

$$SEI = \frac{P}{\dot{V}^{in}} \tag{10}$$

In the present work, a variant of the specific energy input *SEI* is introduced, in the following referred to as *SEI**, in which the electrical power input P is divided not by the total volumetric feed flow rate $\dot{V}^{in}$, but only by that of the reactants (here: CH_4 and O_2), disregarding the inert components (here: Ar). The *SEI** is defined in Equation (11)

$$SEI^* = \frac{P}{\dot{V}^{in}_{CH_4} + \dot{V}^{in}_{O_2}} \tag{11}$$

As a result, the specific energy input *SEI** accounts not only for the influence of the residence time τ and the electrical power input P, but also for the mole fraction of the inert carrier gas in the feed as the volumetric feed flow rates of the reactants change at constant residence time when varying the mole fraction of argon in the feed. To the best of our knowledge, *SEI** has not been used in any other study.

3 Results and Discussion

3.1 Overview of Experiments

The experiments were conducted with three different molar reactant ratios CH_4:O_2 in the feed of 2:1, 3:1, and 4:1 (in the following simply CH_4:O_2 ratio for brevity) and with two different mole fractions of argon in the feed x_{Ar}^{in} of 0.19 and 0.75 mol mol^{-1}, resulting in feed compositions that were all above the upper explosion limit, see Appendix A.2. In the experiments of the present work, the residence time τ and the primary voltage were varied and were in the range of 0.4 to 4.7 s and 12 to 59 V, respectively. For all experiments, the necessary frequency to ignite the DBD cold plasma was in a range from 10 to 16 kHz. Finally, the resulting electrical power input P and the specific energy input SEI^* were in a range from 14 to 153 W and from 0.9 to 23.8 J cm^{-3}, respectively. Table 4 gives an overview of the range of the process parameters that was covered in the experiments of the present work.

Table 4: Overview of the process parameter ranges covered in the experiments of the present work. A detailed list of the individual experiments is given in the Appendix G, Table G.3.

CH_4:O_2	x_{Ar}^{in}	τ	P	SEI^*	Number of
mol mol^{-1}	mol mol^{-1}	s	W	J cm^{-3}	experiments
2:1	0.19	0.4 to 1.6	23 to 153	0.9 to 8.0	6
	0.75	0.5 to 4.7	16 to 33	1.4 to 23.8	23
3:1	0.19	0.8 to 1.6	24 to 133	1.8 to 7.9	5
	0.75	3.5	16 to 43	8.3 to 22.9	4
4:1	0.75	0.9 to 2.8	14 to 36	2.7 to 14.4	5

The covered range of parameters is the widest in which a stable operation of the present DBD cold plasma reactor was possible. A detailed list of all 43 experiments and their results is given in the Appendix G, Table G.3.

The electrical energy required to produce one mole of product was in a range from 0.3 to 1.0 kWh mol^{-1} and was calculated from the power input, the residence time, and the product molar flow. The products are defined hereby as all components, excluding the non-converted reactants as well as H_2O and CO_2.

The H-selectivities shown in the present work do not sum up to 1 mol mol^{-1} as only H_2O and H_2 are shown and the difference from 1 mol mol^{-1} is basically a measure for the hydrogen bound in the products that contain carbon. In contrast, as the elemental balance for carbon is closed within the uncertainty of measurement, the C-selectivities were normalized and sum up to 1 mol mol^{-1}.

3.2 Influence of the Mole Fraction of Argon

The results from experiments with an argon mole fraction in the feed x_{Ar}^{in} of 0.19 and 0.75 mol mol^{-1} were plotted against *SEI* and *SEI**, cf. Equations (10) and (11), and the data sets were compared to each other. The comparison led to the finding that the resulting trends in conversions and selectivities showed no significant difference

when plotted against *SEI**. This justifies the use of the newly introduced *SEI** rather than the use of the *SEI*, commonly used in the literature. An example that illustrates this finding is given in Figure 8, which shows results for the conversion of O_2, X_{O_2}, plotted against a) *SEI* and b) *SEI**, respectively. The plots in Figure 8 also include linear fits to the data at partial conversion of O_2.

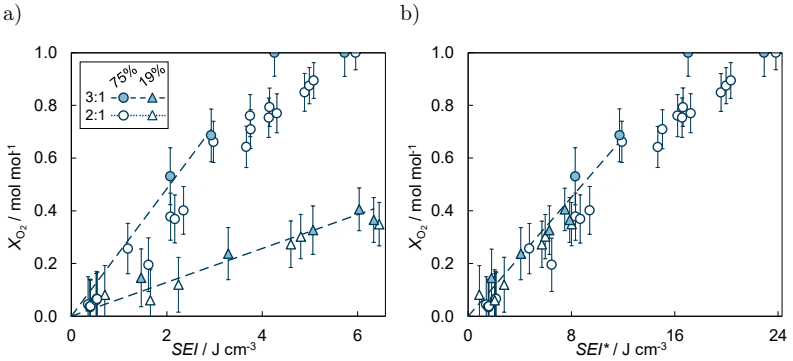

Figure 8: Conversion of O_2 plotted against a) *SEI* and b) *SEI** at CH_4:O_2 ratios of 2:1 (open symbols, dotted line), 3:1 (light filled symbols, dashed line), and at argon mole fractions x_{Ar}^{in} of 0.75 (circles) and 0.19 mol mol^{-1} (triangles). The lines were obtained from a linear fit to the data in the region below full conversion of oxygen through the origin as a guide to the eye.

When plotted against *SEI*, cf. Figure 8 panel a), the results for the conversion of O_2 at constant CH_4:O_2 ratio deviate strongly for the two different argon mole fractions (circles and triangles). This is observed for both CH_4:O_2 ratios of 2:1 and 3:1 (open and light filled symbols). When plotted against *SEI**, cf. Figure 8 panel b), the differences between the results for the two argon mole fractions vanish. Hence, the presence of argon does not have an influence on the conversions when plotted against *SEI**. It is remarkable that the influence of the process parameters residence time τ, electrical power input P, and argon mole fraction x_{Ar}^{in} on the results can be represented by a single variable, the *SEI**. This holds not only for the conversion of O_2 shown in Figure 2, but also for the conversion of CH_4 and for all selectivities. For

comparison, all individual results plotted against the *SEI* are presented in Appendix C and individual results plotted against the *SEI** are presented in Appendix D.

This finding is in line with previous reports from the literature: Bhatnagar and Mallison [32] found no discontinuity in the results with and without helium in the feed and also Aghamir [11] reported that the inclusion of helium in the feed changes neither product selectivity nor the conversion rate. Zhou et al. [31] stated that their feed gas component nitrogen was not converted and that dependencies of reactant conversions and methanol production on parameter variation were quite similar in mixtures with and without nitrogen in the feed.

3.3 Lumping of the Data

To reduce the scattering of the data and facilitate the identification of trends from corresponding plots, results from experiments with approximately the same *SEI** (interval width 2 J cm^{-3}) were used to obtain a single averaged value for the data points of the conversions, H-selectivities, and C-selectivities. Hence, all results presented in Section 3.4 to Section 3.5 are lumped results from the individual experiments and the lumped value is plotted together with its standard deviation. In case of only a single value in the interval, the error bar was obtained from the average of the standard deviations of all other intervals. The full set of numerical results is given in Appendix G.

3.4 Conversions

Figure 9 shows the conversion X_j of the reactants CH_4 and O_2 at three different CH_4:O_2 ratios plotted against the *SEI**.

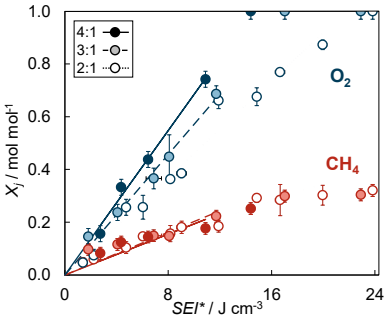

Figure 9: Conversions of CH_4 and O_2 at CH_4:O_2 ratios of 2:1 (open symbols, dotted line), 3:1 (light filled symbols, dashed line), and 4:1 (dark filled symbols, solid line). The lines were obtained from a linear fit to the data in the region below full conversion of oxygen through the origin as a guide to the eye.

The conversion of O_2 increases linearly with increasing *SEI** until full conversion is reached. The slope depends on the CH_4:O_2 ratio and is steeper the higher the excess of CH_4 over O_2 is. Consequently, full conversion is reached earlier for higher CH_4:O_2 ratios. Also the conversion of CH_4 increases linearly, as long as there is O_2 left. Interestingly, the slope of the conversion of CH_4 does not depend significantly on the CH_4:O_2 ratio. As expected, the conversion of CH_4 cannot increase further if O_2 is fully converted. The *SEI** for which full conversion of O_2 is reached (SEI^*_{FC,O_2}) is shown as a function of the CH_4:O_2 ratio in Figure 10. The values for SEI^*_{FC,O_2} were obtained from the linear fits to the data for the conversion of O_2 shown in Figure 9. Statistical uncertainties shown as error bars were obtained from the uncertainties of the linear fits.

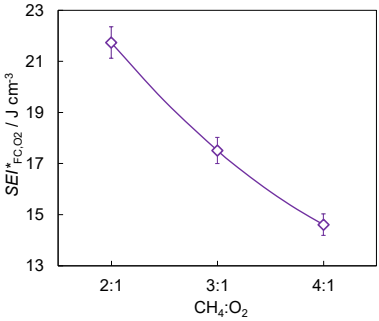

Figure 10: *SEI** for which full conversion of oxygen is reached (SEI^*_{FC,O_2}) as a function of the CH_4:O_2 ratio. The line is a guide to the eye.

Figure 10 illustrates that the dependency of SEI^*_{FC,O_2} on the CH_4:O_2 ratio is close to linear. With decreasing excess of CH_4 it becomes more difficult to reach full conversion.

3.5 Selectivities

For the discussion of the selectivities to the various reaction products, the results are grouped according to the product component groups as introduced in Table 2 in Section 2.4.1:

- H-selectivity to products without carbon (H_2O and H_2),
- C-selectivity to products without hydrogen (CO and CO_2),
- C-selectivity to products without oxygen (C_2H_6 and C_2H_4),
- C-selectivity to products with one carbon atom and hydrogen and oxygen (MeOH, MeOOH, FA, and FAc), and
- C-selectivity to products with more than one carbon atom and hydrogen and oxygen (MeFo, HAc, MeAc, EtOH, Ace, and EG).

Elemental balances were checked for all 43 experiments and for all three elements, i.e., carbon, hydrogen, and oxygen. The results are presented in the Supporting Information. The elemental balances are closed within 10% in most of the cases, except for experiments at low molar flow rates of the elements, for which higher deviations were observed for hydrogen and oxygen.

In all cases, the influence of the CH_4:O_2 ratio as well as that of the *SEI** are discussed. For that purpose, the results for the selectivity are plotted as a function of the *SEI** for the different CH_4:O_2 ratios. As in the previous figures, also linear fits to the data at partial conversion of O_2 are shown; however, they are meant rather as a guide to the eye than for claiming that the relation is actually linear. The influence of the *SEI** on the selectivities is difficult to predict, even only qualitatively (will an increase of the *SEI** yield more or less of a given component?). It could be assumed that predicting the influence of the CH_4:O_2 ratio on the selectivity, at least qualitatively, is an easier task. Changing the CH_4:O_2 ratio shifts the atom ratios C:O and H:O. Hence, it might be expected that an increase of these atom ratios leads to components that have larger values of these ratios as preferred products. It will become apparent that this is a too simplistic picture and reflects the reality in the complex reaction network of the DBD cold plasma reactor only in some cases.

3.6.1 H-Selectivity to Products without Carbon

Figure 11 shows the results for the H-selectivity to products without carbon (H_2O and H_2).

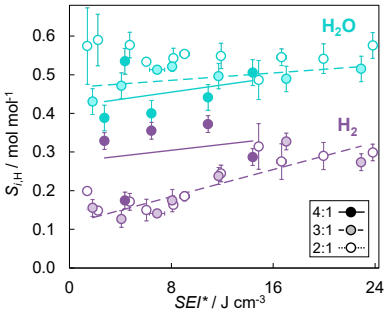

Figure 11: H-selectivities to H_2O and H_2 at CH_4:O_2 ratios of 2:1 (open symbols, dotted line), 3:1 (light filled symbols, dashed line), and 4:1 (dark filled symbols, solid line). The lines were obtained from a linear fit to the data as a guide to the eye.

The selectivity to H_2O is roughly twice as high as that to H_2, with maximal values of about 0.6 mol mol^{-1} for H_2O and 0.3 mol mol^{-1} for H_2. Despite the scattering of the results, trends can be observed. For both components, an increase of *SEI** tends to lead to an increase of the H-selectivity to both H_2O and H_2. The influence of the CH_4:O_2 ratio seems to be different for the two products: an increase yields more H_2 compared to H_2O, which is not unexpected. In fact, for some of the experiments at high values of CH_4:O_2, the selectivity to H_2 is almost as high as that to H_2O, see, e.g., those for the H_2 selectivity for CH_4:O_2 of 4:1. However, these trends need to be interpreted cautiously, as the results strongly scatter.

3.6.2 C-Selectivity to Products without Hydrogen

Figure 12 shows the results for the C-selectivity to products without hydrogen (CO and CO_2).

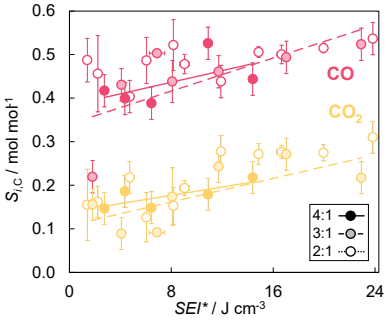

Figure 12: C-selectivities to CO and CO_2 at CH_4:O_2 ratios of 2:1 (open symbols, dotted line), 3:1 (light filled symbols, dashed line), and 4:1 (dark filled symbols, solid line). The lines were obtained from a linear fit to the data as a guide to the eye.

The selectivity to CO is roughly twice that to CO_2 and in both cases, an increase of the *SEI** leads to an increase of the selectivity. An increase of the CH_4:O_2 ratio leads to a decrease of the selectivity to CO_2, which is as expected. For the selectivity to CO, no such trend is found.

3.6.3 C-Selectivity to Products without Oxygen

Figure 13 shows the results for the C-selectivity to products without oxygen (C_2H_6 and C_2H_4).

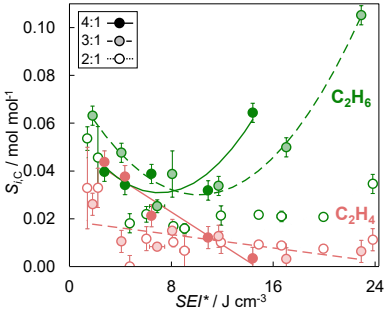

Figure 13: C-selectivities to C_2H_6 and C_2H_4 at CH_4:O_2 ratios of 2:1 (open symbols, dotted line), 3:1 (light filled symbols, dashed line), and 4:1 (dark filled symbols, solid line). The lines were obtained from a polynomial fit to the data of C_2H_6 and a linear fit to the data of C_2H_4 as a guide to the eye.

The selectivities to C_2H_6 are generally above those to C_2H_4. Increasing the *SEI** leads to a decrease of the selectivity to C_2H_4, which is most pronounced for the highest value of the CH_4:O_2 ratio. The results for C_2H_6 reveal complex dependencies, interestingly with clearer patterns than many of the other results. For all three CH_4:O_2 ratios, there is a minimum of the selectivity as a function of the *SEI**. For high values of the *SEI**, an increase of the CH_4:O_2 ratio leads to an increase of the selectivity to C_2H_6, which is as expected. The trend is less clear at *SEI** values below the minimum and seems to be inverted sometimes.

3.6.4 C-Selectivity to Products that Contain One Carbon Atom and Hydrogen and Oxygen

Figure 14 shows the results for the C-selectivity to MeOH, MeOOH, FA, and FAc, which belong to the product group that contain one carbon atom and hydrogen and oxygen.

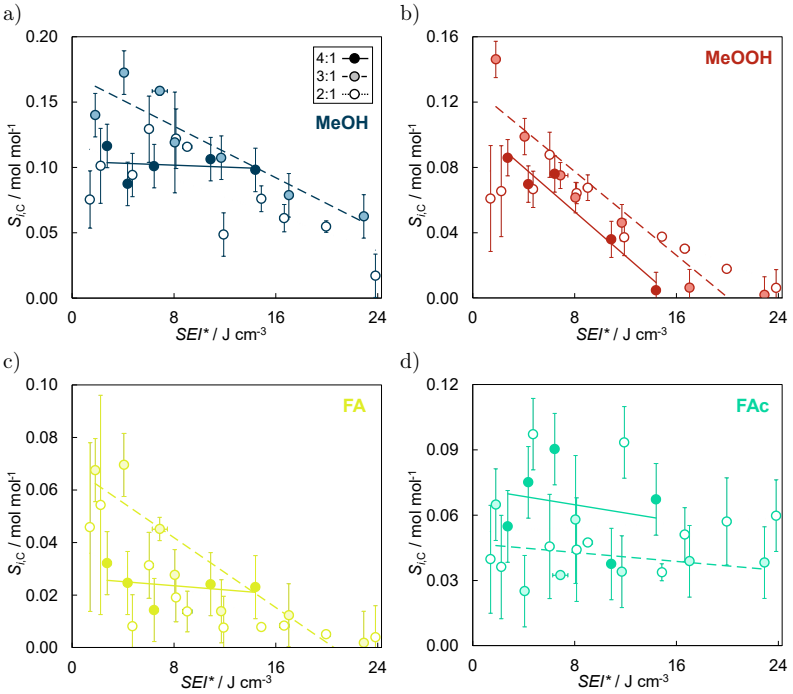

Figure 14: C-selectivities to a) MeOH, b) MeOOH, c) FA, and d) FAc at CH_4:O_2 ratios of 2:1 (open symbols, dotted line), 3:1 (light filled symbols, dashed line), and 4:1 (dark filled symbols, solid line). The lines were obtained from a linear fit to the data as a guide to the eye.

In the product group discussed here, the products with the highest selectivities are MeOH, MeOOH (with maximal selectivities above 0.1 mol mol^{-1}), followed by FA and FAc (with maximal selectivities below 0.1 mol mol^{-1}). For all product components of this group, the selectivities generally show a decreasing trend with increasing *SEI**, except for the results for FAc and for the highest CH_4:O_2 ratio of MeOH and FA, where the influence of the *SEI** is hard to discern. The results are not clearly correlated with the C:O ratio or the H:O ratio in the products, which underlines the need for the development of mechanistic reaction kinetic models to understand the complex processes in cold plasma DBD.

3.6.5 C-Selectivity to Products that Contain More than One Carbon Atom and Hydrogen and Oxygen

Figure 15 shows the results for the C-selectivity to the products that contain more than one carbon atom and hydrogen and oxygen, i.e., MeFo, EtOH, HAc, MeAc, Ace, and EG.

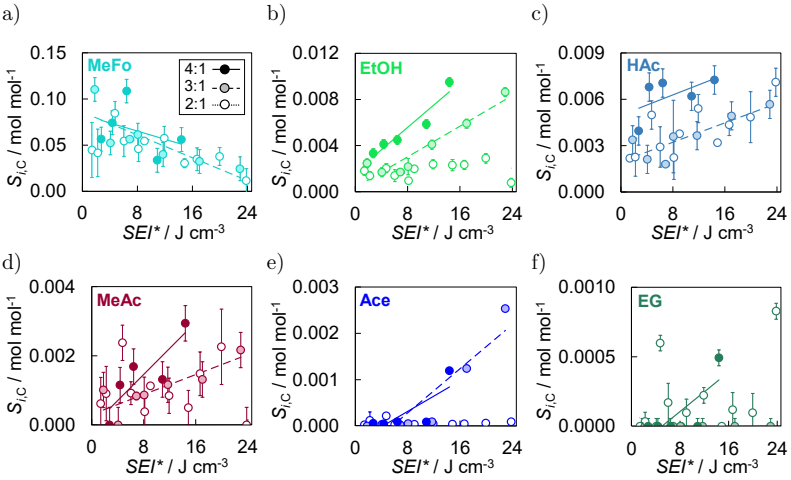

Figure 15: C-selectivities to a) MeFo, b) EtOH, c) HAc, d) MeAc, e) Ace, and f) EG at CH_4:O_2 ratios of 2:1 (open symbols, dotted line), 3:1 (light filled symbols, dashed line), and 4:1 (dark filled symbols, solid line). The lines were obtained from a linear fit to the data as a guide to the eye.

In the product group discussed here, the product with the highest selectivity is MeFo with a maximal selectivity of 0.12 mol mol^{-1}. For all other components in this group, the maximal selectivity is below 0.01 mol mol^{-1}. The selectivity to EtOH shows a remarkably clear trend even at those low values: at a CH_4:O_2 ratio of 2:1, the selectivity is independent of the *SEI**, whereas at 3:1 and 4:1 an increasing *SEI**

leads to an increasing selectivity with a higher gradient of the trend at 4:1. The lowest C-selectivities in the present work were observed for MeAc, Ace, and EG (maximal selectivities below 0.003 mol mol^{-1}). It is to be mentioned, that the measurement uncertainty of NMR analysis of the condensable fraction of 0.01 g g^{-1} is much higher than the highest measured amount of EG, Ace, or even MeAc, which was below $3 \cdot 10^{-3}$ g g^{-1}. In general, the influence of the CH_4:O_2 ratio and the *SEI** on the selectivity of this product group is (where such an influence can be inferred from the data) not clearly correlated with the chemical structure of the product. Again, this indicates that obviously a mechanistic model of the reaction network is needed to gain a better understanding of the findings.

3.6 Temperature Increase

In most of the experiments carried out in the present work, the temperature increase between the reactor inlet and outlet was below 10 K, i.e., the temperature was still near ambient. Obviously, the cooling of the DBD cold plasma reactor by the jacket was not sufficient to ensure isothermal conditions for the overall exothermal reactions. In some of the experiments, distinctly higher outlet temperatures were measured (below 320 K in all cases but one in which the outlet temperature was 348 K). This was only observed for some of the experiments with residence times τ below 2 s. There is no obvious correlation of this higher temperature increase with other process parameters or with the results for the conversions and selectivities. As there were no obvious trends, the data were evaluated making no distinction between the experiments with high temperature difference and those with low temperature difference. It is to mention here that artifacts in the measurement results of the outlet temperature caused by the plasma cannot be strictly excluded. In future experiments, it would be desirable to study the caloric side of the cold plasma reactor in more detail – such studies were beyond the scope of the present work. For comparison, the results without a high temperature difference in the experiments are presented in Appendix E.

3.7 Comparison with the Literature

In the following, the results of the present work are qualitatively compared to results from studies of the uncatalyzed partial oxidation of CH_4 with O_2 using a DBD cold plasma reactor from the literature. A quantitative comparison to the experimental data from the literature makes no sense, as conditions and reactor set-ups differ. Nonetheless, trends can be compared. The qualitative results for the dependencies of conversions and selectivities on the *SEI** and the molar CH_4:O_2 ratio in the feed from the literature and the present work are compared in Table 5 (*SEI**) and Table 6 (CH_4:O_2 ratio). Also two modeling studies from the literature were included in the comparison. The trends were classified as follows: increase (↑), constant or not significant (→), decrease (↓), curve with minimum (↓↑), or curve with maximum (↑↓). For cases in which this classification was ambiguous due to different trends observed for different conditions, the predominant result was chosen.

Table 5: Influence of increasing the *SEI** on conversions and selectivities leading to responses classified as follows: increase (↑), constant or not significant (→), decrease (↓), curve with minimum (↓↑), or curve with maximum (↑↓). No entry means: not studied.

		This work	**Aghamir et al. [15]**	**Bhatnagar and Mallinson [47]**	**Gao et al. [48]**	**Indarto et al. [36]**	**Indarto et al. [38]**	**Larkin et al. [32]**	**Larkin et al. [43]**	**Nozaki et al. [44]**	**Nozaki et al. [14]**	**Okumoto et al. [25]**	**Yao et al. [27]**	**Yi et al. [45]**	**De Bie et al. [51]**	**Yi et al. [45]**
		experiment													**model**	
X_j	CH_4	↑	↑	↑	→	↑	↑	↑	↑	↑	↑	↑	↑	↑		
	O_2	↑		↑	↑			↑	↑	↑		↑	↑			
$S_{i,H}$	H_2O	→								↑					↑	
	H_2	↑			↑	↑	↑		↑	↑					↑	
$S_{i,C}$	CO	↑		→	↑	→	↑		↑	↑	↑	↑	↑	↑	↑	
	CO_2	↑		↑	↑	→	↑		↑	↑	↑	↑	→	↑	↑↓	↑
	C_2H_6	↓↑		→	↑				→	↑			↓		↑↓	
	C_2H_4	↓			↓								↓			
	C_3H_8				→										→	
	MeOH	↓	↑↓	→	↓	↓		↓	↓	↓		↑↓	↑	↓	↑	↓
	MeOOH	↓													↑↓	
	FA	↓			↑↓			↑	→	→		↓		↓	↑↓	↓
	FAc	→						↑	→	↓				↓		
	MeFo	↓						↑	↑↓							
	EtOH	↑		↓	↓											→
	HAc	↑			↓											→

Table 6: Influence of increasing the CH_4:O_2 ratio on conversions and selectivities leading to responses classified as follows: increase (↑), constant or not significant (→), decrease (↓), curve with minimum (↓↑), or curve with maximum (↑↓). No entry means: not studied.

		This work	**Aghamir et al. [15]**	**Bhatnagar and Mallinson [47]**	**Gao et al. [48]**	**Larkin et al. [32]**	**Nozaki et al. [44]**	**Nozaki et al. [14]**	**Okumoto et al. [25]**	**Yao et al. [27]**	**Yi et al. [45]**	**Zhou et al. [46]**	**De Bie et al. [51]**	**Qian et al. [60]**
		experiment											**model**	
X_j	CH_4	→	↓	↓	↓	↓	↑↓			↓	↓	↓	→	↓
	O_2	↑		↑	→	↑	↑			↑			↓	↑
$S_{i,H}$	H_2O	↓					↓					↓	→	
	H_2	↑				↑	→					↑	→	↑
$S_{i,C}$	CO	→		↓	↓	→	↓		↓	↓	→	↓	→	↓
	CO_2	↓		↓	↓	→	↓		↓	↓	→	↓	→	
	C_2H_6	↑		↑	↑	→	↑		↑	↑	↑		↑	
	C_2H_4	↑	↑										→	
	C_3H_8				↑								→	
	MeOH	→	↑	↑	↑	↑	↑↓	↑	↑↓	→		↑↓	→	↑↓
	MeOOH	↓											↑	
	FA	→			↑	→	↑↓	↑	↑↓	→	↓		→	↓
	FAc	→				↓	↑↓	↓			↑			
	MeFo	→				→								
	EtOH	↑		↑	↑								↑	
	HAc	↑			↑									

First, the dependency of the different studied properties on the *SEI** is discussed (cf. Table 5). The findings from the literature for the trends in the dependency of the conversions on *SEI** are generally in line with those from the present work. The same holds also for the H-selectivity to products without carbon (H_2O and H_2), and also for the C-selectivity to products without hydrogen (CO and CO_2). For the remaining selectivities, generally different trends are reported by different sources, which in part agree with those found in the present work, and in part disagree.

This mixed picture was also found for the results for the dependency of the studied properties from the CH_4:O_2 ratio that are presented in Table 6. In assessing these results, it is important to realize that the conditions in the experiments differ, and that therefore, there is no compelling reason why the results should agree, even if it is only for the trends. Hence, the results underline the limitations of purely empirical studies and the need for reaction kinetic modeling. From the overview given in Table 5 and Table 6, it also becomes clear that the study from the present work is by far the most comprehensive that has been carried out so far. Moreover, it shows that all product components that have ever been reported on in the literature were also analyzed in the present work, with the only exceptions being hydrogen peroxide, acetaldehyde, ethyl hydroxy peroxide, and ozone. Finally, the trends in selectivities to the product components MeAc, Ace, and EG are not reported in Table 5 and Table 6 as they have not been studied in the literature.

4 Conclusions

In this work, a series of 43 experiments on partial oxidation of methane (CH_4) with pure oxygen (O_2) in a dielectric barrier discharge (DBD) cold plasma reactor was performed. The DBD cold plasma reactor was operated near ambient conditions and argon was used as inert gas. A comprehensive qualitative and quantitative analysis of the product spectrum as well as unconverted feed components was conducted by a combination of NMR spectroscopy, wet-chemistry methods, and gas chromatography. All in all, quantitative results are reported for 16 components, more than in any previous study of partial oxidation of CH_4 with O_2 in cold plasma. From the sophisticated analysis of the product spectrum conversions of CH_4 and O_2 are obtained together with H-selectivities to water (H_2O) and hydrogen (H_2) and C-selectivities to 14 products, i.e., carbon monoxide (CO) and carbon dioxide (CO_2); ethane (C_2H_6) and ethene (C_2H_4); methanol (MeOH), methyl hydroperoxide (MeOOH), formaldehyde (FA), and formic acid (FAc); and methyl formate (MeFo), ethanol (EtOH), acetic acid (HAc), methyl acetate (MeAc), acetone (Ace), and ethylene glycol (EG).

The dependencies of the conversions and selectivities to the 14 product components on the following parameters was studied: the molar reactant ratio CH_4:O_2 in the feed, the mole fraction of argon in the feed x_{Ar}^{in}, the residence time τ, and the electrical power input P fed into the reactor. To the best of our knowledge this is by far the most comprehensive study on the partial oxidation of CH_4 in a DBD cold plasma reactor.

The results at two different mole fractions of argon in the feed x_{Ar}^{in} of 0.19 mol mol^{-1} and 0.75 mol mol^{-1} clearly show that the presence of argon has no influence on the trends of conversions and selectivities. This is derived as the results at different mole fractions of argon coincide if the residence times are calculated only referring to the volumetric flow rate of the reactants, disregarding argon in the calculation. This is

why a normalized specific energy input *SEI** is introduced to describe the process parameters, in which the electrical power is related to the volumetric flow rate of the reactants, and not to the total volumetric flow rate, as it is commonly done in the literature. Hence, the dependencies of conversions and selectivities on the four varied parameters can be described by using only the specific energy input *SEI** and the molar reactant ratio CH_4:O_2 in the feed. In the series of experiments, the specific energy input *SEI** was in a range from 0.9 to 23.8 J cm^{-3} and the molar reactant ratio CH_4:O_2 in the feed was varied from 2:1, 3:1, and 4:1.

The dependency of the conversions on the *SEI** and the CH_4:O_2 ratio is found to be the following: an increasing *SEI** always leads to increasing conversion for both reactants. The conversion of O_2 increases linearly with increasing *SEI** up to full conversion. The slope of the conversion of O_2 increases with increasing CH_4:O_2 ratio. In the studied range of parameters, the conversions of CH_4 are always below 0.3 mol mol^{-1} and, in contrast to O_2, the conversion of CH_4 is hardly affected by the molar reactant ratio CH_4:O_2, as long as there is O_2 left.

The dependencies of the selectivities to the 14 product components on the *SEI** show more sundry trends: at a constant CH_4:O_2 ratio, with an increasing *SEI**, the H-selectivity to H_2 and the C-selectivities to CO, CO_2, HAc, EtOH, MeAc, and Ace increase, while the C-selectivities to MeOH, MeOOH, FA, MeFo, and C_2H_4 decrease. The H-selectivity to H_2O and the C-selectivities to FAc and EG show no significant trend and, lastly, the C-selectivities to C_2H_6 show a minimum. The largest C-selectivity to CO was 0.5 mol mol^{-1} and the selectivities to CO_2 were about half of those to CO. For the H-selectivities to H_2, values of up to 0.3 mol mol^{-1} were found. The largest C-selectivities to the product components containing carbon, hydrogen, and oxygen were found for MeOH (0.18 mol mol^{-1}), MeOOH and MeFo (both 0.12 mol mol^{-1}), and FAc and FA (both 0.09 mol mol^{-1}). However, these large selectivities were found for low conversions.

The variation of the molar reactant ratio CH_4:O_2 showed a less significant influence on the selectivities. With an increasing CH_4:O_2 ratio, the H-selectivity to H_2 and the C-selectivities to C_2H_6, C_2H_4, EtOH, HAc, and MeAc increased, while the H-selectivity to H_2O and the C-selectivities to CO_2 and MeOOH decreased. The selectivities to all other components did not show a significant dependence on the CH_4:O_2 ratio.

A comparison of the results of the present work to results from the literature obtained from other authors was carried out where this was possible. However, basically only trends can be compared, and even this is hampered by the fact that the conditions in the experiments are different. While for the conversions and the C-selectivities to CO_2 and CO, most trends reported in the literature are consistent and agree with the findings from the present work. For all other results, no clear picture emerges from the literature data. All this underlines that an understanding of partial oxidation of methane with pure oxygen in a DBD cold plasma reactor requires reaction kinetic modeling. Also the modeling of the caloric side of the process should be addressed. The present results provide an excellent basis for this. In future work, as a step towards technical applications, it is also desirable to attend to the question of the separation of the products and the recycling of reactants.

References

[1] A. Fridman: Plasma Chemistry, *Cambridge University Press* (2008).

[2] U. Kogelschatz: Dielectric-Barrier Discharges: Their History, Discharge Physics, and Industrial Applications, Plasma Chemistry and Plasma Processing 23 (2003) 1–46. https://doi.org/10.1023/A:1022470901385.

[3] A. Fridman, L.A. Kennedy: Plasma physics and engineering, *CRC Press* Boca Raton (2004).

[4] B. Eliasson, U. Kogelschatz: Nonequilibrium Volume Plasma Chemical Processing, IEEE Transactions on Plasma Science 19 (1991) 1063–1077. https://doi.org/10.1109/27.125031.

[5] A. Bogaerts, E. Neyts, R. Gijbels, J. van der Mullen: Gas Discharge Plasmas and Their Applications, Spectrochimica Acta Part B: Atomic Spectroscopy 57 (2002) 609–658. https://doi.org/10.1016/S0584-8547(01)00406-2.

[6] W. Siemens: Ueber die elektrostatische Induction und die Verzögerung des Stroms in Flaschendrähten, Annalen der Physik und Chemie 178 (1857) 66–122. https://doi.org/10.1002/andp.18571780905.

[7] U. Kogelschatz, B. Eliasson, W. Egli: From Ozone Generators to Flat Television Screens: History and Future Potential of Dielectric-Barrier Discharges, Pure and Applied Chemistry 71 (1999) 1819–1828. https://doi.org/10.1351/pac199971101819.

[8] M.A. Malik, A. Ghaffar, S.A. Malik: Water Purification by Electrical Discharges, Plasma Sources Science and Technology 10 (2001) 82–91. https://doi.org/10.1088/0963-0252/10/1/311.

[9] C. Tapp, R.G. Rice: Generation and Control of Ozone, in: Ozone in Food Processing, (2012): pp. 33–54 https://doi.org/10.1002/9781118307472.ch4.

[10] P.A. Mikheyev, A.V. Demyanov, I.V. Kochetov, A.A. Sludnova, A.P. Torbin, A.M. Mebel, V.N. Azyazov: Ozone and Oxygen Atoms Production in a Dielectric Barrier Discharge in Pure Oxygen and O_2/CH_4 Mixtures Modeling and Experiment, Plasma Sources Science and Technology 29 (2020) 015012. https://doi.org/10.1088/1361-6595/ab5da3.

[11] H.-H. Kim, A.A. Abdelaziz, Y. Teramoto, T. Nozaki, D.-Y. Kim, R. Brandenburg, M. Schiorlin, K. Hensel, Y.-H. Song, D.-H. Lee: Revisiting Why DBDs Can Generate O_3 against the Thermodynamic Limit, International Journal of Plasma Environmental Science & Technology (IJPEST) 17 (2023).

[12] T. Nitsche, C. Unger, E. Weidner: Plasma Catalytical Reactors for Atmospheric Gas Conversions, Chemie Ingenieur Technik 90 (2018) 1453–1464. https://doi.org/10.1002/cite.201800024.

[13] A. Indarto: A Review of Direct Methane Conversion to Methanol by Dielectric Barrier Discharge, IEEE Transactions on Dielectrics and Electrical Insulation 15 (2008) 1038–1043. https://doi.org/10.1109/TDEI.2008.4591225.

[14] T. Nozaki, A. Ağıral, S. Yuzawa, J.G.E. Han Gardeniers, K. Okazaki: A Single Step Methane Conversion into Synthetic Fuels Using Microplasma Reactor, Chemical Engineering Journal 166 (2011) 288–293. https://doi.org/10.1016/j.cej.2010.08.001.

[15] F.M. Aghamir, N.S. Matin, A.H. Jalili, M.H. Esfarayeni, M.A. Khodagholi, R. Ahmadi: Conversion of Methane to Methanol in an Ac Dielectric Barrier Discharge, Plasma Sources Science and Technology 13 (2004) 707–711. https://doi.org/10.1088/0963-0252/13/4/021.

[16] H. Suhr: Application of Nonequilibrium Plasmas in Organic Chemistry, Plasma Chemistry and Plasma Processing 3 (1983) 1–61. https://doi.org/10.1007/BF00566027.

[17] R. Aerts, W. Somers, A. Bogaerts: Carbon Dioxide Splitting in a Dielectric Barrier Discharge Plasma: A Combined Experimental and Computational Study, ChemSusChem 8 (2015) 702–716. https://doi.org/10.1002/cssc.201402818.

[18] K. Thanyachotpaiboon, S. Chavadej, T.A. Caldwell, L.L. Lobban, R.G. Mallinson: Conversion of Methane to Higher Hydrocarbons in AC Nonequilibrium Plasmas, AIChE Journal 44 (1998) 2252–2257. https://doi.org/10.1002/aic.690441014.

[19] M.C. Alvarez-Galvan, N. Mota, M. Ojeda, S. Rojas, R.M. Navarro, J.L.G. Fierro: Direct Methane Conversion Routes to Chemicals and Fuels, Catalysis Today 171 (2011) 15–23. https://doi.org/10.1016/j.cattod.2011.02.028.

[20] N. Seyed Matin, H.A. Savadkoohi, S.Y. Feizabadi: Methane Conversion to C_2 Hydrocarbons Using Dielectric-Barrier Discharge Reactor: Effects of System Variables, Plasma Chemistry and Plasma Processing 28 (2008) 189–202. https://doi.org/10.1007/s11090-008-9123-5.

[21] T. Nozaki, V. Goujard, S. Yuzawa, S. Moriyama, A. Ağıral, K. Okazaki: Selective Conversion of Methane to Synthetic Fuels Using Dielectric Barrier Discharge Contacting Liquid Film, Journal of Physics D: Applied Physics 44 (2011) 274010. https://doi.org/10.1088/0022-3727/44/27/274010.

[22] J. Zhou, Y. Xu, X. Zhou, J. Gong, Y. Yin, H. Zheng, H. Guo: Direct Oxidation of Methane to Hydrogen Peroxide and Organic Oxygenates in a Double Dielectric Plasma Reactor, ChemSusChem 4 (2011) 1095–1098. https://doi.org/10.1002/cssc.201100093.

[23] M. Okumoto, A. Mizuno: Conversion of Methane for Higher Hydrocarbon Fuel Synthesis Using Pulsed Discharge Plasma Method, Catalysis Today 71 (2001) 211–217. https://doi.org/10.1016/S0920-5861(01)00431-X.

[24] B. Pietruszka, K. Anklam, M. Heintze: Plasma-Assisted Partial Oxidation of Methane to Synthesis Gas in a Dielectric Barrier Discharge, Applied Catalysis A: General 261 (2004) 19–24. https://doi.org/10.1016/j.apcata.2003.10.027.

[25] M. Okumoto, H.H. Kim, K. Takashima, S. Katsura, A. Mizuno: Reactivity of Methane in Nonthermal Plasma in the Presence of Oxygen and Inert Gases at Atmospheric Pressure, IEEE Transactions on Industry Applications 37 (2001) 1618–1624. https://doi.org/10.1109/28.968169.

[26] D.W. Larkin, T.A. Caldwell, L.L. Lobban, R.G. Mallinson: Oxygen Pathways and Carbon Dioxide Utilization in Methane Partial Oxidation in Ambient Temperature Electric Discharges, Energy & Fuels 12 (1998) 740–744. https://doi.org/10.1021/ef970217n.

[27] S.L. Yao, T. Takemoto, F. Ouyang, A. Nakayama, E. Suzuki, A. Mizuno, M. Okumoto: Selective Oxidation of Methane Using a Non-Thermal Pulsed Plasma, Energy & Fuels 14 (2000) 459–463. https://doi.org/10.1021/ef9901692.

[28] M. Okumoto, K. Tsunoda, S. Katsura, A. Mizuno: Direct Methanol Synthesis Using Non-Thermal Pulsed Plasma Generated by a Solid State Pulse Generator, Journal of Electrostatics 42 (1997) 167–175. https://doi.org/10.1016/S0304-3886(97)00147-2.

[29] M. Okumoto, Z. Su, S. Katsura, A. Mizuno: Dilution Effect with Inert Gases in Direct Synthesis of Methanol from Methane Using Nonthermal Plasma, IEEE Transactions on Industry Applications 35 (1999) 1205–1210. https://doi.org/10.1109/28.793386.

[30] S.P. Bugaev, A.V. Kozyrev, V.A. Kuvshinov, N.S. Sochugov, P.A. Khryapov: Plasma-Chemical Conversion of Lower Alkanes with Stimulated Condensation of Incomplete Oxidation Products, Plasma Chemistry and Plasma Processing 18 (1998) 15.

[31] D.W. Larkin, L.L. Lobban, R.G. Mallinson: Production of Organic Oxygenates in the Partial Oxidation of Methane in a Silent Electric Discharge Reactor, Industrial & Engineering Chemistry Research 40 (2001) 1594–1601. https://doi.org/10.1021/ie000527k.

[32] D.W. Larkin, L.L. Lobban, R.G. Mallinson: The Direct Partial Oxidation of Methane to Organic Oxygenates Using a Dielectric Barrier Discharge Reactor as a Catalytic Reactor Analog, Catalysis Today 71 (2001) 199–210. https://doi.org/10.1016/S0920-5861(01)00430-8.

[33] T. Nozaki, K. Okazaki: Plasma Enhanced C_1-Chemistry: Towards Greener Methane Conversion, Green Processing and Synthesis 1 (2012) 517–523. https://doi.org/10.1515/gps-2012-0074.

[34] T. Nozaki, S. Abe, S. Moriyama, S. Kameshima, K. Okazaki, V. Goujard, A. Ağıral: One Step Methane Conversion to Syngas by Dielectric Barrier Discharge, Japanese Journal of Applied Physics 54 (2015) 01AG01. http://dx.doi.org/10.7567/JJAP.54.01AG01.

[35] B. Wang, X. Zhang, Y. Liu, G. Xu: Conversion of CH_4, Steam and O_2 to Syngas and Hydrocarbons via Dielectric Barrier Discharge, Journal of Natural Gas Chemistry 18 (2009) 94–97. https://doi.org/10.1016/S1003-9953(08)60089-4.

[36] A. Indarto, J.-W. Cho, H. Lee, H.K. Song, J. Palgunadi: Partial Oxidation of Methane with Sol-Gel Fe/Hf/YSZ Catalyst in Dielectric Barrier Discharge: Catalyst Activation by Plasma, Journal of Rare Earths 24 (2006) 513–518. https://doi.org/10.1016/S1002-0721(06)60154-3.

[37] B. Loenders, Y. Engelmann, A. Bogaerts: Plasma-Catalytic Partial Oxidation of Methane on Pt(111): A Microkinetic Study on the Role of Different Plasma Species, The Journal of Physical Chemistry C 125 (2021) 2966–2983. https://doi.org/10.1021/acs.jpcc.0c09849.

[38] A. Indarto, D.R. Yang, J. Palgunadi, J.-W. Choi, H. Lee, H.K. Song: Partial Oxidation of Methane with Cu–Zn–Al Catalyst in a Dielectric Barrier Discharge, Chemical Engineering and Processing: Process Intensification 47 (2008) 780–786. https://doi.org/10.1016/j.cep.2006.12.015.

[39] S.A. Nair, T. Nozaki, K. Okazaki: Methane Oxidative Conversion Pathways in a Dielectric Barrier Discharge Reactor—Investigation of Gas Phase Mechanism, Chemical Engineering Journal 132 (2007) 85–95. https://doi.org/10.1016/j.cej.2007.01.022.

[40] P. Chawdhury, Y. Wang, D. Ray, S. Mathieu, N. Wang, J. Harding, F. Bin, X. Tu, Ch. Subrahmanyam: A Promising Plasma-Catalytic Approach towards Single-Step Methane Conversion to Oxygenates at Room Temperature, Applied Catalysis B: Environmental 284 (2021) 119735. https://doi.org/10.1016/j.apcatb.2020.119735.

[41] J.-J. Zou, Y. Zhang, C.-J. Liu, Y. Li, B. Eliasson: Starch-Enhanced Synthesis of Oxygenates from Methane and Carbon Dioxide Using Dielectric-Barrier Discharges, Plasma Chemistry and Plasma Processing 23 (2003) 69–82. https://doi.org/10.1023/A:1022416819132.

[42] A. Ağıral, T. Nozaki, M. Nakase, S. Yuzawa, K. Okazaki, J.G.E. (Han) Gardeniers: Gas-to-Liquids Process Using Multi-Phase Flow, Non-Thermal Plasma Microreactor, Chemical Engineering Journal 167 (2011) 560–566. https://doi.org/10.1016/j.cej.2010.10.050.

[43] D.W. Larkin, L. Zhou, L.L. Lobban, R.G. Mallinson: Product Selectivity Control and Organic Oxygenate Pathways from Partial Oxidation of Methane in a Silent Electric Discharge Reactor, Industrial & Engineering Chemistry Research 40 (2001) 5496–5506. https://doi.org/10.1021/ie010298h.

[44] T. Nozaki, A. Hattori, K. Okazaki: Partial Oxidation of Methane Using a Microscale Non-Equilibrium Plasma Reactor, Catalysis Today 98 (2004) 607–616. https://doi.org/10.1016/j.cattod.2004.09.053.

[45] Y. Yi, S. Li, Z. Cui, Y. Hao, Y. Zhang, L. Wang, P. Liu, X. Tu, X. Xu, H. Guo, A. Bogaerts: Selective Oxidation of CH_4 to CH_3OH through Plasma Catalysis: Insights from Catalyst Characterization and Chemical Kinetics Modelling, Applied Catalysis B: Environmental 296 (2021) 120384. https://doi.org/10.1016/j.apcatb.2021.120384.

[46] L.M. Zhou, B. Xue, U. Kogelschatz, B. Eliasson: Partial Oxidation of Methane to Methanol with Oxygen or Air in a Nonequilibrium Discharge Plasma, Plasma Chemistry and Plasma Processing 18 (1998) 375–393.

[47] R. Bhatnagar, R.G. Mallinson: Methane Conversion in AC Electric Discharges at Ambient Conditions, in: Methane and Alkane Conversion Chemistry, *Springer, Boston, MA* (1995): pp. 249–264 https://doi.org/10.1007/978-1-4615-1807-5_27.

[48] Y. Gao, L. Dou, B. Feng, C. Zhang, T. Shao: Catalyst-Free Activation of CH_4 and Air into Platform Chemicals and H_2 Using Parametrized Nanosecond Pulsed Plasma, Energy Conversion and Management 276 (2023) 116570. https://doi.org/10.1016/j.enconman.2022.116570.

[49] V. Goujard, T. Nozaki, S. Yuzawa, A. Ağıral, K. Okazaki: Plasma-Assisted Partial Oxidation of Methane at Low Temperatures: Numerical Analysis of Gas-Phase Chemical Mechanism, Journal of Physics D: Applied Physics 44 (2011) 274011. https://doi.org/10.1088/0022-3727/44/27/274011.

[50] B. Pietruszka, M. Heintze: Methane Conversion at Low Temperature: The Combined Application of Catalysis and Non-Equilibrium Plasma, Catalysis Today 90 (2004) 151–158. https://doi.org/10.1016/j.cattod.2004.04.021.

[51] C. De Bie, J. van Dijk, A. Bogaerts: The Dominant Pathways for the Conversion of Methane into Oxygenates and Syngas in an Atmospheric Pressure Dielectric Barrier Discharge, The Journal of Physical Chemistry C 119 (2015) 22331–22350. https://doi.org/10.1021/acs.jpcc.5b06515.

[52] I. Adamovich, S.D. Baalrud, A. Bogaerts, P.J. Bruggeman, M. Cappelli, V. Colombo, U. Czarnetzki, U. Ebert, J.G. Eden, P. Favia, D.B. Graves, S. Hamaguchi, G. Hieftje, M. Hori, I.D. Kaganovich, U. Kortshagen, M.J. Kushner, N.J. Mason, S. Mazouffre, S.M. Thagard, H.-R. Metelmann, A. Mizuno, E. Moreau, A.B. Murphy, B.A. Niemira, G.S. Oehrlein, Z.L. Petrovic, L.C. Pitchford, Y.-K. Pu, S. Rauf, O. Sakai, S. Samukawa, S. Starikovskaia, J. Tennyson, K. Terashima, M.M. Turner, M.C.M. van de Sanden, A. Vardelle: The 2017 Plasma Roadmap: Low Temperature Plasma Science and Technology, Journal of Physics D: Applied Physics 50 (2017) 323001. https://doi.org/10.1088/1361-6463/aa76f5.

[53] T. Nozaki, A. Bogaerts, X. Tu, R. Sanden: Special Issue: Plasma Conversion, Plasma Processes and Polymers 14 (2017) 1790061. https://doi.org/10.1002/ppap.201790061.

[54] A.H. Khoja, M. Tahir, N.A.S. Amin: Recent Developments in Non-Thermal Catalytic DBD Plasma Reactor for Dry Reforming of Methane, Energy Conversion and Management 183 (2019) 529–560. https://doi.org/10.1016/j.enconman.2018.12.112.

[55] T. Shao, R. Wang, C. Zhang, P. Yan: Atmospheric-Pressure Pulsed Discharges and Plasmas: Mechanism, Characteristics and Applications, High Voltage 3 (2018) 14–20. https://doi.org/10.1049/hve.2016.0014.

[56] R. Snoeckx, A. Ozkan, F. Reniers, A. Bogaerts: The Quest for Value-Added Products from Carbon Dioxide and Water in a Dielectric Barrier Discharge: A Chemical Kinetics Study, ChemSusChem 10 (2017) 409–424. https://doi.org/10.1002/cssc.201601234.

[57] J. Hong, S. Prawer, A.B. Murphy: Production of Ammonia by Heterogeneous Catalysis in a Packed-Bed Dielectric-Barrier Discharge: Influence of Argon Addition and Voltage, 42 (2014) 2.

[58] N.R. Pinhao, A. Janeco, J.B. Branco: Influence of Helium on the Conversion of Methane and Carbon Dioxide in a Dielectric Barrier Discharge, Plasma Chemistry and Plasma Processing (2011) 13.

[59] R. Snoeckx, W. Wang, X. Zhang, M.S. Cha, A. Bogaerts: Plasma-Based Multi-Reforming for Gas-To-Liquid: Tuning the Plasma Chemistry towards Methanol, Scientific Reports 8 (2018) 15929. https://doi.org/10.1038/s41598-018-34359-x.

[60] M. Qian, W. Zhong, J. Kang, S. Liu, C. Ren, J. Zhang, D. Wang: Global Modeling on Partial Oxidation of Methane to Oxygenates and Syngas in Non-Equilibrium Plasma, Japanese Journal of Applied Physics 59 (2020) 066003. https://doi.org/10.35848/1347-4065/ab91cd.

[61] A. Bogaerts, C.D. Bie, R. Snoeckx, T. Kozák: Plasma Based CO_2 and CH_4 Conversion: A Modeling Perspective, Plasma Processes and Polymers 14 (2017) 1600070. https://doi.org/10.1002/ppap.201600070.

[62] R. Kircher, N. Schmitz, J. Berje, K. Münnemann, W.R. Thiel, J. Burger, H. Hasse: Generalized Chemical Equilibrium Constant of Formaldehyde Oligomerization, Industrial & Engineering Chemistry Research 59 (2020) 11431–11440. https://doi.org/10.1021/acs.iecr.0c00974.

[63] N. Schmitz, F. Homberg, J. Berje, J. Burger, H. Hasse: Chemical Equilibrium of the Synthesis of Poly(Oxymethylene) Dimethyl Ethers from Formaldehyde and Methanol in Aqueous Solutions, Industrial & Engineering Chemistry Research 54 (2015) 6409–6417. https://doi.org/10.1021/acs.iecr.5b01148.

[64] C. Kuhnert, M. Albert, S. Breyer, I. Hahnenstein, H. Hasse, G. Maurer: Phase Equilibrium in Formaldehyde Containing Multicomponent Mixtures: Experimental Results for Fluid Phase Equilibria of (Formaldehyde + (Water or Methanol) + Methylal)) and (Formaldehyde + Water + Methanol + Methylal) and Comparison with Predictions, Industrial & Engineering Chemistry Research 45 (2006) 5155–5164. https://doi.org/10.1021/ie060131u.

[65] M. Maiwald, H.H. Fischer, M. Ott, R. Peschla, C. Kuhnert, C.G. Kreiter, G. Maurer, H. Hasse: Quantitative NMR Spectroscopy of Complex Liquid Mixtures: Methods and Results for Chemical Equilibria in Formaldehyde–Water–Methanol at Temperatures up to 383 K, Industrial & Engineering Chemistry Research 42 (2003) 259–266. https://doi.org/10.1021/ie0203072.

[66] I. Hahnenstein, H. Hasse, C.G. Kreiter, G. Maurer: ^{1}H- and ^{13}C-NMR-Spectroscopic Study of Chemical Equilibria in Solutions of Formaldehyde in Water, Deuterium Oxide, and Methanol, Industrial & Engineering Chemistry Research 33 (1994) 1022–1029. https://doi.org/10.1021/ie00028a033.

[67] G. Maurer: Vapor-Liquid Equilibrium of Formaldehyde-and Water-Containing Multicomponent Mixtures, AIChE Journal 32 (1986) 932–948. https://doi.org/10.1002/aic.690320604.

[68] M. Hołub: On the Measurement of Plasma Power in Atmospheric Pressure DBD Plasma Reactors, International Journal of Applied Electromagnetics and Mechanics 39 (2012) 81–87. https://doi.org/10.3233/JAE-2012-1446.

[69] M. Dyga, A. Keller, H. Hasse: Vapor–Liquid Equilibria and Chemical Equilibria in the System (Formaldehyde + Water + Isoprenol), Industrial & Engineering Chemistry Research 60 (2021) 4471–4483. https://doi.org/10.1021/acs.iecr.1c00168.

[70] M. Albert, I. Hahnenstein, H. Hasse, G. Maurer: Vapor–Liquid and Liquid–Liquid Equilibria in Binary and Ternary Mixtures of Water, Methanol, and Methylal, Journal of Chemical & Engineering Data 46 (2001) 897–903. https://doi.org/10.1021/je000352l.

[71] M. Albert, B. Coto García, C. Kuhnert, R. Peschla, G. Maurer: Vapor–Liquid Equilibrium of Aqueous Solutions of Formaldehyde and Methanol, AIChE Journal 46 (2000) 1676–1687. https://doi.org/10.1002/aic.690460818.

[72] A. Scheithauer, E. von Harbou, H. Hasse, T. Grützner, C. Rijksen, D. Zollinger, W.R. Thiel: ^{1}H- and ^{13}C-NMR Spectroscopic Study of Chemical Equilibria in the System Acetaldehyde + Water, AIChE Journal 61 (2015) 177–187. https://doi.org/10.1002/aic.14623.

[73] A. Scheithauer, T. Grützner, C. Rijksen, D. Zollinger, E. von Harbou, W.R. Thiel, H. Hasse: NMR Spectroscopic Study of the Aldoxane Formation in Aqueous Acetaldehyde Solutions, Industrial & Engineering Chemistry Research 53 (2014) 8395–8403. https://doi.org/10.1021/ie5004043.

[74] aprentas, ed.: Wasserbestimmung nach Karl Fischer, in: Laborpraxis Band 4: Analytische Methoden, *Springer International Publishing* Cham (2017): pp. 105–111 https://doi.org/10.1007/978-3-0348-0972-6_9.

[75] J.F. Walker: Formaldehyde, 2nd ed., *ACS Monograph Series, Reinhold Publishing Corp.* New York (1953).

[76] M. Rivlin, U. Eliav, G. Navon: NMR Studies of the Equilibria and Reaction Rates in Aqueous Solutions of Formaldehyde, The Journal of Physical Chemistry B 119 (2015) 4479–4487. https://doi.org/10.1021/jp513020y.

[77] I. Hahnenstein, M. Albert, H. Hasse, C.G. Kreiter, G. Maurer: NMR Spectroscopic and Densimetric Study of Reaction Kinetics of Formaldehyde Polymer Formation in Water, Deuterium Oxide, and Methanol, Industrial & Engineering Chemistry Research 34 (1995) 440–450. https://doi.org/10.1021/ie00041a003.

[78] K.Z. Gaca, J.A. Parkinson, L. Lue, J. Sefcik: Equilibrium Speciation in Moderately Concentrated Formaldehyde–Methanol–Water Solutions Investigated Using ^{13}C and ^{1}H Nuclear Magnetic Resonance Spectroscopy, Industrial & Engineering Chemistry Research 53 (2014) 9262–9271. https://doi.org/10.1021/ie403252x.

[79] M. Dyga, A. Keller, H. Hasse: 13C-NMR Spectroscopic Study of the Kinetics of Formaldehyde Oligomerization Reactions in the System (Formaldehyde + Water + Isoprenol), Industrial & Engineering Chemistry Research (2021) https://doi.org/10.1021/acs.iecr.1c03911.

[80] A.E. Lawson Jr., J.M. Miller: Thermal Conductivity Detectors in Gas Chromatography, Journal of Chromatographic Science 4 (1966) 273–284. https://doi.org/10.1093/chromsci/4.8.273.

[81] VDI e. V., ed.: VDI-Wärmeatlas, *Springer Berlin Heidelberg* Berlin, Heidelberg (2013) https://doi.org/10.1007/978-3-642-19981-3.

[82] C.J. Cowper, A.J. Derose: The Analysis of Gases by Chromatography, *Elsevier* (2013).

[83] K. Snavely, B. Subramaniam: Thermal Conductivity Detector Analysis of Hydrogen Using Helium Carrier Gas and HayeSep® D Columns, Journal of Chromatographic Science 36 (1998) 6.

Appendix

A Supporting Information on Experiments

A.1 Setting of the Two-Position Valves of the Analytical System

The three two-position valves V-I, V-II, and V-III are connected in such a way that the analytical system can be evacuated, purged, and connected to a calibration gas supply for the different operation modes, i.e., *pre-run*, *sampling*, and *calibration*. The valves provide connections to two cold traps (CT) and to a sample loop for the gas chromatographic analysis (GC). The sample loop can either be evacuated (Vac), loaded with an external reference gas, or the product stream, or injected into the GC. The GC can be operated with two carrier gases.
Figure A.**1** to a)
b)

Figure A.3 show the set-up of the valves V-I to V-III in the *pre-run mode*, the *sampling mode*, and the *calibration mode* with either the loading or the injecting mode of the sample loop.

a)

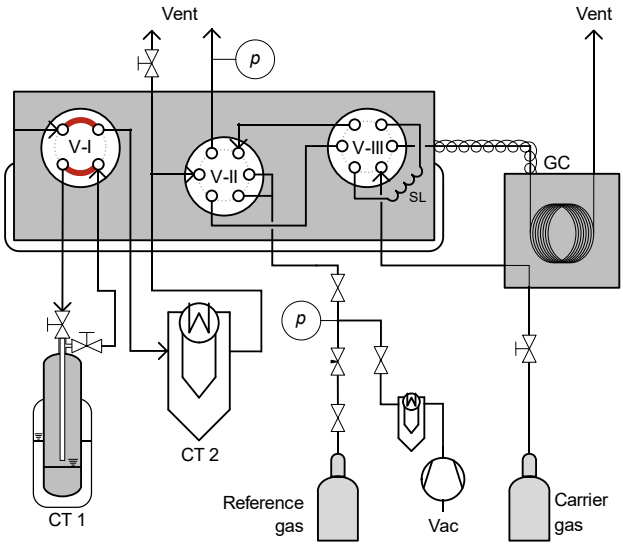

b)

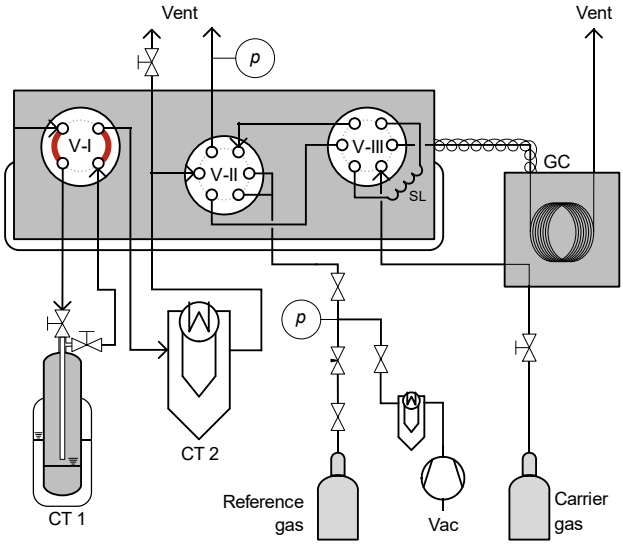

Figure A.1: Setting of valve V-I in the analytical system for a) the *pre-run mode* and b) the *sampling mode*.

a)

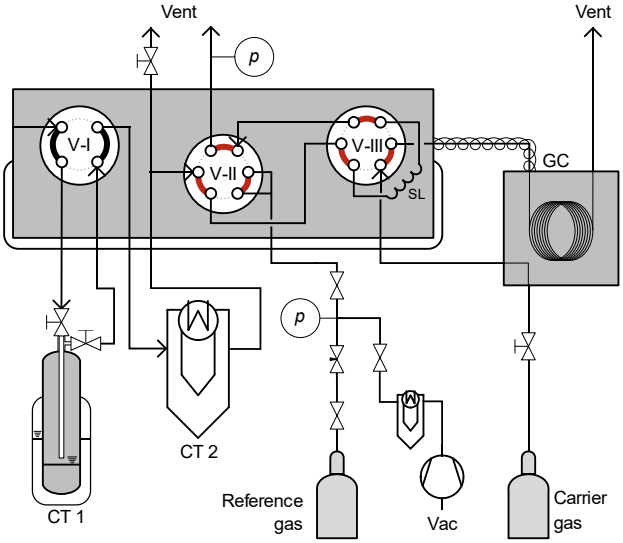

b)

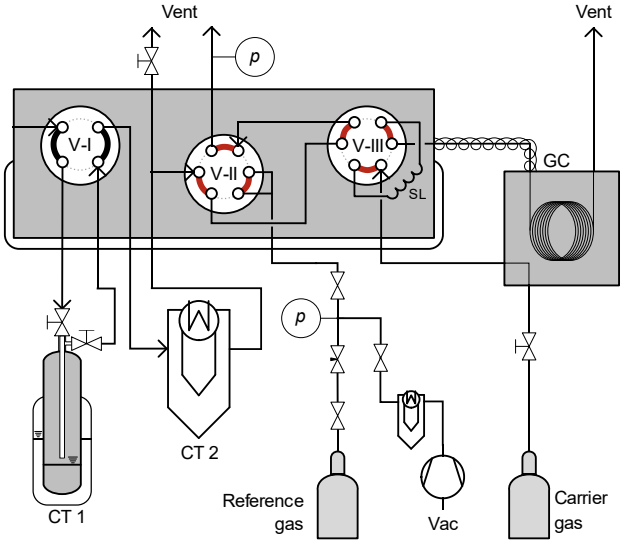

Figure A.2: Setting of valve V-II and V-III in the analytical system in the *sampling mode* for a) loading and b) injecting the sample loop.

a)

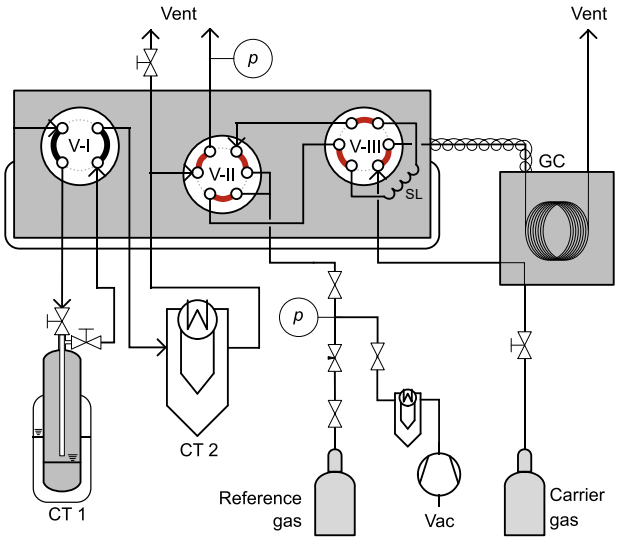

b)

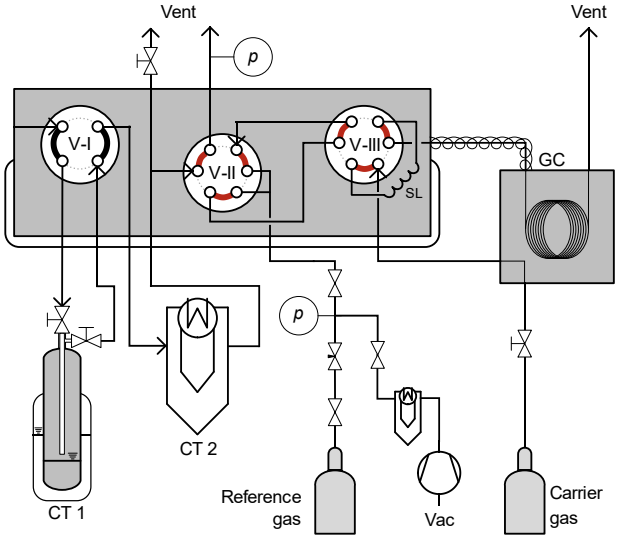

Figure A.3: Setting of valves V-II and V-III in the analytical system in the *calibration mode* for a) loading and b) injecting the sample loop.

A.2 Feed Composition

The experiments were conducted with three different molar reactant ratios of CH_4 to O_2 (referred to as CH_4:O_2 ratio) in the feed of 2:1, 3:1, and 4:1 and with two different mole fractions of argon in the feed x_{Ar}^{in} of 0.19 and 0.75 mol mol^{-1}, resulting in feed compositions that were all above the upper explosion limit. Figure A.4 shows the explosion region of the ternary system at 100 °C.

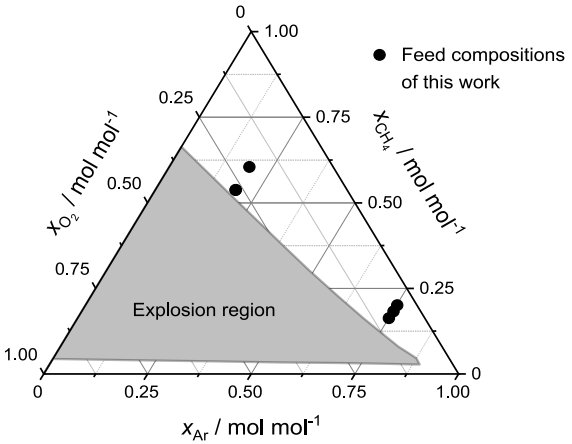

Figure A.4: Feed compositions and explosion region of the ternary system argon, methane, and oxygen at 100 °C.

The temperature was lower than 100 °C in all experiments, so that the explosion region was smaller than that shown here.

B Supporting Information on Measurements

B.1 Measurement Uncertainties

The measurement uncertainty of the mass flow controllers was 0.4% from reading (Rd) based upon a 95% confidence limit as stated by the manufacturer. Assuming a mixture of ideal gases, an uncertainty of 0.4% Rd also applies to the results of the volumetric feed flow rate $\dot{V}_j^{\text{in}}$ of the feed gas components *j*. From error propagation, this leads to an uncertainty of 0.8% Rd. For instance, at a CH_4:O_2 ratio of 2:1 and at 75% of argon in the feed, the mole fractions of the feed components correspond to:

$$x_{\text{Ar}}^{\text{in}} = 0.7500 \pm 0.0060 \text{ mol mol}^{-1},$$
$$x_{\text{CH}_4}^{\text{in}} = 0.1667 \pm 0.0013 \text{ mol mol}^{-1},$$
$$x_{\text{O}_2}^{\text{in}} = 0.0833 \pm 0.0007 \text{ mol mol}^{-1}.$$

The measurement uncertainty of the pressure sensor (at 293 K) was 0.05% Rd in the range of up to 1.6 bar as stated by the manufacturer, corresponding to an uncertainty of about around 0.5 mbar at ambient conditions. The outlet temperature was measured with a platinum resistance thermometer, and both the inlet and outlet temperature were averaged over the experiment runtime and their uncertainties were 1 K.

For the quantitative analytical measurements of the product stream components, the measurement uncertainties were considered separately for each product, depending on

the analytical method. An overview on all product stream components, the abbreviation for the components used in the present work, their quantitative analytical measurement method, and corresponding uncertainty is listed in Table B.1.

Table B.1: Overview on quantified components of the feed and the product stream, the corresponding analytical measurement method, measured variable, and measurement uncertainty.

Component	Abbreviation	Analysis method	Variable	Uncertainty
Acetic acid	HAc	NMR	$x_{\mathrm{HAc}}^{(\mathrm{m})}$	0.01 g g^{-1}
Acetone	Ace	NMR	$x_{\mathrm{Ace}}^{(\mathrm{m})}$	0.01 g g^{-1}
Argon	Ar	MFC	$\dot{V}_{\mathrm{Ar}}^{\mathrm{in}}$	0.4% Rd
		GC	$p_{\mathrm{Ar}}^{\mathrm{in}}$	14.6 mbar
Carbon dioxide	$CO_{2,cond}$	NMR	$x_{\mathrm{CO_2,cond}}^{(\mathrm{m})}$	0.01 g g^{-1}
	CO_2	GC	$p_{\mathrm{CO_2}}$	4.4 mbar
Carbon monoxide	CO	GC	p_{CO}	2.6 mbar
Ethane	C_2H_6	GC	$p_{\mathrm{C_2H_6}}$	1.0 mbar
Ethanol	EtOH	NMR	$x_{\mathrm{EtOH}}^{(\mathrm{m})}$	0.01 g g^{-1}
Ethene	C_2H_4	GC	$p_{\mathrm{C_2H_4}}$	0.2 mbar
Ethylene glycol	EG	NMR	$x_{\mathrm{EG}}^{(\mathrm{m})}$	0.01 g g^{-1}
Formaldehyde	FA	Sodium sulfite titration	$x_{\mathrm{FA}}^{(\mathrm{m})}$	0.01 g g^{-1}
Formic acid	FAc	NMR	$x_{\mathrm{FAc}}^{(\mathrm{m})}$	0.01 g g^{-1}
Hydrogen	H_2	GC	$p_{\mathrm{H_2}}$	2.9 mbar
Methane	CH_4	MFC	$\dot{V}_{\mathrm{CH_4}}^{\mathrm{in}}$	0.4% Rd
		GC	$p_{\mathrm{CH_4}}$	6.6 mbar
Methanol	MeOH	NMR	$x_{\mathrm{MeOH}}^{(\mathrm{m})}$	0.01 g g^{-1}
Methyl acetate	MeAc	NMR	$x_{\mathrm{MeAc}}^{(\mathrm{m})}$	0.01 g g^{-1}
Methyl formate	MeFo	NMR	$x_{\mathrm{MeFo}}^{(\mathrm{m})}$	0.01 g g^{-1}
Methyl hydroperoxide	MeOOH	NMR	$x_{\mathrm{MeOOH}}^{(\mathrm{m})}$	0.01 g g^{-1}
Oxygen	O_2	MFC	$\dot{V}_{\mathrm{O_2}}^{\mathrm{in}}$	0.4% Rd
		GC	$p_{\mathrm{O_2}}$	5.4 mbar
Water	H_2O	Karl Fischer titration	$x_{\mathrm{H_2O}}^{(\mathrm{m})}$	0.02 g g^{-1}

The uncertainties of the results from wet-chemistry are specified from average deviation from repeated measurements including the weighing error and are 0.02 g g^{-1} for the mass fraction of water $x_{H_2O}^{(m)}$ and 0.01 g g^{-1} for the mass fraction of formaldehyde $x_{FA}^{(m)}$. Reaction products of FA, i.e., hemiformal, hemiformal hydroperoxide, and methylene glycol are not evaluated quantitatively but are reported by the overall concentration of formaldehyde. The uncertainty of the mass fractions of the products obtained from quantitative NMR spectroscopy $x_i^{(m)}$ is derived from the deviation between the results from ^{1}H and ^{13}C NMR spectra including the weighing error and is 0.01 g g^{-1}. Finally, the uncertainty of the measurement results in the gaseous fraction from gas chromatography on the partial pressure p_i are the root mean squared error from linear regression of the calibration data. Further details on the measurement methods, i.e., wet-chemistry, NMR spectroscopy, and gas chromatography, are given in Appendix B.2 to B.4.

B.2 Wet-chemistry

The Karl Fischer titration to determine the overall mass fraction of water in the condensable fraction was carried out with an 870 KF Titrino plus from Metrohm. To carry out the measurement at an optimum pH value, either Hydranal imidazole or Hydranal composite 5 from Honeywell was added to the titration solution. The sodium sulfite titration method to determine the overall mass fraction of formaldehyde in the condensable fraction was carried out with a 916 TI-Touch from Metrohm.

B.3 NMR Spectroscopy

B.3.1 Acquisition and Processing Parameters

Quantitative NMR spectra were recorded with a ^{1}H standard sequence and ^{13}C inverse-gated ^{1}H-decoupled (hereafter referred to as ^{13}C) pulse sequence. These sequences ensure that the peak areas are proportional to the mole numbers of the corresponding functional groups. Table B.2 lists the NMR acquisition and processing parameters used in this work.

Table B.2: Acquisition and processing parameters of the quantitative NMR experiments.

	^{1}H	^{13}C
Acquisition parameters		
Temperature / K	303.15	303.15
Pulse program	zg	zgig
Decoupling sequence	-	Waltz16
Number of scans	8 … 32	400 … 1024
Flip angle / °	10	30
Excitation frequency offset / ppm	7	120
Sweep width / ppm	16	260
Relaxation delay / s	60	120
Acquisition time / s	5	2.6
Acquired size / kB	44	64
Processing parameters		
Apodization / Hz	none	0.3 … 1
Zero filling / kB	64	256

To ensure quantitative measurements, the sum of acquisition time and relaxation delay at a 90° flip angle should be five times the relaxation time (T_1). The longest relaxation time was measured for the carboxylate ester group of MeFo, which was about 8 s of the ^{1}H and about 30 s of the ^{13}C NMR experiment, such that quantitative measurement is ensured with the set relaxation delays and flip angles.

B.3.2 Structure Elucidation

The quantitative ^{1}H and ^{13}C NMR spectra for the sample of the condensable fraction of experiment 15 are presented in Section 2.4.3. Four additional types of NMR spectra were acquired for the structure elucidation of the products in the CT samples: ^{13}C DEPT-135; ^{13}C without ^{1}H decoupling; ^{1}H,^{13}C HSQC; and ^{1}H,^{13}C HMBC. Figure B.1 to Figure B.4 show the four additional NMR spectra of the sample of the condensable fraction of experiment 15, see Appendix G, Table G.3. For an overview on labels and peak assignment to the components, see Table 3 in Section 2.4.3. Peaks that have not been assigned to a component are labeled with a question mark (?) and peaks labeled with an asterisk (*) are ^{13}C satellites. 1,4-dioxane (S) is used as internal standard.

Figure B.1 is a ^{13}C DEPT-135 (Distortionless Enhancement by Polarization Transfer) NMR spectrum. With the specific sequence of pulses used in this technique one can tell how many H atoms are bound to a C atom based on the peak intensity: a positive intensity corresponds to either a CH or a CH_3 group, a negative intensity corresponds to a CH_2 group. If the intensity equals zero in the spectrum, this corresponds to no H atom bound to the C atom. Figure B.2 shows the ^{13}C NMR spectrum without ^{1}H-decoupling, where additionally C atoms are detected, which have no H atom. The multiplicity of a peak depends on how many H atoms are directly bound to a C atom: a singlet corresponds to no H atom bound to the C atom, a doublet to one, a triplet to two and so forth. Figure B.3 shows the ^{1}H,^{13}C HSQC (Heteronuclear Single Quantum Coherence) NMR spectrum. With this two-dimensional NMR technique single bond correlations between ^{1}H and ^{13}C are visualized topographically, so that one can tell which peaks in the ^{1}H and ^{13}C NMR spectra correspond to atoms that are only one bond length apart from each other in the same molecule. Figure B.4 shows the ^{1}H,^{13}C HMBC (Heteronuclear Multiple Bond Correlation) NMR spectrum. With this two-dimensional NMR technique one can tell which peaks in the ^{1}H and

^{13}C NMR spectra correspond to atoms that are two, three, and sometimes even four bonds apart from each other in the same molecule.

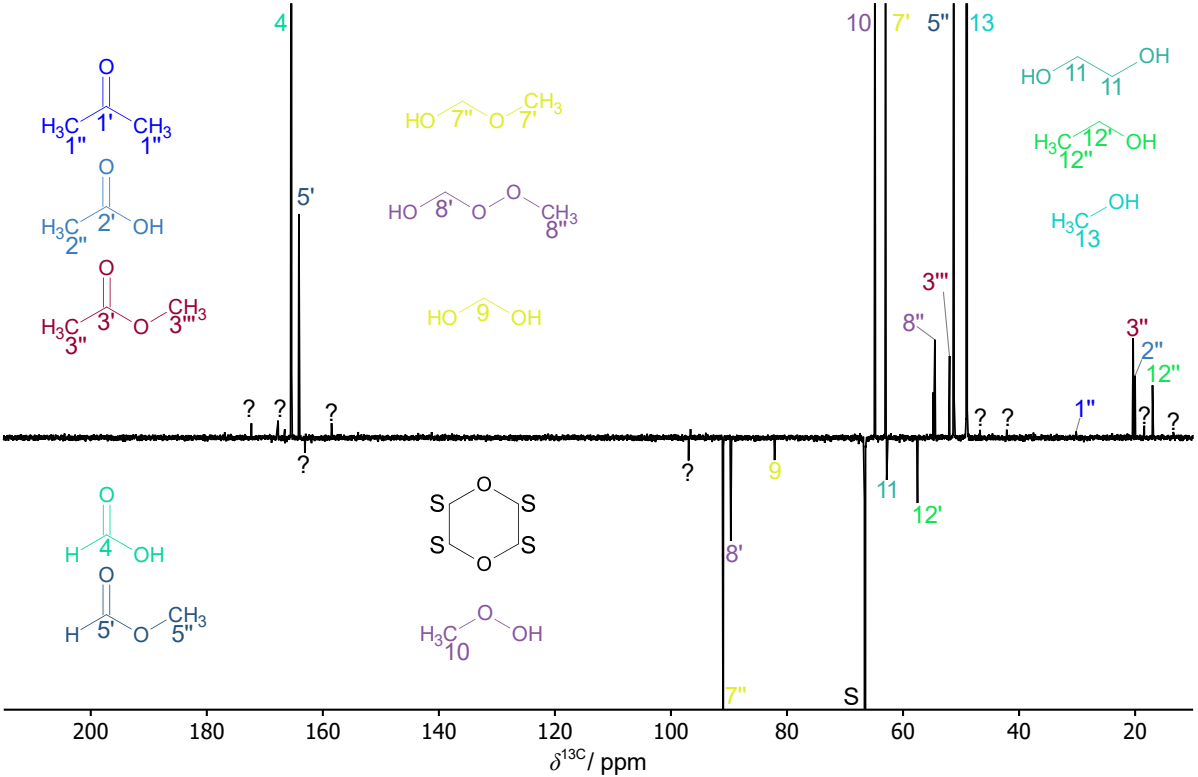

Figure B.1: ^{13}C DEPT-135 NMR spectrum of the sample of the condensable fraction of experiment 15. The full intensities of some peaks are truncated for better visibility.

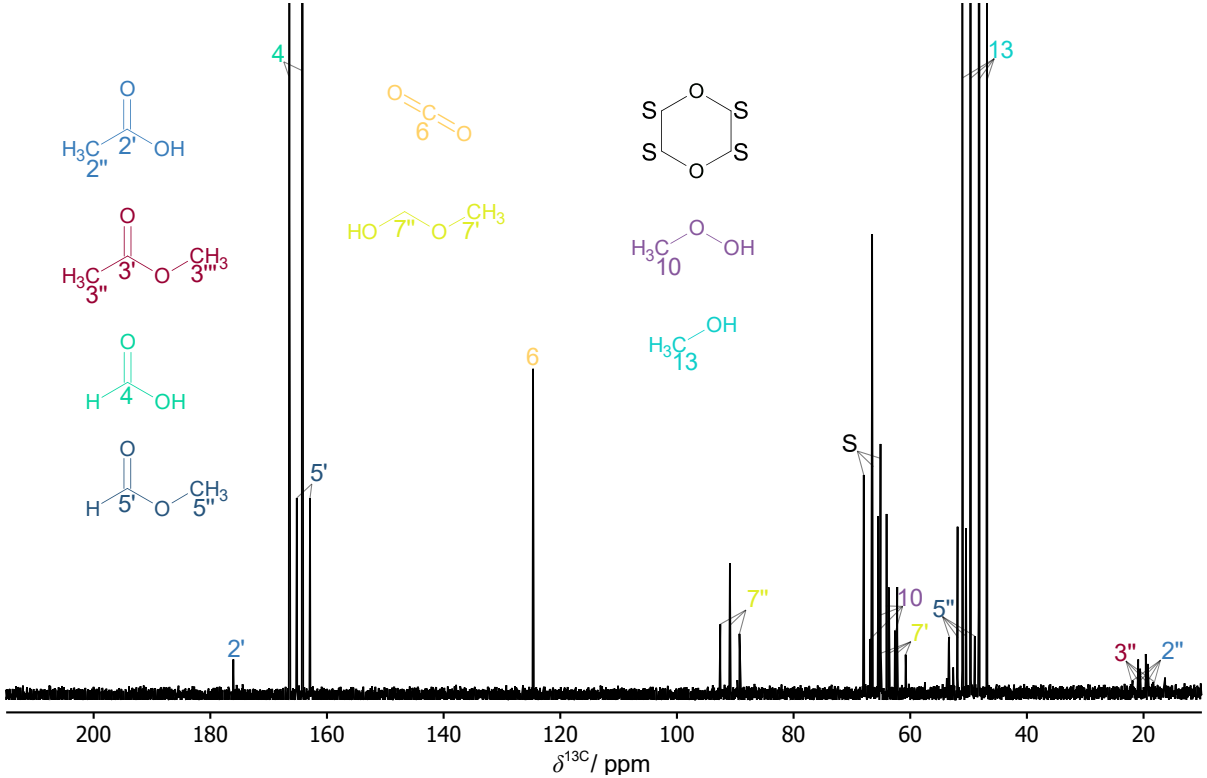

Figure B.2: ^{13}C without ^{1}H decoupling NMR spectrum of the sample the condensable fraction of experiment 15. The full intensities of some peaks are truncated for better visibility.

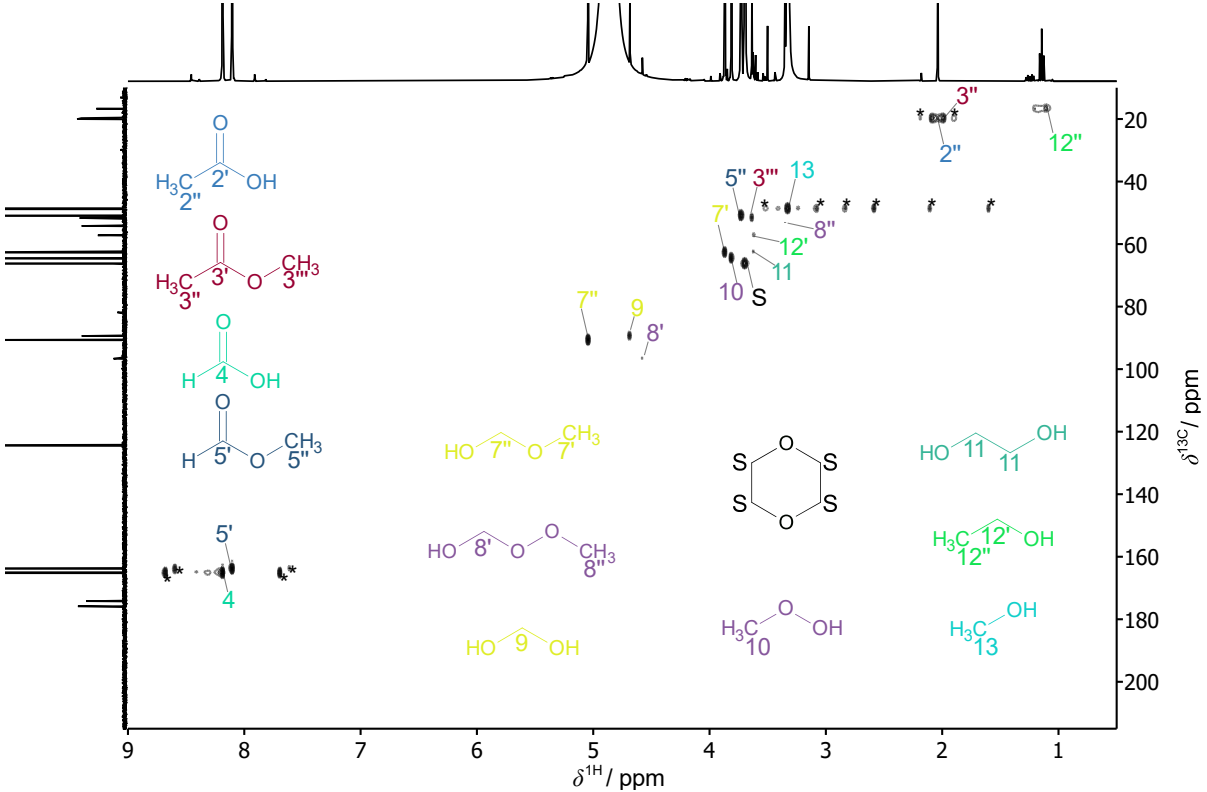

Figure B.3: ^{1}H,^{13}C HSQC NMR spectrum of the sample of the condensable fraction of experiment 15.

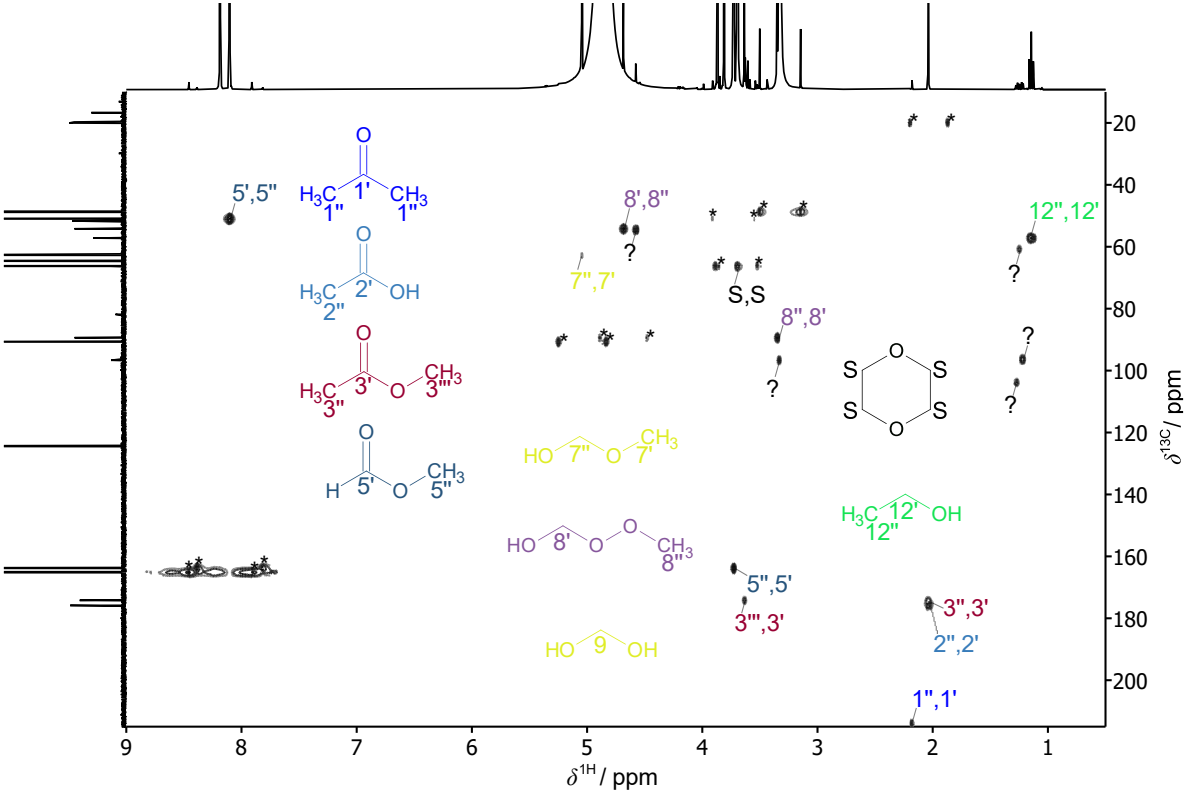

Figure B.4: ^{1}H,^{13}C HMBC NMR spectrum of the sample of the condensable fraction of experiment 15.

As the spectra of the samples of the condensable fraction were sufficiently alike it was not necessary to acquire all four additional types of NMR spectra, i.e., ^{13}C DEPT-135; ^{13}C without ^{1}H decoupling; ^{1}H,^{13}C HSQC; and ^{1}H,^{13}C HMBC, for every sample of the condensable fraction. For comparison, two more sets of ^{1}H and ^{13}C NMR spectra are provided in Figure B.5 to Figure B.8. Hence, only ^{1}H and ^{13}C NMR spectra were acquired for the quantitative analysis. These spectra correspond to the samples of the condensable fraction of experiments 3 and 43, see Appendix G, Table G.3. Again, an overview on labels and peak assignment to the components is presented in Table 3 in Section 2.4.3. Peaks that have not been assigned to a component are labeled with a question mark (?) and peaks labeled with an asterisk (*) are ^{13}C satellites. 1,4-dioxane (S) is used as internal standard. It should be noted, that the -OH peak has shifted compared to other experiments, which may be due to a shift in pH value.

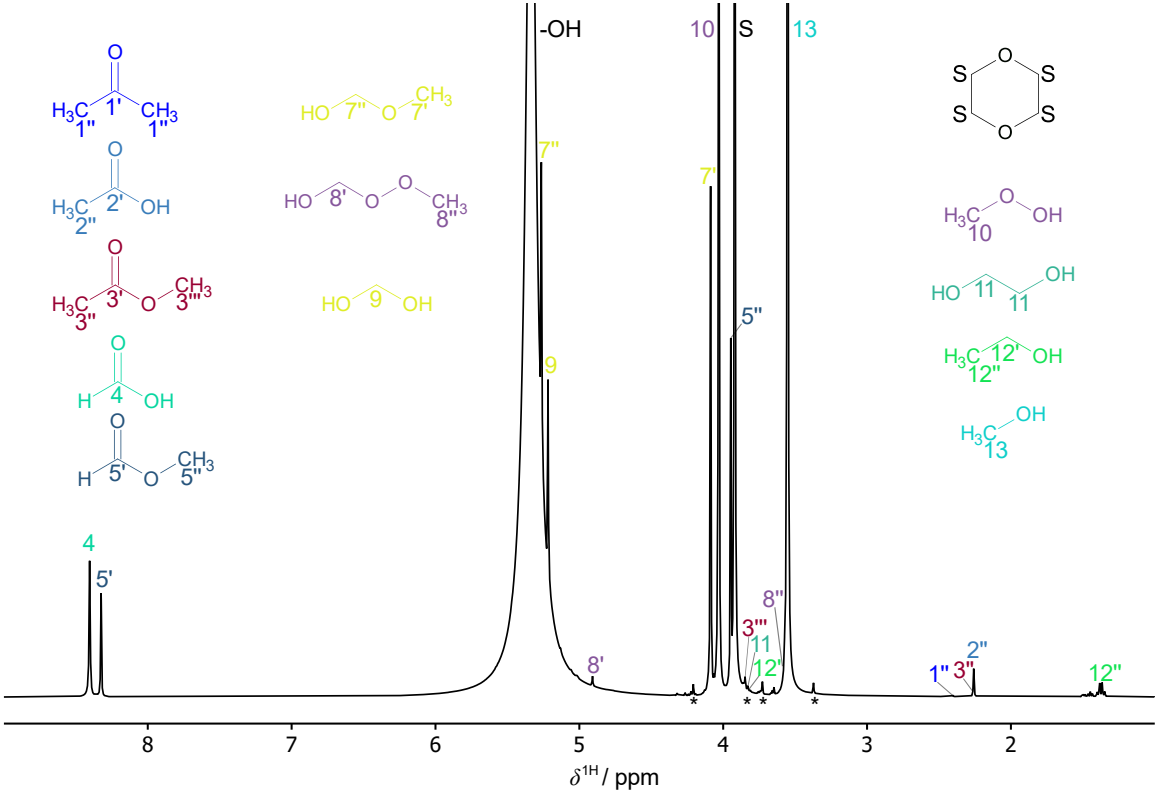

Figure B.5: ^{1}H NMR spectrum of the sample of the condensable fraction of experiment 3. The full intensities of some peaks are truncated for better visibility.

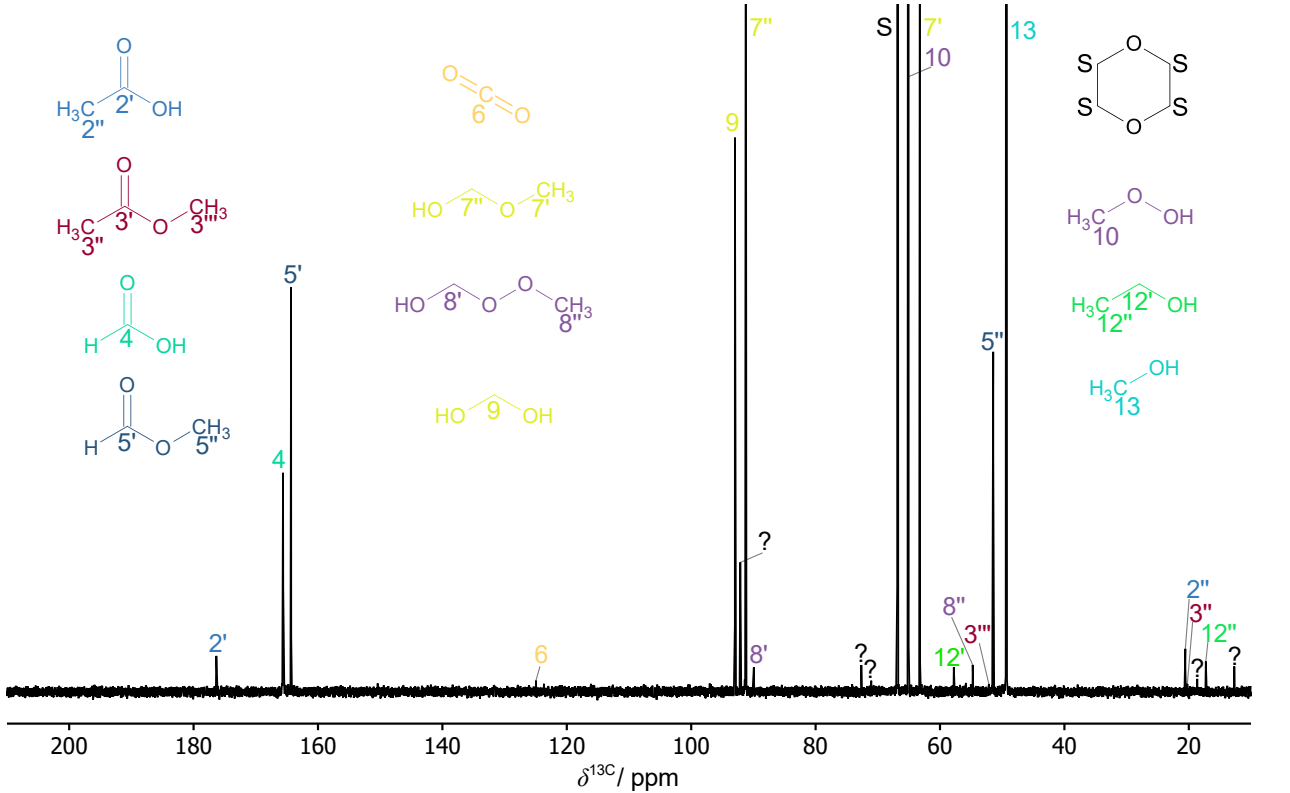

Figure B.6: ^{13}C NMR spectrum of the sample of the condensable fraction of experiment 3. The full intensities of some peaks are truncated for better visibility.

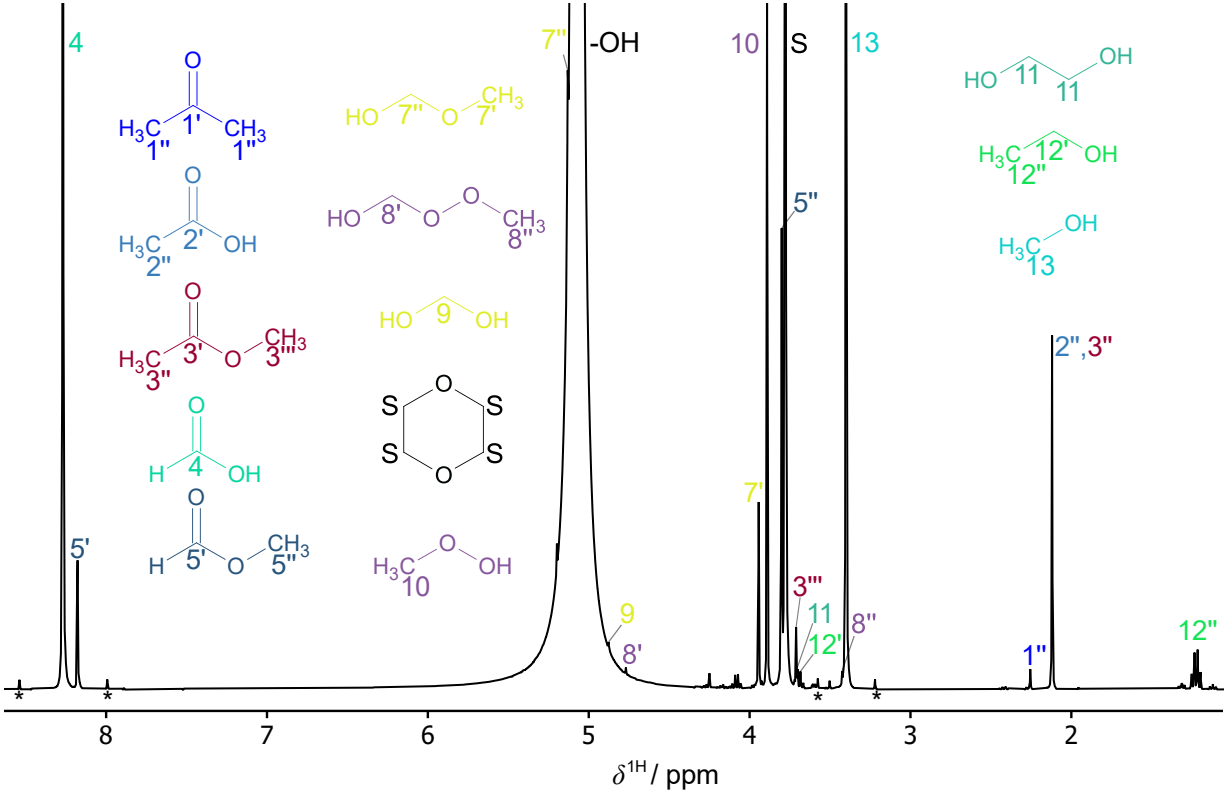

Figure B.7: ^{1}H NMR spectrum of the sample of the condensable fraction of experiment 43. The full intensities of some peaks are truncated for better visibility.

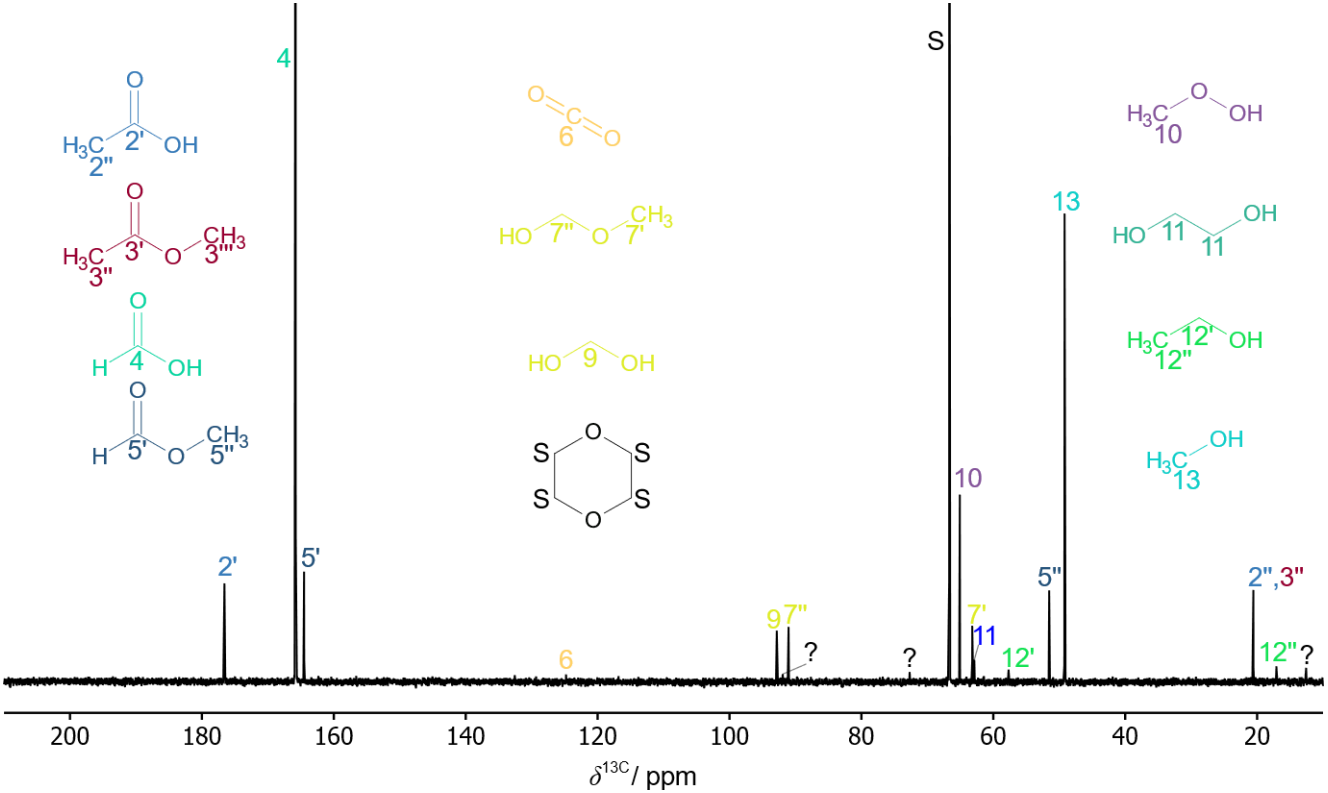

Figure B.8: ^{13}C NMR spectrum of the sample of the condensable fraction of experiment 43. The full intensities of some peaks are truncated for better visibility.

B.4 Gas Chromatography

B.4.1 Acquisition Parameters and Specification of the Methods

The gas chromatograph used in this work detects the components with a thermal conductivity detector. The measuring principle is based on the difference in thermal conductivity between two measuring chambers, one with pure carrier gas and one with the carrier gas including the sample [80]. The carrier gas helium yields good results for a majority of product components, except for the detection of hydrogen, as the thermal conductivity of helium (0.209 W $(m\ K)^{-1}$, [81]) is too close to that of hydrogen (0.246 W $(m\ K)^{-1}$, [81]) in the range of interest at 1 bar and 473.5 K. Hence, the approach was to use two carrier gases, i.e., helium (He) and nitrogen (N_2). Nitrogen was selected as the carrier gas for hydrogen analysis. Table B.3 shows the acquisition parameters of Method 1 (carrier gas: He) and Method 2 (carrier gas: N_2) used for the gas chromatographic analysis in the present work.

Table B.3: Acquisition parameters of the gas chromatographic analysis methods.

Parameter	Method 1	Method 2
Carrier gas	He	N_2
Inlet temperature / K	423.15	423.15
Inlet pressure / bar	0.7	0.6
Total volume flow / ml min^{-1}	87	120
Split ratio	30:1	50:1
Initial oven temperature / K	313.15	313.15
Initial hold time / min	20	21
1^{st} oven temperature / K	333.15	-
1^{st} hold time / min	13.5	-
Detector temperature / K	473.15	523.15

B.4.2 Retention Times and Quantitative Evaluation

The GC was equipped with a dual column from Agilent (GC: Series 6890, column: CP7430 comprised of PoraBOND Q and Molsieve 5 Å) so that, in general, there are two signals in the chromatograms per component and per method. To assign these signals, their retention times were compared to the retention times of known components. External reference gases used in this work are CO_2, H_2, CO, C_2H_6, and C_2H_4. While calibrations of these components are conducted in *calibration mode*, the calibrations of the feed gases Ar, CH_4, and O_2 are conducted in *sampling mode* without operation of plasma.

Figure B.9 and Figure B.10 show the chromatograms and
Table B.**4** shows the corresponding retention times and assigned components from the GC analysis of the gaseous product stream obtained from experiment 15, see Appendix G, Table G.3.

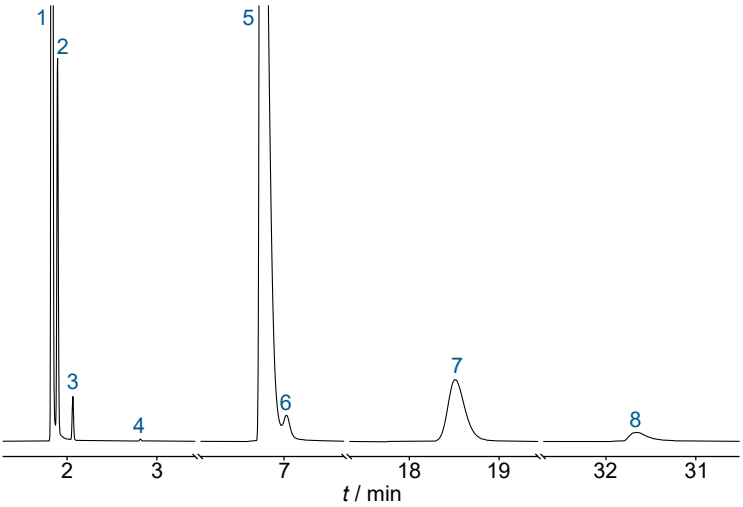

Figure B.9: Chromatogram from Method 1 of the gaseous fraction of the product stream of experiment 15. The full intensities of some peaks are truncated for better visibility.

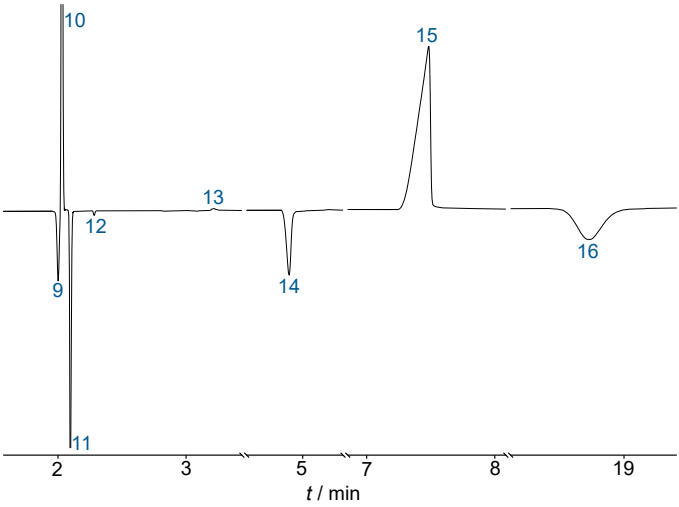

Figure B.10: Chromatogram from Method 2 of the gaseous fraction of the product stream of experiment 15. The full intensities of some peaks are truncated for better visibility.

Table B.4: Overview on retention times of the different components and their calibration factors k_i of Methods 1 and 2.

Signal	t / min	Component	k_i / mbar (µVs)$^{-1}$
Method 1			
1	1.8	H_2, O_2, Ar, CO	-
2	1.9	CH_4	-
3	2.1	CO_2	1.0
-	2.4	C_2H_4	1.0
4	2.8	C_2H_6	1.0
-	4.4	H_2	99.0
5	6.7	Ar	0.6
6	7.0	O_2	0.6
7	18.5	CH_4	0.8
8	31.3	CO	0.7
Method 2			
9	2.0	H_2, O_2	-
10	2.0	Ar	-
11	2.1	CH_4	-
12	2.3	C_2H_4	2.3
13	3.2	C_2H_6	0.5
14	4.7	H_2	0.3
15	7.5	Ar	2.2
-	7.6	O_2	9.1
16	18.7	CH_4	0.8

In
Table B.**4**, unnumbered signals are not visible in the chromatograms shown in Figure B.9 and Figure B.10. Signals without calibration factor have not been evaluated quantitatively.

The components CO_2, C_2H_6, and C_2H_4 have only one signal in each method since they do not elute from the Molsieve 5Å column but are adsorbed by it. For H_2, O_2, Ar, CO, and CH_4, the first signals in the chromatograms of both methods coincide at a

retention time of about 2 min and, thus, are hard to integrate. For the quantitative analysis of these components, only the areas from the second signals at a higher retention time are used. When more than one area was available for quantitative evaluation, the average was calculated. This was except for O_2, for which the calibration factor in Method 2 was subject to significantly higher uncertainties than with Method 1. In Method 2, some areas were negative. Interestingly, the area of C_2H_6 changes from positive to negative at high concentrations. This phenomenon has already been described for hydrogen [82, 83]. For H_2, the results from Method 1 were exclusively used for the quantification in experiments 2 – 5 and 8 – 10, as the detection limit was 0.02 mol mol^{-1}.

B.5 Stability of the Condensable Fraction

The time stability was analyzed for the condensable fraction from an experiment with a residence time of 4.7 s and an electrical power input of 26 W, corresponding to a specific energy input SEI^* of 19.2 J cm^{-3}. The sample was stored in the NMR sample tube at room temperature for 14 weeks and analyzed by NMR spectroscopy at different lifetimes of the sample. Figure B.11 shows the results of normalized, true mass fractions of the components FAc, MeOH, MeOOH, water and CO_2 over the sample lifetime.

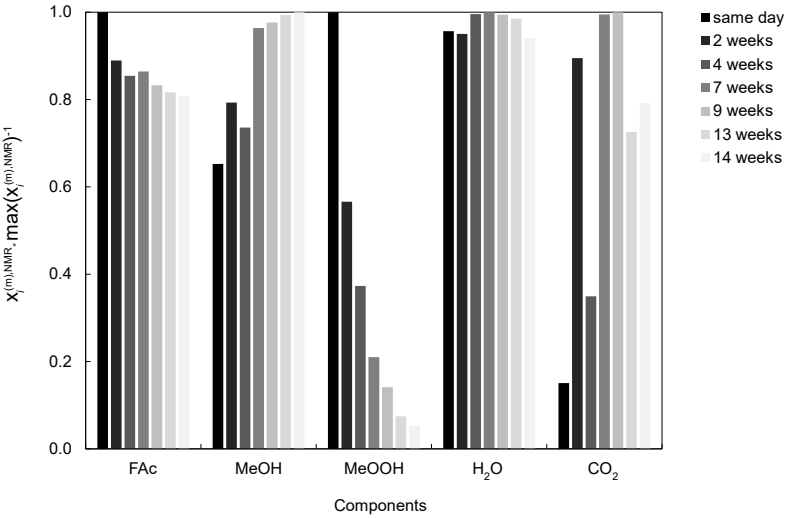

Figure B.11: Normalized, true mass fractions of the components FAc, MeOH, MeOOH, H_2O, and CO_2 as a function of the sample lifetime.

The mass fractions of FAc and MeOOH decrease and the mass fractions of MeOH and CO_2 increase with increasing lifetime of the sample of the condensable fraction and almost no change was detected for H_2O. These observations can be attributed to subsequent reactions in the condensable fraction following the oxidation of methane in the cold plasma. Accordingly, the significant reduction in the mass fraction of MeOOH might occur due to the radical decomposition of MeOOH. The decomposition of MeOOH can also lead to the formation of MeOH, for which an increasing mass fraction is observed with increasing lifetime of the sample. The decreasing mass fractions of FAc might occur due to reactions with peroxides, from which CO_2 and H_2O are formed. This assumption is supported by the increase in the mass fraction of CO_2.

C Influence of Argon

C.1 Conversions

The individual results on the conversion X_j of the reactants CH_4 and O_2 at three different CH_4:O_2 ratios are plotted against *SEI* in Figure C.1.

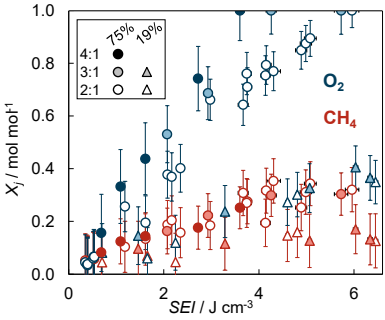

Figure C.1: Conversions of CH_4 and O_2 of individual experiments plotted against *SEI* at CH_4:O_2 ratios of 2:1 (open symbols), 3:1 (light filled symbols), and 4:1 (dark filled symbols) and at argon mole fractions x_{Ar}^{in} of 0.75 mol mol^{-1} (circles) and 0.19 mol mol^{-1} (triangles).

C.2 Selectivities

C.2.1 H-Selectivity to Products without Carbon

Figure C.2 shows the results for the H-selectivity to products without carbon (H_2O and H_2) of individual experiments plotted against *SEI*.

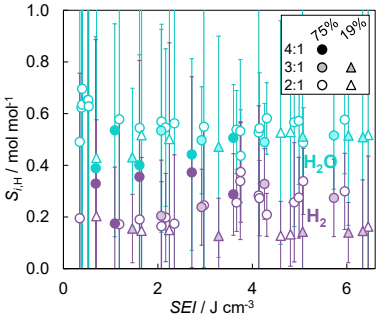

Figure C.2: H-selectivities to H_2O and H_2 of individual experiments plotted against *SEI* at CH_4:O_2 ratios of 2:1 (open symbols), 3:1 (light filled symbols), and 4:1 (dark filled symbols) and at argon mole fractions x_{Ar}^{in} of 0.75 mol mol^{-1} (circles) and 0.19 mol mol^{-1} (triangles).

C.2.2 C-Selectivity to Products without Hydrogen

Figure C.3 shows the results for the C-selectivity to products without hydrogen (CO and CO_2) of individual experiments plotted against *SEI*.

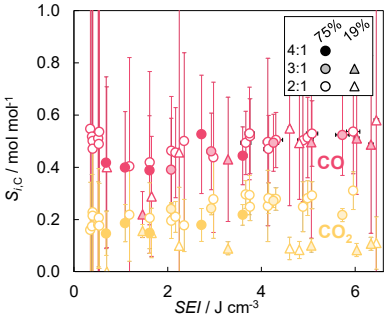

Figure C.3: C-selectivities to CO and CO_2 of individual experiments plotted against *SEI* at CH_4:O_2 ratios of 2:1 (open symbols), 3:1 (light filled symbols), and 4:1 (dark filled symbols) and at argon mole fractions x_{Ar}^{in} of 0.75 mol mol^{-1} (circles) and 0.19 mol mol^{-1} (triangles).

C.2.3 C-Selectivity to Products without Oxygen

Figure C.4 shows the results for the C-selectivity to products without oxygen (C_2H_6 and C_2H_4) of individual experiments plotted against *SEI*.

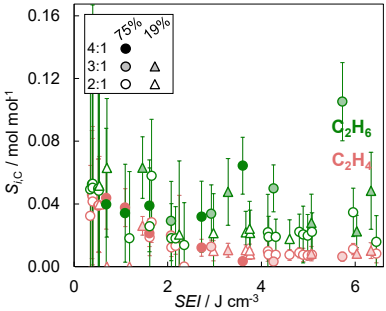

Figure C.4: C-selectivities to C_2H_6 and C_2H_4 of individual experiments plotted against *SEI* at CH_4:O_2 ratios of 2:1 (open symbols), 3:1 (light filled symbols), and 4:1 (dark filled symbols) and at argon mole fractions x_{Ar}^{in} of 0.75 mol mol^{-1} (circles) and 0.19 mol mol^{-1} (triangles).

C.2.4 C-Selectivity to Products that Contain One Carbon and Hydrogen and Oxygen

Figure C.5 shows the results for the C-selectivity to products that contain one carbon and hydrogen and oxygen (MeOH, MeOOH, FA, and FAc) of individual experiments plotted against *SEI*.

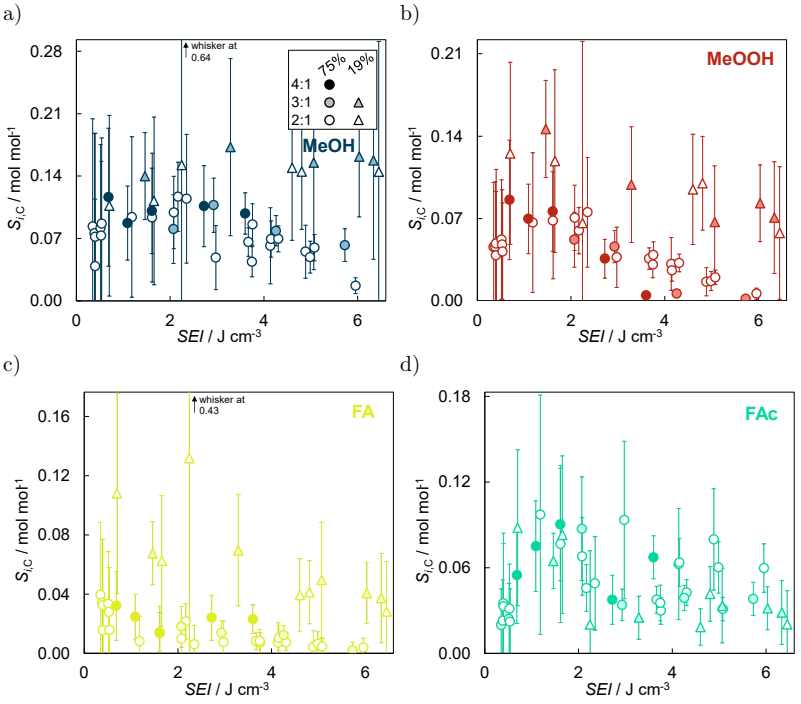

Figure C.5: C-selectivities to a) MeOH, b) MeOOH, c) FA, and d) FAc of individual experiments plotted against *SEI* at CH_4:O_2 ratios of 2:1 (open symbols), 3:1 (light filled symbols), and 4:1 (dark filled symbols) and at argon mole fractions x_{Ar}^{in} of 0.75 mol mol^{-1} (circles) and 0.19 mol mol^{-1} (triangles).

C.2.5 C-Selectivity to Products that Contain More than One Carbon Atom and Hydrogen and Oxygen

Figure C.6 shows the results for the C-selectivity to products that contain more than one carbon atom and hydrogen and oxygen (MeFo, EtOH, HAc, MeAc, Ace, and EG) of individual experiments plotted against *SEI*.

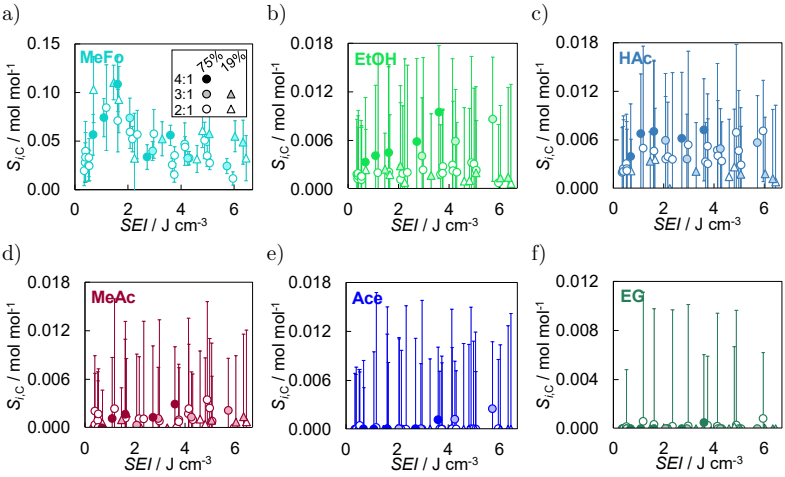

Figure C.6: C-selectivities to a) MeFo, b) EtOH, c) HAc, d) MeAc, e) Ace, and f) EG of individual experiments plotted against *SEI* at CH_4:O_2 ratios of 2:1 (open symbols), 3:1 (light filled symbols), and 4:1 (dark filled symbols) and at argon mole fractions x_{Ar}^{in} of 0.75 mol mol^{-1} (circles) and 0.19 mol mol^{-1} (triangles).

D Individual Results

D.1 Conversions

For comparison, the individual results on the conversion X_j of the reactants CH_4 and O_2 at three different CH_4:O_2 ratios and at argon mole fractions x_{Ar}^{in} of 0.75 mol mol^{-1} and 0.19 mol mol^{-1} are plotted in Figure D.1 in the same manner as in Section 3.4.

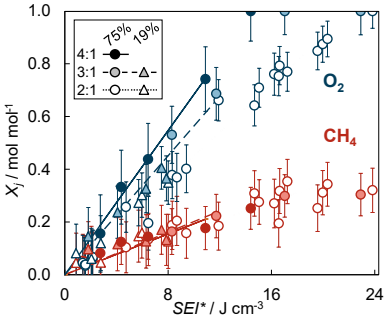

Figure D.1: Conversions of CH_4 and O_2 of individual experiments at CH_4:O_2 ratios of 2:1 (open symbols), 3:1 (light filled symbols), and 4:1 (dark filled symbols) and argon mole fractions x_{Ar}^{in} of 0.75 mol mol^{-1} (circles) and 0.19 mol mol^{-1} (triangles). The lines were obtained from a linear fit to the data in the region below full conversion of oxygen through the origin as a guide to the eye.

The SEI^* for which full conversion of O_2 is reached SEI^*_{FC,O_2} is shown as a function of the CH_4:O_2 ratio in Figure D.2. The values were obtained from the linear fits to the data for the conversion of O_2 shown in Figure D.1. Statistical uncertainties shown as error bars were obtained from the uncertainties of the linear fits.

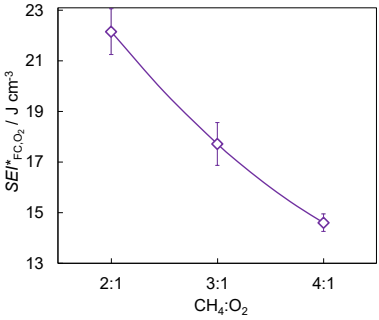

Figure D.2: SEI^* for which full conversion of oxygen is reached SEI^*_{FC,O_2} as a function of the CH_4:O_2 ratio. The line is a guide to the eye.

D.2 Selectivities

For comparison, the individual results on the selectivities to the product components at three different CH_4:O_2 ratios and at argon mole fractions x^{in}_{Ar} of 0.75 mol mol^{-1} and 0.19 mol mol^{-1} are plotted in Figure E.3 (H-selectivities $S_{i,H}$ to H_2O and H_2), Figure E.4 (C-selectivities $S_{i,C}$ to CO and CO_2), Figure E.5 (C-selectivities $S_{i,C}$ to C_2H_6 and C_2H_4), Figure E.6 (C-selectivities $S_{i,C}$ to MeOH, MeOOH, FA, and FAc), and Figure E.7 (C-selectivities $S_{i,C}$ to MeFo, EtOH, HAc, MeAc, Ace, and EG) in the same manner as in Section 3.5. In these Figures, error bars indicate the uncertainty calculated from the analytical uncertainties with error propagation.

D.2.1 H-Selectivity to Products without Carbon

Figure D.3 shows the results for the H-selectivity to products without carbon (H_2O and H_2).

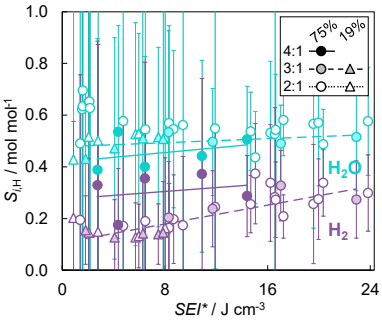

Figure D.3: H-selectivities to H_2O and H_2 of individual experiments at CH_4:O_2 ratios of 2:1 (open symbols), 3:1 (light filled symbols), and 4:1 (dark filled symbols) and argon mole fractions x_{Ar}^{in} of 0.75 mol mol^{-1} (circles) and 0.19 mol mol^{-1} (triangles). The lines were obtained from a linear fit to the data as a guide to the eye.

D.2.2 C-Selectivity to Products without Hydrogen

Figure D.4 shows the results for the C-selectivity to products without hydrogen (CO and CO_2).

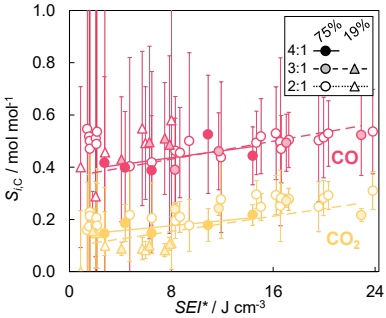

Figure D.4: C-selectivities to CO and CO_2 of individual experiments at CH_4:O_2 ratios of 2:1 (open symbols, dotted line), 3:1 (light filled symbols, dashed line), and 4:1 (dark filled symbols, solid line) and argon mole fractions x_{Ar}^{in} of 0.75 mol mol^{-1} (circles) and 0.19 mol mol^{-1} (triangles). The lines were obtained from a linear fit to the data as a guide to the eye.

D.2.3 C-Selectivity to Products without Oxygen

Figure D.5 shows the results for the C-selectivity to products without oxygen (C_2H_6 and C_2H_4).

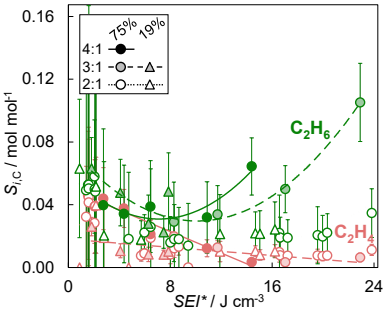

Figure D.5: C-selectivities to C_2H_6 and C_2H_4 of individual experiments at CH_4:O_2 ratios of 2:1 (open symbols, dotted line), 3:1 (light filled symbols, dashed line), and 4:1 (dark filled symbols, solid line) and argon mole fractions x_{Ar}^{in} of 0.75 mol mol^{-1} (circles) and 0.19 mol mol^{-1} (triangles). The lines were obtained from a polynomial fit to the data of C_2H_6 and a linear fit to the data of C_2H_4 as a guide to the eye.

D.2.4 C-Selectivity to Products that Contain One Carbon Atom and Hydrogen and Oxygen

Figure D.6 shows the results for the C-selectivity to products that contain one carbon atom and hydrogen and oxygen (MeOH, MeOOH, FA, and FAc).

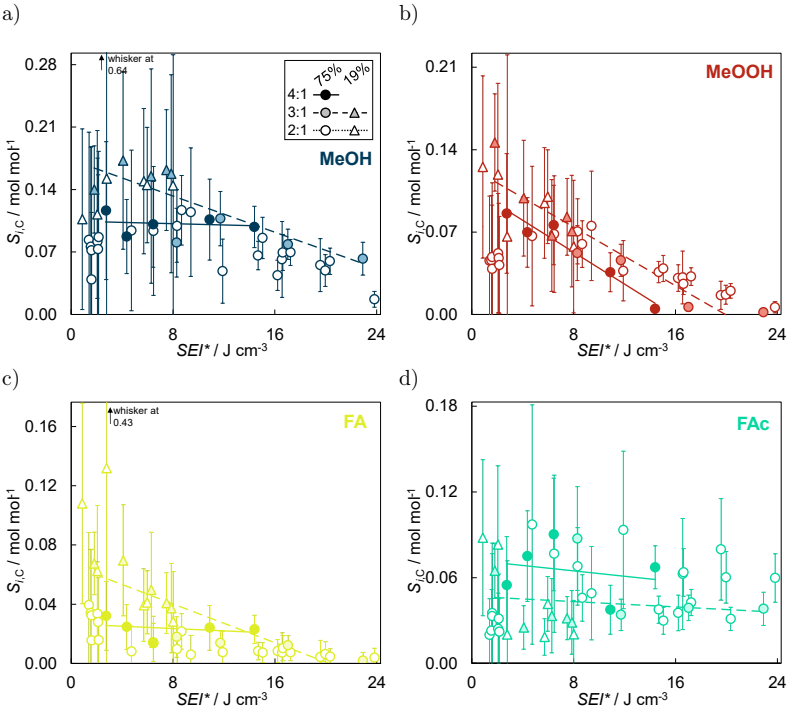

Figure D.6: C-selectivities to a) MeOH, b) MeOOH, c) FA, and d) FAc of individual experiments at CH_4:O_2 ratios of 2:1 (open symbols, dotted line), 3:1 (light filled symbols, dashed line), and 4:1 (dark filled symbols, solid line) and argon mole fractions x_{Ar}^{in} of 0.75 mol mol^{-1} (circles) and 0.19 mol mol^{-1} (triangles). The lines were obtained from a linear fit to the data as a guide to the eye.

D.2.5 C-Selectivity to Products that Contain More than One Carbon Atom and Hydrogen and Oxygen

Figure D.7 shows the results for the C-selectivity to products that contain more than one carbon atom and hydrogen and oxygen (MeFo, EtOH, HAc, MeAc, Ace, and EG) of individual experiments plotted against *SEI**.

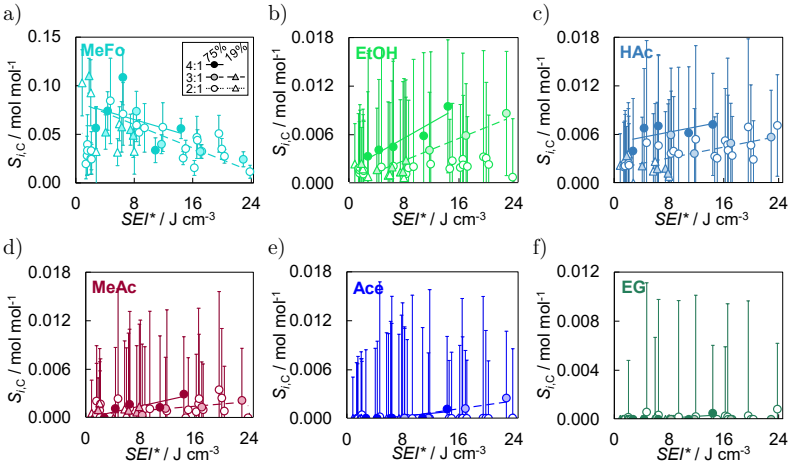

Figure D.7: C-selectivities to a) MeFo, b) EtOH, c) HAc, d) MeAc, e) Ace, and f) EG of individual experiments at CH_4:O_2 ratios of 2:1 (open symbols, dotted line), 3:1 (light filled symbols, dashed line), and 4:1 (dark filled symbols, solid line) and argon mole fractions x_{Ar}^{in} of 0.75 mol mol^{-1} (circles) and 0.19 mol mol^{-1} (triangles). The lines were obtained from a linear fit to the data as a guide to the eye.

E Results without a High Temperature Difference

E.1 General Remarks

From a total of 43 experiments conducted, 14 experiments showed a high temperature difference, i.e., T^{in} - T^{out}, between inlet and outlet of the reactor of more than 10 K, see Appendix G, Table G.3. The high temperature difference only occurred for experiments with a residence time of $\tau < 2$ s, but not for all of those. From a principal component analysis, the best correlation of the temperature difference was found for the ratio ξ which is defined as

$$\xi = \frac{\tau}{P^2} \tag{12}$$

where P is the electrical power input. The dependency of the temperature difference on ξ is plotted in Figure E.1.

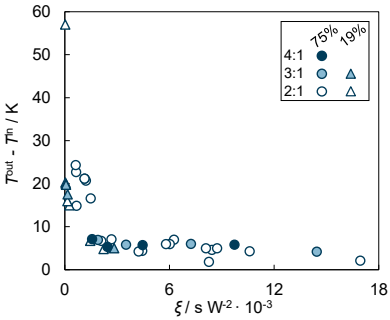

Figure E.1: Temperature difference between outlet and inlet of the reactor of the individual experiments as a function of ξ at CH_4:O_2 ratios of 2:1 (open symbols), 3:1 (light filled symbols), and 4:1 (dark filled symbols) and argon mole fractions x_{Ar}^{in} of 0.75 mol mol^{-1} (circles) and 0.19 mol mol^{-1} (triangles).

It is not intended to claim that this correlation has a physical background. A sound analysis would require a thermal modelling of the reactor and the reaction network. Furthermore, for an investigation of thermal effects, other experimental set-ups might have been more appropriate than the present one.

However, the following comparison in Sections E.2 and E.3 shows that when the data of experiments with a higher temperature difference are excluded in the results, basically the same trends as in the main document are observed. For comparison, the lumped results excluding those experiments with a high temperature difference (i.e., $\Delta T > 10$ K) are plotted in the same manner as in Section 3.4 and Section 3.5.

E.2 Conversions

The lumped results on the conversion X_j of the reactants CH_4 and O_2 without a high temperature difference at three different CH_4:O_2 ratios are plotted in Figure E.2.

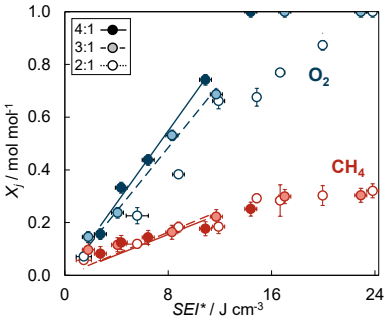

Figure E.2: Conversions of CH_4 and O_2 with $\Delta T < 10$ K at CH_4:O_2 ratios of 2:1 (open symbols), 3:1 (light filled symbols), and 4:1 (dark filled symbols). The lines were obtained from a linear fit to the data in the region below full conversion of oxygen through the origin as a guide to the eye.

E.3 Selectivities

E.3.1 H-Selectivity to Products without Carbon

Figure E.3 shows the results for the H-selectivity to products without carbon (H_2O and H_2) without a high temperature difference.

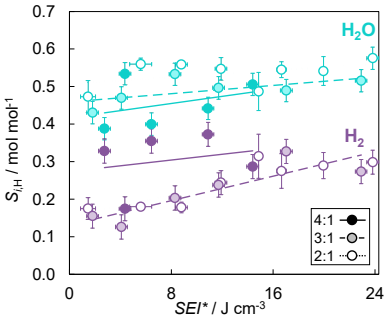

Figure E.3: H-selectivities to H_2O and H_2 with $\Delta T < 10$ K at CH_4:O_2 ratios of 2:1 (open symbols), 3:1 (light filled symbols), and 4:1 (dark filled symbols). The lines were obtained from a linear fit to the data as a guide to the eye.

E.3.2 C-Selectivity to Products without Hydrogen

Figure E.4 shows the results for the C-selectivity to products without hydrogen (CO and CO_2) without a high temperature difference.

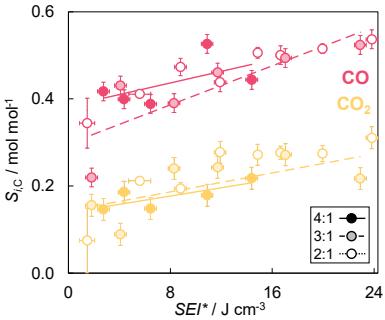

Figure E.4: C-selectivities to CO and CO_2 with $\Delta T < 10$ K at CH_4:O_2 ratios of 2:1 (open symbols), 3:1 (light filled symbols), and 4:1 (dark filled symbols). The lines were obtained from a linear fit to the data as a guide to the eye.

E.3.3 C-Selectivity to Products without Oxygen

Figure E.5 shows the results for the C-selectivity to products without oxygen (C_2H_6 and C_2H_4) without a high temperature difference.

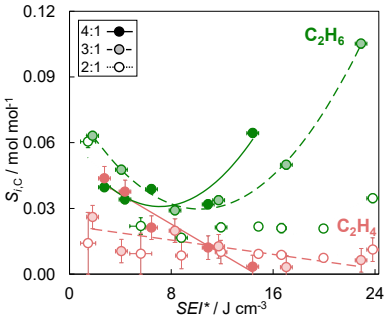

Figure E.5: C-selectivities to C_2H_6 and C_2H_4 with $\Delta T < 10$ K at CH_4:O_2 ratios of 2:1 (open symbols), 3:1 (light filled symbols), and 4:1 (dark filled symbols). The lines were obtained from a polynomial fit to the data of C_2H_6 and a linear fit to the data of C_2H_4 as a guide to the eye.

E.3.4 C-Selectivity to Products that Contain One Carbon and Hydrogen and Oxygen

Figure E.6 shows the results for the C-selectivity to products that contain one carbon and hydrogen and oxygen (MeOH, MeOOH, FA, and FAc) without a high temperature difference.

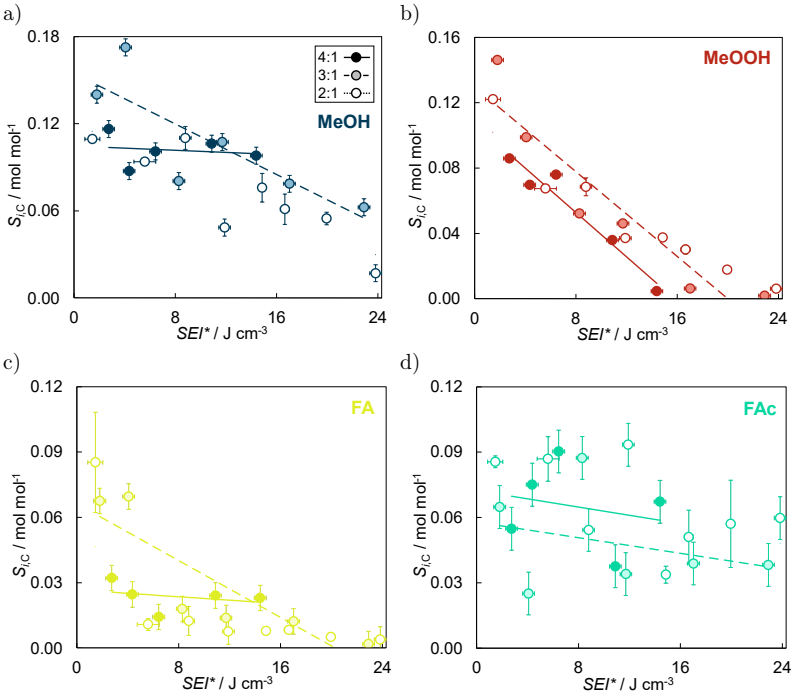

Figure E.6: C-selectivities to a) MeOH, b) MeOOH, c) FA, and d) FAc with $\Delta T < 10$ K at CH_4:O_2 ratios of 2:1 (open symbols), 3:1 (light filled symbols), and 4:1 (dark filled symbols). The lines were obtained from a linear fit to the data as a guide to the eye.

E.3.5 C-Selectivity to Products that Contain More than One Carbon Atom and Hydrogen and Oxygen

Figure E.7 shows the results for the C-selectivity to products that contain more than one carbon atom and hydrogen and oxygen (MeFo, EtOH, HAc, MeAc, Ace, and EG) without a high temperature difference.

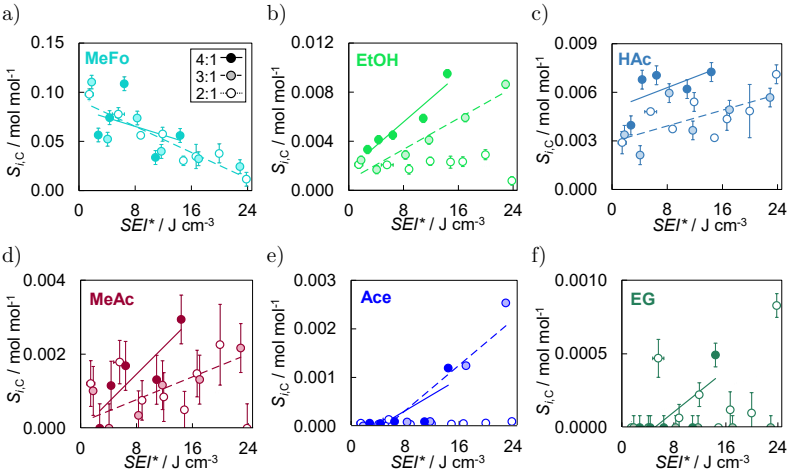

Figure E.7: C-selectivities to a) MeFo, b) EtOH, c) HAc, d) MeAc, e) Ace, and f) EG with $\Delta T < 10$ K at CH_4:O_2 ratios of 2:1 (open symbols), 3:1 (light filled symbols), and 4:1 (dark filled symbols). The lines were obtained from a linear fit to the data as a guide to the eye.

F Elemental Balance

An elemental balance was conducted for all elements e (carbon, hydrogen, and oxygen) and for all individual experiments. In case of a complete elucidation of the product stream, the difference of the molar flow of elements between inlet and outlet of the reactor (i.e., $\dot{n}_e^{\text{in}}$ - $\dot{n}_e^{\text{out}}$) would equal 0 for each element e. Hence, the value of ($\dot{n}_e^{\text{in}}$ - $\dot{n}_e^{\text{out}}$) represents the remaining molar flow of elements that have not been quantified by the analysis methods at the outlet of the reactor. Figure F.1 shows a) the molar flow $\dot{n}_e^{\text{in}}$ of carbon and oxygen at the inlet of the reactor and b) the difference of the molar flows of elements between inlet and outlet ($\dot{n}_e^{\text{in}}$ - $\dot{n}_e^{\text{out}}$) calculated from the elemental balance. In Figure F.1 panel a), the molar flow of hydrogen at the inlet of the reactor is not plotted as it is simply four times the flow of carbon. Additionally, at CH_4:O_2 ratios of 2:1, the molar flow of carbon and oxygen are equal. Since the symbols for carbon are plotted in the front, the ones for oxygen are not visible. In Figure F.1 panel b), the error bars indicate the uncertainty calculated from the analytical uncertainties with error propagation.

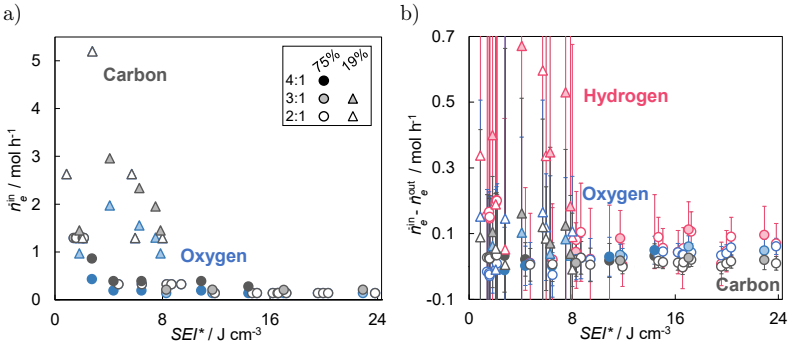

Figure F.1: a) Molar flow of elements at the inlet of the reactor $\dot{n}_e^{\text{in}}$ and b) difference of the molar flows of elements between inlet and outlet ($\dot{n}_e^{\text{in}}$ - $\dot{n}_e^{\text{out}}$) of the individual experiments at CH_4:O_2 ratios of 2:1 (open symbols), 3:1 (light filled symbols), and 4:1 (dark filled symbols) and argon mole fractions $x_{\text{Ar}}^{\text{in}}$ of 0.75 mol mol^{-1} (circles) and 0.19 mol mol^{-1} (triangles).

G Numerical Experimental Data

G.1 Lumped Experimental Data

Table G.1 lists the specific energy input *SEI**, the CH_4:O_2 ratio, and the conversion X_j of the reactants CH_4 and O_2 of the lumped results and the uncertainties calculated from standard deviation from average. Table G.2 lists the H-selectivities $S_{i,H}$ to the product components H_2 and H_2O and the C-selectivities $S_{i,C}$ to the product components CO and CO_2; C_2H_6 and C_2H_4; MeOH, MeOOH, FA, and FAc; and MeFo, EtOH, HAc, MeAc, Ace, and EG of the lumped results and the uncertainties calculated from standard deviation from average.

Table G.1: Overview on specific energy input *SEI**, CH_4:O_2 ratio, and conversion X_j of the reactants CH_4 and O_2 of the lumped results including the standard deviation from average.

Exp.	***SEI****	**CH_4:O_2**	X_{CH_4}	X_{O_2}
	J cm^{-3}	mol mol^{-1}	mol mol^{-1}	mol mol^{-1}
1	1.4 ± 0.3	2:1	0.048 ± 0.012	0.047 ± 0.011
2	2.2 ± 0.3		0.059 ± 0.027	0.074 ± 0.020
3	4.7 ± 0.3		0.104 ± 0.027	0.256 ± 0.020
4	6.0 ± 0.3		0.146 ± 0.027	0.257 ± 0.020
5	8.2 ± 0.2		0.157 ± 0.027	0.363 ± 0.020
6	9.0 ± 0.4		0.181 ± 0.015	0.385 ± 0.031
7	11.9 ± 0.3		0.185 ± 0.027	0.661 ± 0.020
8	14.9 ± 0.2		0.292 ± 0.027	0.676 ± 0.020
9	16.7 ± 0.4		0.284 ± 0.019	0.769 ± 0.014
10	20.0 ± 0.3		0.302 ± 0.027	0.873 ± 0.020
11	23.8 ± 0.3		0.320 ± 0.027	1.000 ± 0.020
12	1.8 ± 0.3	3:1	0.097 ± 0.027	0.146 ± 0.020
13	4.1 ± 0.3		0.115 ± 0.027	0.237 ± 0.020
14	6.9 ± 0.6		0.149 ± 0.016	0.366 ± 0.034
15	8.1 ± 0.2		0.148 ± 0.059	0.448 ± 0.015
16	11.7 ± 0.3		0.222 ± 0.027	0.686 ± 0.020
17	17.0 ± 0.3		0.299 ± 0.037	1.000 ± 0.018
18	22.9 ± 0.3		0.304 ± 0.027	1.000 ± 0.020
19	2.7 ± 0.3	4:1	0.082 ± 0.023	0.156 ± 0.031
20	4.4 ± 0.3		0.124 ± 0.023	0.332 ± 0.031
21	6.4 ± 0.3		0.144 ± 0.023	0.438 ± 0.031
22	10.9 ± 0.3		0.177 ± 0.023	0.742 ± 0.031
23	14.4 ± 0.3		0.252 ± 0.023	1.000 ± 0.031

Table G.2: Overview on H-selectivities $S_{i,H}$ and C-selectivities $S_{i,C}$ to the product components of the lumped results including the standard deviation from average. All values are given in mol mol^{-1}.

Exp.	$S_{H_2O,H}$	$S_{H_2,H}$	$S_{CO,C}$	$S_{CO_2,C}$	$S_{C_2H_6,C}$	$S_{C_2H_4,C}$	$S_{MeOH,C}$	$S_{MeOOH,C}$
1	0.574 ± 0.043	0.199 ± 0.029	0.487 ± 0.056	0.155 ± 0.074	0.054 ± 0.003	0.033 ± 0.014	0.075 ± 0.003	0.061 ± 0.003
2	0.590 ± 0.030	0.148 ± 0.032	0.456 ± 0.021	0.162 ± 0.025	0.046 ± 0.002	0.033 ± 0.005	0.101 ± 0.006	0.065 ± 0.003
3	0.577 ± 0.030	0.171 ± 0.032	0.404 ± 0.021	0.218 ± 0.025	0.018 ± 0.002	0.000 ± 0.005	0.094 ± 0.006	0.067 ± 0.003
4	0.533 ± 0.030	0.150 ± 0.032	0.487 ± 0.021	0.126 ± 0.025	0.022 ± 0.002	0.012 ± 0.005	0.129 ± 0.006	0.088 ± 0.003
5	0.543 ± 0.030	0.163 ± 0.032	0.522 ± 0.021	0.153 ± 0.025	0.017 ± 0.002	0.010 ± 0.005	0.122 ± 0.006	0.064 ± 0.003
6	0.554 ± 0.016	0.185 ± 0.009	0.478 ± 0.008	0.194 ± 0.006	0.016 ± 0.004	0.007 ± 0.009	0.116 ± 0.000	0.068 ± 0.001
7	0.549 ± 0.030	0.245 ± 0.032	0.438 ± 0.021	0.277 ± 0.025	0.021 ± 0.002	0.010 ± 0.005	0.049 ± 0.006	0.037 ± 0.003
8	0.486 ± 0.030	0.314 ± 0.032	0.506 ± 0.021	0.272 ± 0.025	0.022 ± 0.002	0.009 ± 0.005	0.076 ± 0.006	0.038 ± 0.003
9	0.545 ± 0.010	0.275 ± 0.014	0.500 ± 0.019	0.276 ± 0.013	0.021 ± 0.002	0.009 ± 0.006	0.061 ± 0.008	0.030 ± 0.007
10	0.541 ± 0.030	0.290 ± 0.032	0.515 ± 0.021	0.274 ± 0.025	0.021 ± 0.002	0.007 ± 0.005	0.055 ± 0.006	0.018 ± 0.003
11	0.576 ± 0.030	0.299 ± 0.032	0.536 ± 0.021	0.310 ± 0.025	0.035 ± 0.002	0.011 ± 0.005	0.017 ± 0.006	0.006 ± 0.003
12	0.431 ± 0.030	0.155 ± 0.032	0.219 ± 0.021	0.156 ± 0.025	0.063 ± 0.002	0.026 ± 0.005	0.140 ± 0.006	0.146 ± 0.003
13	0.472 ± 0.030	0.127 ± 0.032	0.431 ± 0.021	0.089 ± 0.025	0.048 ± 0.002	0.011 ± 0.005	0.172 ± 0.006	0.099 ± 0.003
14	0.513 ± 0.051	0.141 ± 0.059	0.503 ± 0.013	0.092 ± 0.024	0.025 ± 0.000	0.008 ± 0.001	0.158 ± 0.010	0.075 ± 0.002
15	0.521 ± 0.021	0.174 ± 0.046	0.438 ± 0.021	0.174 ± 0.015	0.039 ± 0.002	0.015 ± 0.001	0.119 ± 0.010	0.061 ± 0.002
16	0.496 ± 0.030	0.238 ± 0.032	0.461 ± 0.021	0.243 ± 0.025	0.034 ± 0.002	0.013 ± 0.005	0.107 ± 0.006	0.046 ± 0.003
17	0.489 ± 0.038	0.327 ± 0.035	0.494 ± 0.011	0.271 ± 0.019	0.050 ± 0.001	0.003 ± 0.000	0.079 ± 0.004	0.006 ± 0.002
18	0.515 ± 0.030	0.273 ± 0.032	0.524 ± 0.021	0.217 ± 0.025	0.105 ± 0.002	0.006 ± 0.005	0.062 ± 0.006	0.002 ± 0.003
19	0.388 ± 0.033	0.329 ± 0.032	0.417 ± 0.021	0.146 ± 0.025	0.040 ± 0.004	0.044 ± 0.005	0.116 ± 0.017	0.086 ± 0.011
20	0.535 ± 0.033	0.175 ± 0.022	0.399 ± 0.037	0.186 ± 0.036	0.034 ± 0.004	0.038 ± 0.005	0.087 ± 0.017	0.070 ± 0.011
21	0.400 ± 0.033	0.355 ± 0.022	0.388 ± 0.037	0.148 ± 0.036	0.039 ± 0.004	0.021 ± 0.005	0.101 ± 0.017	0.076 ± 0.011
22	0.441 ± 0.033	0.372 ± 0.022	0.526 ± 0.037	0.179 ± 0.036	0.032 ± 0.004	0.012 ± 0.005	0.106 ± 0.017	0.036 ± 0.011
23	0,506 ± 0.033	0.287 ± 0.022	0.444 ± 0.037	0.218 ± 0.036	0.064 ± 0.004	0.003 ± 0.005	0.098 ± 0.017	0.005 ± 0.011

Table G.2 is continued on the following page

continued from Table G.2 from the previous page

Exp.	$S_{FA,C}$	$S_{FAc,C}$	$S_{MeFo,C}$	$S_{EtOH,C}$	$S_{HAc,C}$	$S_{MeAc,C}$	$S_{Ace,C}$	$S_{EG,C}$
1	0.046 ± 0.023	0.040 ± 0.002	0.103 ± 0.005	0.002 ± 0.000	0.002 ± 0.001	0.001 ± 0.001	0.000 ± 0.000	0.000 ± 0.000
2	0.054 ± 0.006	0.036 ± 0.010	0.042 ± 0.007	0.001 ± 0.000	0.002 ± 0.001	0.001 ± 0.001	0.000 ± 0.000	0.000 ± 0.000
3	0.008 ± 0.006	0.097 ± 0.010	0.084 ± 0.007	0.002 ± 0.000	0.005 ± 0.001	0.002 ± 0.001	0.000 ± 0.000	0.001 ± 0.000
4	0.031 ± 0.006	0.046 ± 0.010	0.054 ± 0.007	0.001 ± 0.000	0.003 ± 0.001	0.001 ± 0.001	0.000 ± 0.000	0.000 ± 0.000
5	0.019 ± 0.006	0.044 ± 0.010	0.046 ± 0.007	0.001 ± 0.000	0.002 ± 0.001	0.000 ± 0.001	0.000 ± 0.000	0.000 ± 0.000
6	0.014 ± 0.003	0.047 ± 0.010	0.054 ± 0.007	0.002 ± 0.000	0.004 ± 0.000	0.001 ± 0.001	0.000 ± 0.000	0.000 ± 0.000
7	0.008 ± 0.006	0.093 ± 0.010	0.057 ± 0.007	0.002 ± 0.000	0.005 ± 0.001	0.001 ± 0.001	0.000 ± 0.000	0.000 ± 0.000
8	0.008 ± 0.006	0.034 ± 0.010	0.030 ± 0.007	0.002 ± 0.000	0.003 ± 0.001	0.000 ± 0.001	0.000 ± 0.000	0.000 ± 0.000
9	0.008 ± 0.007	0.051 ± 0.010	0.035 ± 0.003	0.002 ± 0.000	0.004 ± 0.000	0.001 ± 0.001	0.000 ± 0.000	0.000 ± 0.000
10	0.005 ± 0.006	0.057 ± 0.010	0.038 ± 0.007	0.003 ± 0.000	0.005 ± 0.001	0.002 ± 0.001	0.000 ± 0.000	0.000 ± 0.000
11	0.004 ± 0.006	0.060 ± 0.010	0.012 ± 0.007	0.001 ± 0.000	0.007 ± 0.001	0.000 ± 0.001	0.000 ± 0.000	0.001 ± 0.000
12	0.068 ± 0.006	0.065 ± 0.010	0.110 ± 0.007	0.002 ± 0.000	0.003 ± 0.001	0.001 ± 0.001	0.000 ± 0.000	0.000 ± 0.000
13	0.070 ± 0.006	0.025 ± 0.010	0.052 ± 0.007	0.002 ± 0.000	0.002 ± 0.001	0.000 ± 0.001	0.000 ± 0.000	0.000 ± 0.000
14	0.045 ± 0.000	0.032 ± 0.004	0.056 ± 0.005	0.002 ± 0.000	0.002 ± 0.000	0.001 ± 0.000	0.000 ± 0.000	0.000 ± 0.000
15	0.028 ± 0.001	0.058 ± 0.012	0.061 ± 0.012	0.002 ± 0.000	0.004 ± 0.001	0.001 ± 0.001	0.000 ± 0.000	0.000 ± 0.000
16	0.014 ± 0.006	0.034 ± 0.010	0.040 ± 0.007	0.004 ± 0.000	0.004 ± 0.001	0.001 ± 0.001	0.000 ± 0.000	0.000 ± 0.000
17	0.012 ± 0.001	0.039 ± 0.020	0.032 ± 0.010	0.006 ± 0.000	0.005 ± 0.002	0.001 ± 0.001	0.001 ± 0.000	0.000 ± 0.000
18	0.002 ± 0.006	0.038 ± 0.010	0.024 ± 0.007	0.009 ± 0.000	0.006 ± 0.001	0.002 ± 0.001	0.003 ± 0.000	0.000 ± 0.000
19	0.032 ± 0.006	0.055 ± 0.010	0.057 ± 0.007	0.003 ± 0.000	0.004 ± 0.001	0.000 ± 0.001	0.000 ± 0.000	0.000 ± 0.000
20	0.025 ± 0.012	0.075 ± 0.016	0.074 ± 0.013	0.004 ± 0.000	0.007 ± 0.001	0.001 ± 0.001	0.000 ± 0.000	0.000 ± 0.000
21	0.014 ± 0.012	0.090 ± 0.016	0.109 ± 0.013	0.004 ± 0.000	0.007 ± 0.001	0.002 ± 0.001	0.000 ± 0.000	0.000 ± 0.000
22	0.024 ± 0.012	0.038 ± 0.016	0.034 ± 0.013	0.006 ± 0.000	0.006 ± 0.001	0.001 ± 0.001	0.000 ± 0.000	0.000 ± 0.000
23	0.023 ± 0.012	0.067 ± 0.016	0.056 ± 0.013	0.010 ± 0.000	0.007 ± 0.001	0.003 ± 0.001	0.001 ± 0.000	0.000 ± 0.000

G.2 Individual Experimental Data

Table G.3 lists the specific energy inputs *SEI** and *SEI*, electrical power input P, residence time τ, mole fraction of argon in the feed $x_{\mathrm{Ar}}^{\mathrm{in}}$, CH_4:O_2 ratio, temperature at the inlet T^{in} and outlet T^{out} of the reactor, pressure p, and conversion X_j of CH_4 and O_2 of all individual experiments. Table G.4 lists the corresponding H-selectivities $S_{i,\mathrm{H}}$ to the product components H_2 and H_2O and the C-selectivities $S_{i,\mathrm{C}}$ to the product components CO and CO_2; C_2H_6 and C_2H_4; MeOH, MeOOH, FA, and FAc; and MeFo, EtOH, HAc, MeAc, Ace, and EG of the individual experiments.

Table G.3: Overview on the specific energy inputs *SEI** and *SEI*, electrical power input P, residence time τ, mole fraction of argon in the feed x_{Ar}^{in}, CH_4:O_2 ratio, temperature at the inlet T^{in} and outlet T^{out} of the reactor, pressure p, and conversion X_j of CH_4 and O_2 of all individual experiments.

Exp.	*SEI**	*SEI*	*P*	τ	x_{Ar}^{in}	CH_4:O_2	T^{in}	T^{out}	*p*	X_{CH_4}	X_{O_2}
	J cm^{-3}	J cm^{-3}	W	s	mol mol^{-1}		K		mbar	mol mol^{-1}	
1	0.9	0.7	23	0.8	0.19	2:1	292.3	299.1	979	0.045	0.081
2	1.4	0.3	18	0.5	0.75	2:1	294.1	310.6	984	0.052	0.044
3	1.5	0.4	20	0.5	0.75	2:1	294.6	315.2	970	0.049	0.036
4	1.6	0.4	21	0.5	0.75	2:1	294.0	315.1	987	0.046	0.034
5	1.6	0.4	21	0.5	0.75	2:1	294.5	315.6	982	0.047	0.038
6	1.8	1.5	24	1.6	0.19	3:1	291.5	296.5	993	0.097	0.146
7	2.1	1.7	27	1.6	0.19	2:1	296.6	301.4	985	0.070	0.060
8	2.1	0.5	27	0.5	0.75	2:1	295.3	310.1	985	0.060	0.059
9	2.1	0.5	28	0.5	0.75	2:1	294.6	317.2	965	0.062	0.066
10	2.2	0.5	28	0.5	0.75	2:1	294.3	318.6	983	0.057	0.065
11	2.7	0.7	20	0.9	0.75	4:1	[a]	[a]	995	0.082	0.156
12	2.8	2.2	148	0.4	0.19	2:1	291.6	348.6	984	0.046	0.120
13	4.1	3.3	109	0.8	0.19	3:1	294.0	[a]	991	0.115	0.237
14	4.4	1.1	14	2.0	0.75	4:1	293.2	299.0	984	0.124	0.332
15	4.7	1.2	16	2.0	0.75	2:1	297.5	299.3	979	0.104	0.256
16	5.7	4.6	153	0.8	0.19	2:1	297.7	317.9	982	0.146	0.273
17	6.0	4.8	78	1.6	0.19	2:1	293.1	308.1	978	0.159	0.302
18	6.3	5.1	133	1.0	0.19	3:1	292.1	312.0	980	0.127	0.326
19	6.4	1.6	21	2.0	0.75	4:1	294.1	299.8	994	0.144	0.438
20	6.5	1.6	21	2.0	0.75	2:1	296.6	300.9	978	0.134	0.195
21	7.5	6.0	132	1.2	0.19	3:1	291.4	311.1	982	0.170	0.405
22	7.9	6.3	103	1.6	0.19	3:1	291.6	309.1	988	0.132	0.365

Table G.3 is continued on the following page

continued from Table G.3 from the previous page

23	8.0	6.5	105	1.6	0.19	2:1	296.5	312.4	991	0.126	0.349
24	8.3	2.1	16	3.5	0.75	3:1	294.5	298.7	988	0.163	0.531
25	8.3	2.1	27	2.0	0.75	2:1	291.6	298.6	990	0.188	0.378
26	8.7	2.2	29	2.0	0.75	2:1	293.6	298.7	997	0.204	0.369
27	9.4	2.4	31	2.0	0.75	2:1	296.2	302.8	977	0.157	0.401
28	10.9	2.7	36	2.0	0.75	4:1	293.6	300.7	1001	0.177	0.742
29	11.7	2.9	22	3.5	0.75	3:1	292.1	298.1	971	0.222	0.686
30	11.9	3.0	17	4.7	0.75	2:1	296.6	298.7	981	0.185	0.661
31	14.4	3.6	34	2.8	0.75	4:1	295.5	300.8	991	0.252	1.000
32	14.7	3.7	21	4.7	0.75	2:1	291.9	[a]	985	0.308	0.642
33	15.0	3.8	21	4.7	0.75	2:1	294.2	298.5	987	0.275	0.709
34	16.2	3.7	23	4.3	0.75	2:1	295.0	299.5	973	0.270	0.761
35	16.6	4.1	23	4.7	0.75	2:1	297.5	302.5	997	0.195	0.753
36	16.6	4.2	23	4.7	0.75	2:1	[a]	[a]	984	0.317	0.793
37	17.0	4.3	32	3.5	0.75	3:1	294.9	300.7	997	0.299	1.000
38	17.2	4.3	24	4.7	0.75	2:1	291.8	296.7	986	0.354	0.770
39	19.6	4.9	27	4.7	0.75	2:1	296.0	303.0	977	0.253	0.849
40	20.0	5.0	28	4.7	0.75	2:1	294.3	300.2	990	0.311	0.875
41	20.3	5.1	28	4.7	0.75	2:1	294.6	300.6	975	0.343	0.894
42	22.9	5.7	43	3.5	0.75	3:1	293.6	300.5	981	0.304	1.000
43	23.8	6.0	33	4.7	0.75	2:1	295.7	299.9	984	0.320	1.000

[a] temperature was not recorded

Table G.4: Overview on H-selectivities $S_{i,\mathrm{H}}$ and C-selectivities $S_{i,\mathrm{C}}$ to the product components i of the individual experiments. All values are given in mol mol^{-1}.

Exp.	$S_{\mathrm{H_2O,H}}$	$S_{\mathrm{H_2,H}}$	$S_{\mathrm{CO,C}}$	$S_{\mathrm{CO_2,C}}$	$S_{\mathrm{C_xH_x,C}}$	$S_{\mathrm{C_xH_x,C}}$	$S_{\mathrm{MeOH,C}}$	$S_{\mathrm{MeOOH,C}}$	$S_{\mathrm{FA,C}}$	$S_{\mathrm{FAc,C}}$	$S_{\mathrm{MeFo,C}}$	$S_{\mathrm{EtOH,C}}$	$S_{\mathrm{HAc,C}}$	$S_{\mathrm{MeAc,C}}$	$S_{\mathrm{Ace,C}}$	$S_{\mathrm{EG,C}}$
1	0.428	0.203	0.400	0.001	0.063	0.000	0.107	0.125	0.108	0.088	0.103	0.002	0.002	0.001	0.0000	0.0000
2	0.490	0.195	0.547	0.160	0.049	0.032	0.083	0.046	0.039	0.020	0.020	0.002	0.002	0.000	0.0000	0.0000
3	0.623	0.000	0.518	0.174	0.053	0.046	0.076	0.046	0.034	0.023	0.028	0.001	0.002	0.000	0.0000	0.0000
4	0.695	0.000	0.500	0.228	0.053	0.045	0.039	0.039	0.015	0.035	0.039	0.002	0.002	0.002	0.0000	0.0000
5	0.634	0.000	0.471	0.214	0.050	0.041	0.072	0.049	0.032	0.033	0.033	0.002	0.002	0.000	0.0000	0.0000
6	0.516	0.146	0.288	0.149	0.058	0.028	0.112	0.119	0.063	0.083	0.093	0.002	0.004	0.002	0.0001	0.0000
7	0.652	0.000	0.510	0.179	0.050	0.039	0.082	0.052	0.033	0.024	0.025	0.002	0.003	0.001	0.0000	0.0002
8	0.652	0.000	0.489	0.206	0.048	0.039	0.073	0.048	0.028	0.031	0.033	0.001	0.002	0.000	0.0000	0.0000
9	0.627	0.000	0.536	0.176	0.052	0.040	0.087	0.042	0.016	0.022	0.024	0.002	0.002	0.002	0.0005	0.0000
10	0.502	0.150	0.457	0.100	0.020	0.019	0.152	0.066	0.132	0.020	0.032	0.001	0.000	0.000	0.0000	0.0000
11	0.577	0.171	0.404	0.218	0.018	0.000	0.094	0.067	0.008	0.097	0.084	0.002	0.005	0.002	0.0002	0.0006
12	0.527	0.127	0.548	0.089	0.018	0.007	0.149	0.095	0.039	0.018	0.032	0.001	0.001	0.001	0.0000	0.0000
13	0.529	0.133	0.493	0.084	0.022	0.009	0.145	0.100	0.041	0.042	0.061	0.001	0.003	0.000	0.0000	0.0002
14	0.544	0.189	0.419	0.205	0.026	0.019	0.094	0.068	0.014	0.077	0.071	0.002	0.005	0.001	0.0000	0.0003
15	0.517	0.163	0.580	0.110	0.016	0.008	0.145	0.058	0.028	0.020	0.032	0.001	0.001	0.001	0.0000	0.0000
16	0.569	0.163	0.463	0.195	0.018	0.012	0.099	0.071	0.010	0.068	0.059	0.001	0.004	0.000	0.0000	0.0000
17	0.546	0.198	0.456	0.210	0.018	0.013	0.117	0.060	0.022	0.046	0.052	0.002	0.004	0.001	0.0000	0.0000
18	0.562	0.173	0.500	0.177	0.014	0.000	0.115	0.075	0.006	0.049	0.057	0.002	0.004	0.001	0.0000	0.0002
19	0.549	0.245	0.438	0.277	0.021	0.010	0.049	0.037	0.008	0.093	0.057	0.002	0.005	0.001	0.0000	0.0002
20	0.537	0.255	0.493	0.296	0.022	0.011	0.066	0.036	0.008	0.038	0.026	0.002	0.003	0.000	0.0000	0.0000
21	0.436	0.373	0.518	0.248	0.021	0.008	0.086	0.039	0.007	0.030	0.035	0.003	0.003	0.001	0.0000	0.0000
22	0.531	0.338	0.530	0.294	0.024	0.010	0.044	0.031	0.008	0.035	0.015	0.002	0.005	0.001	0.0000	0.0003

Table G.4 is continued on the following page

continued from Table G.4 from the previous page

23	0.526	0.282	0.497	0.252	0.022	0.010	0.062	0.031	0.007	0.063	0.047	0.003	0.005	0.002	0.0001	0.0002
24	0.543	0.273	0.470	0.282	0.019	0.008	0.069	0.026	0.010	0.064	0.044	0.002	0.004	0.002	0.0001	0.0000
25	0.581	0.208	0.505	0.278	0.019	0.007	0.070	0.032	0.007	0.043	0.032	0.002	0.003	0.001	0.0000	0.0000
26	0.566	0.256	0.503	0.249	0.020	0.008	0.055	0.016	0.004	0.080	0.051	0.003	0.007	0.003	0.0001	0.0003
27	0.571	0.275	0.514	0.282	0.020	0.007	0.049	0.017	0.006	0.060	0.035	0.003	0.005	0.002	0.0001	0.0000
28	0.487	0.338	0.529	0.292	0.022	0.008	0.060	0.020	0.005	0.031	0.027	0.002	0.003	0.001	0.0001	0.0000
29	0.576	0.299	0.536	0.310	0.035	0.011	0.017	0.006	0.004	0.060	0.012	0.001	0.007	0.000	0.0001	0.0008
30	0.431	0.155	0.219	0.156	0.063	0.026	0.140	0.146	0.068	0.065	0.110	0.002	0.003	0.001	0.0000	0.0000
31	0.472	0.127	0.431	0.089	0.048	0.011	0.172	0.099	0.070	0.025	0.052	0.002	0.002	0.000	0.0000	0.0000
32	0.511	0.143	0.496	0.100	0.028	0.008	0.155	0.067	0.050	0.033	0.058	0.002	0.002	0.001	0.0000	0.0000
33	0.515	0.139	0.510	0.083	0.023	0.008	0.162	0.083	0.041	0.032	0.055	0.001	0.002	0.001	0.0000	0.0000
34	0.508	0.145	0.487	0.107	0.048	0.010	0.158	0.071	0.037	0.029	0.049	0.001	0.001	0.001	0.0000	0.0000
35	0.534	0.203	0.390	0.240	0.029	0.020	0.080	0.052	0.018	0.087	0.074	0.003	0.006	0.000	0.0001	0.0000
36	0.496	0.238	0.461	0.243	0.034	0.013	0.107	0.046	0.014	0.034	0.040	0.004	0.004	0.001	0.0001	0.0000
37	0.489	0.327	0.494	0.271	0.050	0.003	0.079	0.006	0.012	0.039	0.032	0.006	0.005	0.001	0.0012	0.0000
38	0.515	0.273	0.524	0.217	0.105	0.006	0.062	0.002	0.002	0.038	0.024	0.009	0.006	0.002	0.0025	0.0000
39	0.388	0.329	0.417	0.146	0.040	0.044	0.116	0.086	0.032	0.055	0.057	0.003	0.004	0.000	0.0001	0.0000
40	0.535	0.175	0.399	0.186	0.034	0.038	0.087	0.070	0.025	0.075	0.074	0.004	0.007	0.001	0.0000	0.0000
41	0.400	0.355	0.388	0.148	0.039	0.021	0.101	0.076	0.014	0.090	0.109	0.004	0.007	0.002	0.0001	0.0000
42	0.441	0.372	0.526	0.179	0.032	0.012	0.106	0.036	0.024	0.038	0.034	0.006	0.006	0.001	0.0001	0.0000
43	0.506	0.287	0.444	0.218	0.064	0.003	0.098	0.005	0.023	0.067	0.056	0.010	0.007	0.003	0.0012	0.0005

G.3 Numerical Data for the Elemental Balance

Table G.5 lists the numerical results of the molar flow of elements at the inlet $\dot{n}_e^{\text{in}}$ and outlet $\dot{n}_e^{\text{out}}$ of the reactor.

Table G.5: Molar flow of elements at the inlet $\dot{n}_e^{\text{in}}$ and outlet $\dot{n}_e^{\text{out}}$ of the reactor of carbon, hydrogen, and oxygen of the individual experiments.

Exp.	$\dot{n}_{\text{carbon}}^{\text{in}}$	$\dot{n}_{\text{hydrogen}}^{\text{in}}$	$\dot{n}_{\text{oxygen}}^{\text{in}}$	$\dot{n}_{\text{carbon}}^{\text{out}}$	$\dot{n}_{\text{hydrogen}}^{\text{out}}$	$\dot{n}_{\text{oxygen}}^{\text{out}}$
	mol h^{-1}	mol h^{-1}	mol h^{-1}	mol h^{-1}	mol h^{-1}	mol h^{-1}
1	2.630	10.521	2.631	2.539	10.177	2.478
2	1.290	5.161	1.287	1.262	5.003	1.303
3	1.290	5.161	1.287	1.262	4.993	1.307
4	1.290	5.161	1.287	1.267	5.013	1.316
5	1.290	5.161	1.287	1.265	5.008	1.311
6	1.452	5.809	0.969	1.346	5.404	0.905
7	1.290	5.161	1.287	1.234	4.967	1.295
8	1.290	5.161	1.287	1.255	4.966	1.298
9	1.290	5.161	1.287	1.255	4.957	1.292
10	1.290	5.161	1.287	1.256	4.959	1.278
11	0.860	3.440	0.430	0.826	3.330	0.441
12	5.198	20.793	5.200	5.178	20.681	5.039
13	2.961	11.843	1.975	2.792	11.146	1.864
14	0.387	1.548	0.193	0.365	1.463	0.191
15	0.322	1.289	0.322	0.317	1.277	0.313
16	2.630	10.521	2.631	2.504	9.902	2.460
17	1.290	5.161	1.287	1.203	4.815	1.165
18	2.337	9.349	1.556	2.261	8.977	1.511
19	0.387	1.548	0.193	0.367	1.517	0.191
20	0.322	1.289	0.322	0.315	1.267	0.348
21	1.951	7.804	1.300	1.822	7.255	1.211
22	1.452	5.809	0.969	1.410	5.612	0.931

Table G.5 is continued on the following page

continued from Table G.5 from the previous page

23	1.290	5.161	1.287	1.297	5.061	1.177
24	0.207	0.829	0.138	0.196	0.784	0.119
25	0.323	1.290	0.322	0.303	1.209	0.300
26	0.323	1.290	0.322	0.296	1.184	0.296
27	0.322	1.289	0.322	0.317	1.265	0.302
28	0.387	1.548	0.193	0.368	1.517	0.163
29	0.207	0.829	0.138	0.189	0.743	0.103
30	0.137	0.549	0.137	0.138	0.544	0.109
31	0.277	1.106	0.138	0.244	0.998	0.088
32	0.137	0.549	0.137	0.120	0.459	0.104
33	0.137	0.549	0.137	0.124	0.492	0.092
34	0.137	0.549	0.137	0.126	0.505	0.095
35	0.137	0.549	0.137	0.140	0.551	0.101
36	0.137	0.549	0.137	0.125	0.493	0.102
37	0.205	0.822	0.137	0.179	0.709	0.076
38	0.137	0.549	0.137	0.117	0.442	0.094
39	0.137	0.549	0.137	0.137	0.540	0.103
40	0.137	0.549	0.137	0.128	0.502	0.098
41	0.137	0.549	0.137	0.122	0.458	0.080
42	0.207	0.828	0.138	0.187	0.732	0.089
43	0.137	0.549	0.137	0.127	0.479	0.076

Statement on Authorship

This dissertation contains material that has been published previously. These publications are listed below. The author of the present thesis developed the experimental setup, carried out or supervised the experiments, evaluated the results, and wrote the manuscript.

- S. Müller, E Ströfer, M. Kohns, E. von Harbou, K. Münnemann, H. Hasse: Investigation of Partial Oxidation of Methane in a Cold Plasma Reactor with Detailed Product Analysis, Plasma Chemistry and Plasma Processing 43 (2023) 513 – 532. https://doi.org/10.1007/s11090-022-10308-5.

  The author of the present thesis developed the experimental setup, carried out and supervised the experiments, evaluated the results, and wrote the manuscript.

- S. Müller, E Ströfer, M. Kohns, E. von Harbou, K. Münnemann, H. Hasse: Conversions and Selectivities in Cold Plasma Partial Oxidation of Methane, Plasma Processes and Polymers (2024) e2400027. https://doi.org/10.1002/ppap.202400027

  The author of the present thesis developed the experimental setup, carried out and supervised the experiments, evaluated the results, and wrote the manuscript.

Contributions and Student Reports

The following colleagues and students contributed to this thesis under the supervision of the author by carrying out experiments and measurements, developing the experimental set-up, or evaluating the results (Ferdinand Breit, Tess Seip, Craig McQuillan, Annemarie Rätz, André Bender, Maximilian Koch, Lena Magel, Daniel Stolte, Jana Heiß, Florian Jager, Tobias Laufer, Tanja Breug-Nissen, Kirsten Brunn, Julian Peter, Dirk Feddeck, Eckhard Ströfer, Jürgen Brauch). The following student reports were prepared under the supervision of the author in the context of the present thesis:

- T. Laufer: Investigation of the Partial Oxidation of Methane by means of Cold Plasma Experiments and Simulations of Classical Combustion. Master thesis, Laboratory of Engineering Thermodynamics (LTD), TU Kaiserslautern (2022).

- J. Heiß: Experimental Investigation of Gas Phase Reactions in Cold Plasma. Master thesis, Laboratory of Engineering Thermodynamics (LTD), TU Kaiserslautern (2021).

- D. Stolte: Experimental Investigation of Methane Oxidation in Cold Plasma. Research work, Laboratory of Engineering Thermodynamics (LTD), TU Kaiserslautern (2021).

- L. Magel: Extension of a Laboratory Facility for Studying Gas Phase Reactions in Cold Plasma. Master thesis, Laboratory of Engineering Thermodynamics (LTD), TU Kaiserslautern (2020).

- A. Bender: Experimental Investigation of Methane Oxidization in Cold Plasma. Master thesis, Laboratory of Engineering Thermodynamics (LTD), TU Kaiserslautern (2020).

- C. McQuillan: Process Design for New Experimental Investigations (Focus NMR Spectroscopy). IASTE research project, Laboratory of Engineering Thermodynamics (LTD), TU Kaiserslautern (2018).

- T. Seip: Process Design for New Experimental Investigations (Focus Gas Chromatography). RISE research project, Laboratory of Engineering Thermodynamics (LTD), TU Kaiserslautern (2018).

Curriculum Vitae

Personal information

Name	Silvie Müller
Date of birth	22.07.1991
Place of birth	Ludwigshafen am Rhein, Germany

Education

1997 – 1999	Grundschule Berlin
1999 – 2001	Grundschule Ludwigshafen am Rhein
2001 – 2010	Heinrich-Böll-Gymnasium Ludwigshafen am Rhein
	Degree: Allgemeine Hochschulreife
2010 – 2015	Technische Universität Kaiserslautern
	Course: Energy and Process Engineering
	Degree: B.Sc.
2015 – 2017	Technische Universität Kaiserslautern
	Course: Energy and Process Engineering
	Degree: M.Sc.

Professional experience

10/2017 – 06/2022	PhD student at
	Laboratory of Engineering Thermodynamics (LTD)
	Technische Universität Kaiserslautern
	Prof. Dr.-Ing. Hans Hasse
Since 11/2022	Technical Project Engineer/Manager at
	Merck Group, Darmstadt